UNIVERSITÀ
DEGLI STUDI
DI PADOVA

Sede Amministrativa: Università degli Studi di Padova

Dipartimento di Scienze Biomediche

SCUOLA DI DOTTORATO DI RICERCA IN : BIOSCIENZE E BIOTECNOLOGIE

INDIRIZZO: NEUROBIOLOGIA

CICLO XXV

EFFECTS OF FAMILIAL ALZHEIMER'S DISEASE-LINKED PRESENILIN 2 MUTANTS ON Ca^{2+} HOMEOSTASIS OF GOLGI APPARATUS SUB-COMPARTMENTS

Direttore della Scuola : Ch.mo Prof. Giuseppe Zanotti

Coordinatore d'indirizzo: Ch.ma Prof.ssa Daniela Pietrobon

Supervisore : Dott.ssa Paola Pizzo

Dottoranda : PAOLA CAPITANIO

Index

Riassunto

La malattia di Alzheimer's (AD) è un disordine neurodegenerativo e la forma più comune di demenza senile.
La caratteristica istopatologica di AD è la presenza di depositi neurofibrillari intracellulari e di placche amiloidi, costituite da aggregati di peptide amiloide (Aβ), che si depositano nella matrice extracellulare del cervello. I peptidi Aβ sono il risultato di due tagli sequenziali della Proteina Precursore dell'Amiloide (APP); Aβ viene poi rilasciato dall'enzima γ-secretasi. Le più abbondanti specie peptidiche di Aβ, prodotte anche fisiologicamente per tutta la vita, sono Aβ40 e Aβ42, quest'ultimo più insolubile e più incline all'aggregazione.
Sebbene la maggior parte dei casi di AD siano sporadici, una piccola percentuale di pazienti è affetta dalla forma ereditaria di Alzheimer (malattia familiare di Alzheimer, FAD), causata da mutazioni dominanti in uno dei geni codificanti per APP, presenilina-1 (PS1) e presenilina-2 (PS2); le PSs sono le subunità catalitiche del complesso enzimatico della γ-secretasi ma funzionano anche in maniera indipendente da tale attività enzimatica.
Le mutazioni in PSs legate a FAD portano ad un aumento nel rapporto Aβ42/Aβ40, che promuove la deposizione di placche amiloidi. Oltre a questo effetto, è stato ampiamente dimostrato che molte mutazioni in PS1 e PS2 provocano alterazioni della omeostasi del Ca^{2+} intracellulare, rendendo così i neuroni più sensibili agli stimoli eccitotossici e apoptotici.
L'apparato di Golgi (GA) rappresenta, insieme al reticolo endoplasmatico (ER), il principale deposito intracellulare di Ca^{2+}, IP_3 sensibile, e la sua funzionalità è fondamentale per il controllo delle risposte citosoliche di Ca^{2+}.
Sempre maggiori evidenze suggeriscono che il GA sia un organello eterogeneo in termini di Ca^{2+} *handling*, essendo dotato di un diverso *toolkit* molecolare per il Ca^{2+} rispetto a quello espresso nell' ER. Ad esempio, come meccanismi di *uptake* per il Ca^{2+}, il GA esprime la classica pompa SERCA (*Sarco-Endoplasmic Reticulum* Ca^{2+} *ATPase*) ma anche un ulteriore pompa, detta SPCA1 (*Secretory Pathway* Ca^{2+} *ATPase1*).
L'utilizzo di uno specifico sensore per il Ca^{2+} specificatamente indirizzato al trans-Golgi, ci ha precedentemente permesso di dimostrare

direttamente la eterogeneità funzionale del GA, mostrando il comportamento distinto di questo sub-compartimento: i meccanismi di *uptake* di Ca^{2+} sono mediati esclusivamente dalla SPCA1 (e non dalla SERCA); non rilascia Ca^{2+} in risposta alla generazione IP_3, ma piuttosto si accumula il catione come conseguenza dell'aumento di Ca^{2+} citoplasmatico.
Per quanto riguarda gli altri sub-compartimenti del GA, abbiamo generato un nuovo indicatore per il Ca^{2+} fuso alla sequenza di indirizzamento dell'enzima 1,6 N-acetylglucosaminyltransferasi (C2gnT) residente del cis/medial-Golgi. La nuova sonda co-localizza con il marcatore di cis/medial-Golgi Giantina e quindi è stata utilizzata per studiare le dinamiche di Ca^{2+} in questo sub-compartimento a livello di singola cellula.
Complessivamente i dati ottenuti suggeriscono che il GA sia unico in termini di omeostasi del Ca^{2+}, con tali sub-compartimenti separati da pochi micron, e in equilibrio molto rapido tra loro, ma comunque in grado di mantenere differenze consistenti in termini di concentrazione dello ione e risposta a stimoli esterni .
Le differenze tra i due sub-compartimenti del GA sono confermate dall' effetto specifico sulla omeostasi del Ca^{2+} dell'espressione della forma mutata di PS2T122R legata alla malattia familiare di Alzheimer. Le cellule che esprimono tale proteina mostrano una diminuzione del contenuto di Ca^{2+} nel cis/medial-Golgi ma nessun effetto sull' omeostasi del Ca^{2+} nel trans-Golgi. PS2T122R sembra inibire l'assorbimento di Ca^{2+} nel cis/medial-Golgi, inibendo l'attività della pompa SERCA, mentre non influenza l'assorbimento di Ca^{2+}, mediato dalla SPCA1, nel trans-Golgi.
Il GA sembra quindi giocare un ruolo importante nella patogenesi di AD e comprendere il contributo di tale organello nella patogenesi di AD e la sua base fisiopatologica potrà avere un forte impatto sulla possibilità di sviluppare terapie più efficaci per AD.

Summary

Alzheimer's Disease (AD) is a progressive neurodegenerative disorder and the most common form of senile dementia. The characteristic histopathological hallmarks of AD are the intracellular neurofibrillary tangles and the amyloid plaques, made of aggregated amyloid peptides (Aβ), that deposit in the extracellular matrix of the brain. Aβ peptides are the result of two sequential cleavages of the amyloid precursor protein (APP); Aβ is eventually released by the γ-secretase enzyme. The most abundant Aβ peptide species, both physiologically produced throughout life, are Aβ40 and Aβ42, which is more insoluble and aggregation-prone.

Although most AD cases are sporadic, a small percentage of patients is affected by the hereditary form of AD (Familial Alzheimer's Disease, FAD), caused by dominant mutations in one of three genes. These genes code for the APP, presenilin-1 (PS1) and presenilin-2 (PS2); PSs are the catalytic subunits of the γ-secretase enzyme complex but they also function in a γ-secretase indipendent manner.

FAD-linked mutations in PSs lead to an increased Aβ42/Aβ40 ratio, that promotes Aβ plaques deposition. Beside this effect on Aβ production, many mutations in PS1 and PS2 have been extensively demonstrated to cause alterations in the intracellular Ca^{2+} homeostasis, thus making neurons more sensitive to excitotoxic stimuli and apoptosis.

The Golgi apparatus (GA) represents, together with the endoplasmic reticulum (ER), the major IP_3-sensitive, rapidly mobilizable, intracellular Ca^{2+} store and its functionality is thus important for shaping cytosolic Ca^{2+} responses. Increasing evidence suggests that the GA is an heterogeneous Ca^{2+} handling organelle, equipped with a diverse molecular Ca^{2+} toolkit compared to the one expressed in the ER. For example, as Ca^{2+} uptake mechanisms, the GA expresses the classical sarco-endoplasmic reticulum Ca^{2+} ATPase (SERCA) but also an additional Ca^{2+} pump, the secretory pathway Ca^{2+} ATPase1, SPCA1.

The use of a specific Cameleon Ca^{2+} sensor targeted to the *trans*-Golgi, allowed us to directly demonstrate the functional GA heterogeneity by showing the distinct behavior of this sub-compartment: it takes up Ca^{2+} almost exclusively via SPCA1 (and not by SERCA); it does not release Ca^{2+}

in response to IP_3 generation, but rather accumulates the cation as a consequence of the cytoplasmic Ca^{2+} rise.

As regard to the other GA compartments, we generated a new FRET-based Ca^{2+} indicator fused to the *cis*/medial-Golgi targeting sequence of the enzyme 1,6 N-acetylglucosaminyltransferase (C2gnT). The new probe very nicely co-localizes with the *cis*/medial-Golgi marker Giantin and thus was used to study Ca^{2+} dynamics in this compartment at single cell level.

The data collected suggest that the GA is unique in terms of Ca^{2+} homeostasis, with compartments that are separated by a few microns, and in very rapid equilibrium with each other, that still maintain quite substantial differences in terms of ion concentration and response to external stimuli.

The differences between the two GA sub-compartments, the medial and the *trans*-one, are confirmed by the specific effect on Ca^{2+} homeostasis of the expression of the FAD-linked PS2 T122R mutation. Cells expressing the mutated form of the protein show a decreased Ca^{2+} content in the *cis*/medial-Golgi but no effects on *trans*-Golgi Ca^{2+} homeostasis. PS2-T122R seems to inhibiting Ca^{2+} uptake in the *cis*/medial-Golgi by inhibiting SERCA pump activity while does not affect Ca^{2+} uptake, mediated by SPCA1, in the *trans*-Golgi.

As a major Ca^{2+} store, the GA could play an important role in AD and understanding the contribution of GA Ca^{2+} dysfunction in AD will significantly impact our ability to develop more effective therapies for the disease.

Introduction

1. CALCIUM SIGNALLING

Calcium (Ca^{2+}) is a highly versatile intracellular signal that can regulate many different cellular functions. To achieve this versatility, the Ca^{2+}-signalling system operates in many different ways to regulate cellular processes that function over a wide dynamic range (Berridge M.J. et al., 2003).

Thus, in order to extensively control cellular activity, it is necessary to regulate Ca^{2+} signals (changes in Ca^{2+} concentration) in 3D space, time and amplitude.

Cells normally maintain a low resting 'free' Ca^{2+} concentration in the cytosol ($[Ca^{2+}]c$) of 100-200 nM. This contrasts with a higher concentration (1-2 mM) in the extracellular fluids.

In order to maintain this low resting $[Ca^{2+}]c$, cells remove Ca^{2+} using different energy-dependent mechanisms (fig. 1).

In addition, eukaryotic cells can sequester Ca^{2+} into intracellular organelles, in particular the Endoplasmic Reticulum (ER) and the Golgi Apparatus (GA), but also peroxisomes, mitochondria, and endolysosomal compartments (fig. 1) (Prins D. and Michalak M., 2011).

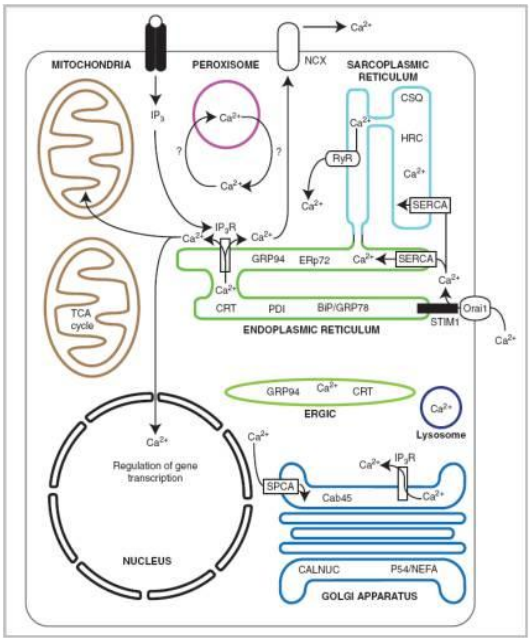

Fig.1: Organellar Ca^{2+} buffering and intracellular Ca^{2+} dynamics (D. Prins and M. Michalak, 2011)

At any time, the level of intracellular Ca^{2+} is determined by a balance between the 'on' reactions, that introduce Ca^{2+} into the cytoplasm, and the 'off ' reactions, through which this ion is removed by the combined action of buffers, pumps and exchangers. Each cell type expresses a unique set of components of the Ca^{2+}-signalling toolkit to create Ca^{2+}-signalling systems with different spatial and temporal properties. Almost all Ca^{2+}-signalling systems have one thing in common: they function by generating brief pulses of Ca^{2+}. The Ca^{2+} signal is derived either from internal stores or from the external medium (Berridge M.J. et al., 2003).

1.1 Intracellular Ca^{2+} stores and Ca^{2+} dynamics

Ca^{2+} is compartmentalized both physically and functionally within the endomembrane system and each organelle has its own distinct Ca^{2+}-handling properties and Ca^{2+}-toolkit (Zampese E. and Pizzo P., 2011).
Main intracellular Ca^{2+} stores are the ER and the GA, but also peroxisomes, mitochondria and endolysosomal compartments are involved in Ca^{2+} signaling.

1.1.1 The Endoplasmic Reticulum as an intracellular Ca^{2+} store

The ER is a continuous membrane network (Csala M. et al., 2006) in the cytosol (fig. 2). Its closed internal compartment, the ER lumen, can comprise up to 10% of the total cell volume.

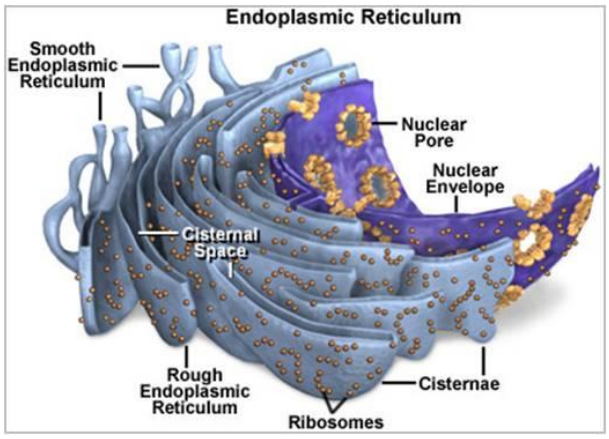

Fig.2: The Endoplasmic Reticulum

Several metabolic pathways are compartmentalized in the ER. These pathways are related to carbohydrate metabolism, biotransformation, steroid metabolism and protein processing (Csala M. et al., 2006).
The ER is also the major intracellular Ca^{2+} store in muscle and non-muscle cells. Sarco/Endoplasmic Reticulum Ca^{2+} ATPases (SERCAs), inositol 1,4,5-trisphosphate receptors ($InsP_3Rs$) and ryanodine receptors (RyRs) Ca^{2+} channels, and intraluminal Ca^{2+}-binding proteins all contribute to the ability of the ER to function as a Ca^{2+} source and Ca^{2+} sink (Pozzan T. et al., 1994).
The ER contains a high intra-luminal Ca^{2+} concentration that has been measured *in situ* in various cell types by several different methods. In particular, reported concentrations of free intra-luminal Ca^{2+}, measured with either Ca^{2+}-sensitive fluorescent dyes or ER-targeted aequorin, range from 100 μM to 5 mM (Meldolesi J. and Pozzan T., 1998).
The high luminal Ca^{2+} concentration is the result of active Ca^{2+} uptake mediated by SERCAs.
The SERCA protein consists of a single polypeptide chain folded into four major domains (fig. 3): a transmembrane (M) domain, composed of 10 transmembrane helices, and three cytosolic domains. Two of these domains, the actuator (A) domain and the phosphorylation (P) domain, are connected to the M domain. The third, the nucleotide-binding (N) domain, is connected to the P domain. Two Ca^{2+}-binding sites are located in the M domain (Wuytack F. et al., 2002).
Depending on the protein conformation, the binding sites can exist in a high-affinity state, allowing access from the cytosolic side (E1 state), or in a low-affinity state, facing the lumenal side of the membrane (E2 state). Either cytosolic ATP or Ca^{2+} can bind first to the E1 conformation. The $2Ca^{2+}$-E1-ATP form undergoes phosphorylation to form $2Ca^{2+}$-E1-P, the high-energy phosphor-intermediate in which the bound Ca^{2+} ions become occluded. This intermediate is also called the ADP-sensitive form, because in the presence of ADP the backward reaction occurs with release of the bound Ca^{2+} and synthesis of ATP. Conversion to the low-energy intermediate is accompanied by a major conformational change to $2Ca^{2+}$-E2-P (ADP-insensitive form), whereby the Ca^{2+}-binding sites are converted to a low-affinity state and reorient towards the lumenal face. The cycle ends with the sequential release of Ca^{2+} and phosphate and a

major conformational change from the E2 to the E1 state (fig. 3) (Wuytack F. et al., 2002).

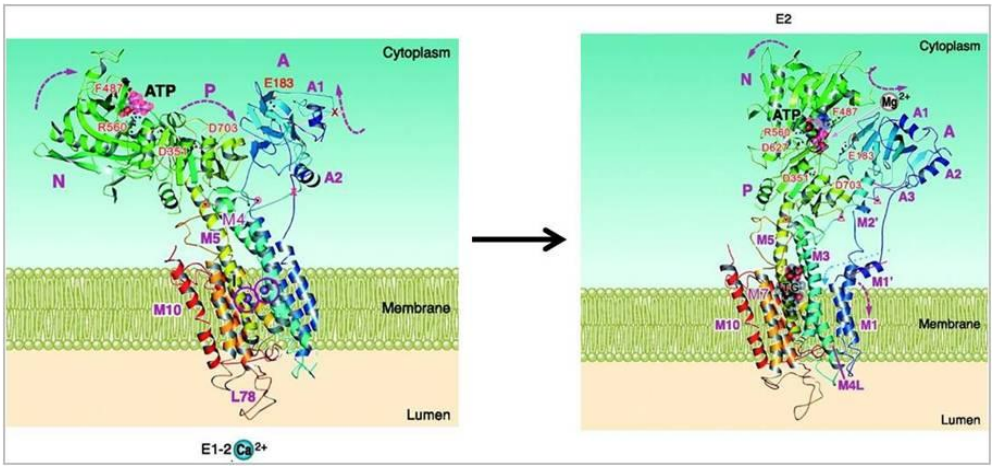

Fig. 3: 3D structure of the SERCA pump showing the open and closed conformation in the E1-2Ca^{2+} and E2 (in presence of thapsigargin) states (M. Brini and E. Carafoli, 2008)

Several studies showed that the pump transports two Ca^{2+} per ATP hydrolyzed and that it counter-transports H^+ in exchange for Ca^{2+}. However, fewer than four H^+ were released to the cytosol per two Ca^{2+} pumped, showing that the transport reaction was partly electrogenic (Brini M. and Carafoli E., 2008).

In mammals, three genes (human nomenclature ATP2A1-3) encode three main SERCA proteins. Each of the three transcripts undergoes tissue-dependent alternative splicing, increasing the number of pump variants (fig. 4). The changes in the expression pattern of the variants during development and tissue differentiation indicate that each isoform is adapted to specific functions.

SERCA1a and SERCA1b variants are expressed in adult and neonatal fast-twitch skeletal muscles, respectively. The SERCA2a variant is selectively expressed in heart and slow-twitch skeletal muscles, whereas the SERCA2b variant is expressed nearly ubiquitously and is thus considered the housekeeping isoform. SERCA3 is instead expressed in a limited number of non-muscle cells (Brini M. and Carafoli E., 2008).

It also known that the SERCA pump was inhibited by La^{3+} and orthovanadate (Szasz I. et al., 1978). Specific inhibitors have also been discovered: thapsigargin (TG, isolated from the roots of Thapsia garganica) (Thastrup O. et al., 1990), cyclopiazonic acid (CPA, produced by Aspergillus and Penicillum) (Seidler N.W. et al., 1989) and 2,5-di(t-

butyl)hydroquinone (tBHQ; Oldershaw K.A. and Taylor C.W., 1990). While the inhibition by CPA and tBHQ is reversible, and disappears following their removal, that by TG is irreversible. TG is the most popular inhibitor of the SERCA pump and its mechanism of action is better characterized than that of the other inhibitors. It binds stechiometrically to the F256 in the M3 helix (Yu M. et al., 1998), locking the pump in an irreversible inactive state (Sagara Y., 1992). Its affinity for the SERCA pump is very high: K_d values in the sub-nanomolar range have been measured (Sagara Y. and Inesi G., 1991).

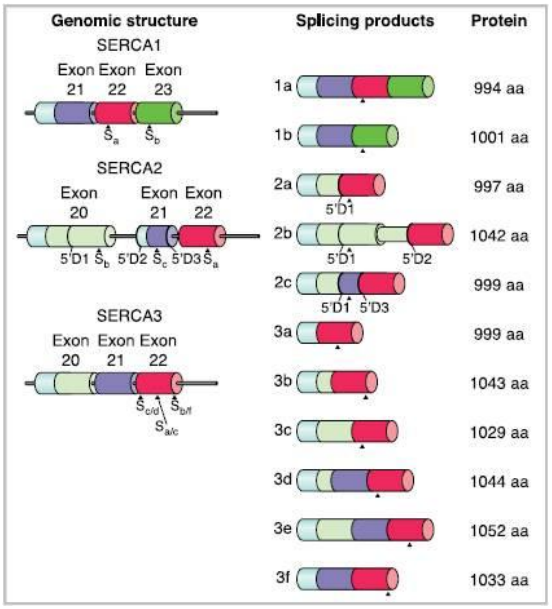

Fig. 4: Generation of multiple SERCA isoforms by alternative splicing of the human ATP2A1-3 genes. Exons are represented by colored boxes, introns by the black line (Brini M. and Carafoli E., 2008)

CPA and tBHQ have lower affinity for the pump than TG (K_d in the low micromolar to high nanomolar range). Recent studies on the structure of the SERCA-CPA complex (Moncoq K. et al., 2007) have shown that CPA occupies the Ca^{2+} access channel in the pump molecule.

Inside the ER, Ca^{2+} is bound by a number of luminal Ca^{2+}-binding proteins, most of them acting both as buffers and protein chaperones (Coe H. and Michalak M., 2009), such as calreticulin (CRT), calsequestrin (CSQ), Glucose-Regulated Protein 78 (GRP78), Glucose-Regulated Protein 94 (GRP94) and Calnexin. These proteins possess a variable number of Ca^{2+}-binding sites (from 1 to ~50 per molecule) while their relatively low affinity for the cation ensures, on the one side, its rapid diffusion

through the organelle and, on the other, its prompt release upon opening of the release channels (Zampese E. and Pizzo P., 2011).

ER Ca^{2+} release relies on two main gated ion channels: the ubiquitous IP_3 receptor (IP_3R), and, in many cells, the Ryanodine Receptors (RyRs).

Inositol 1,4,5-trisphosphate (IP_3) is a second messenger produced through phosphoinositide turnover (fig. 5) in response to many extracellular stimuli (including hormones, growth factors, neurotransmitters, neutrophins, odorants and light) and controls various Ca^{2+}-dependent cell functions (including cell proliferation, differentiation, fertilization, embryonic development, secretion, muscular contraction, immune responses, brain functions, chemical senses and light transduction) by inducing Ca^{2+} release from intracellular Ca^{2+} stores, such as from the ER (Berridge M.J., 1993).

Among the various inositol-phosphates and phospholipids, IP_3 is unique in that it is the only one that has a channel as a target molecule, the IP_3 receptor (IP_3R).

IP_3 diffuses in the cytoplasm and binds to the IP_3R, which is an intracellular ligand-gated Ca^{2+} release channel localized primarily in the ER membrane (Maeda N. et al., 1991).

IP_3Rs are coded by three different genes, and alternatively spliced isoforms have been identified in mammalian cells; the three full-length sequences are 60–80% homologous and have distinct and overlapping patterns of expression that vary during differentiation, with most cells expressing more than one isoform (Foskett J.K. et al., 2007). The different isoforms are probably involved in shaping different types of signaling events (Hattori M. et al., 2004).

Each IP_3R molecule contains ~2,700 amino acids with a molecular mass of ~310 kDa. Structurally, each IP_3R molecule contains a cytoplasmic N-terminus comprising ~85% of the protein mass, a hydrophobic region predicted to contain six membrane-spanning helices that contribute to the ion-conducting pore of the IP_3R channel, and a relatively short cytoplasmic C-terminus (fig. 6) (Foskett J.K. et al., 2007).

Functionally, the N-terminal region can be divided into a proximal IP_3 binding domain and a more distal "regulatory" domain.

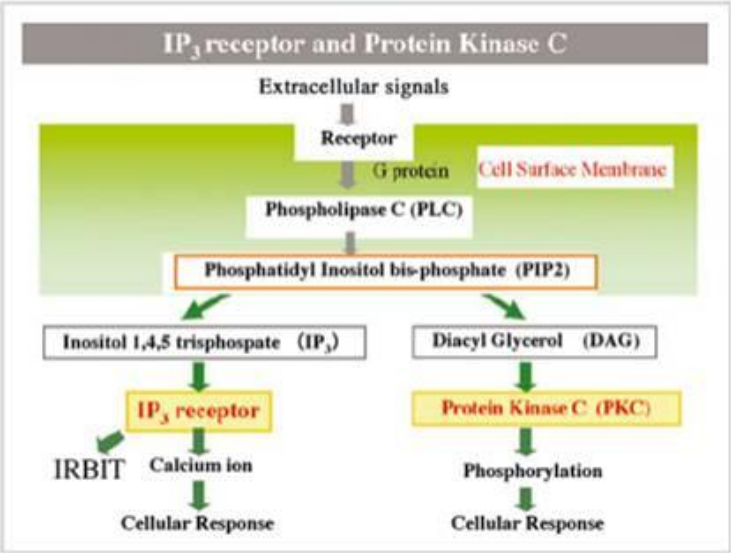

Fig.5: IP_3 receptor and protein kinase C (PKC) signaling cascade system. Both IP_3 and diacylglycerol (DAG) are produced from phosphatidyl inositol bis-phosphate, but both have completely different functions: IP_3 releases Ca^{2+} from internal store and DAG activates PKC for phosphorylation of various proteins.

The IP_3R channel is a tetramer of four IP_3R molecules (fig. 6). Approximately 2,000 amino acids separate the IP_3-binding domain from the pore. This intervening region between the IP_3 binding domain and the pore contains consensus sequences for phosphorylation and binding by nucleotides and various proteins. It may function to integrate, through allosteric coupling, other signaling pathways or metabolic states with the gating of the IP_3R.

The localization of the IP_3 binding region to the N-terminus of the IP_3R was first proposed by Mignery and co-workers based on the discovery that deletion of the first 410 residues of the protein completely eliminated IP_3 binding (Mignery G.A. et al., 1990).

Binding of IP_3 to the receptor is stechiometric (Supattapone S. et al., 1988) with an apparent Kd usually in the range of 10–80 nM.

IP_3 binding to the N-terminus of the channel induces conformational changes that are transduced to the activation gate that then enables ion flow through the channel. The molecular identity of the gate is unknown, and the mechanisms that couple ligand binding to opening and closing of the gate are unknown as well (Foskett K.J. et al., 2007).

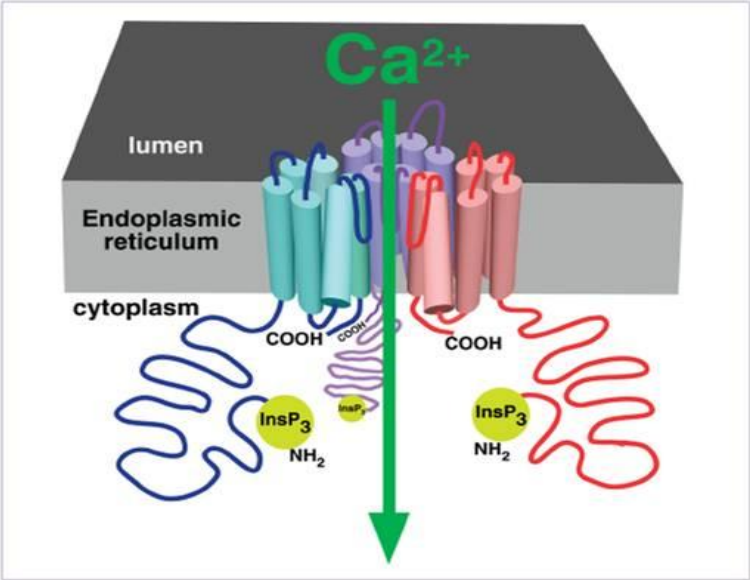

Fig.6: The IP_3R Ca^{2+} release channel. Cartoon depicting three of four IP_3R molecules (in different colors) in a single tetrameric channel structure (Foskett J.K. et al., 2007).

As to the structure of the pore, six transmembrane topology of the IP_3R was established by immunocytochemical techniques and N-linked glycosylation analyses of full-length and truncated proteins. These studies suggested that C-terminal transmembrane helices are involved in ion permeation, with helices 5 and 6 and intervening sequences in IP_3R critical for creating the basic pore structure (Michikawa T. et al., 1994) (fig. 6).

Deletion of the first four transmembrane helices from IP_3R, leaving transmembrane helices 5 and 6, resulted in a channel with normal conductance and selectivity properties (Ramos-Franco J. et al., 1999), consistent with this model. Site-directed mutagenesis of two residues between TM5 and 6, and believed to be located in the putative selectivity filter (Boehning D. et al., 2001), also suggested that such a model provides a rational basis for considering the roles of particular residues that contribute to conductance and selectivity properties of the IP_3R permeation pathway.

The IP_3R is, most fundamentally, a Ca^{2+}-activated ion channel. Ca^{2+} is instead a critical modulator of IP_3R channel function.

The steady-state gating activity of the IP_3-liganded channel is regulated by Ca^{2+} with a biphasic Ca^{2+} concentration dependence (Mak D.O.D. et al., 2001). Modest increases in $[Ca^{2+}]c$ potentiate the responses to IP_3, while more substantial increases inhibit them (Foskett J.K. et al., 2007).

The primary functional effect of IP_3 is to relieve Ca^{2+} inhibition of the channel, enabling Ca^{2+} activation sites to gate it (Mak D.O.D. et al., 1998). In essence, Ca^{2+} is the true channel ligand. Experimental results and insights that have emerged from patch-clamp studies of the IP_3R, together with molecular modeling, indicate that Ca^{2+} regulation of the channel is very complex, involving several distinct Ca^{2+} binding sites. Where are these Ca^{2+} binding sites in the IP_3R structure and sequence is not yet known (Foskett K.J. et al., 2007).

Moreover, the N-terminal regulatory domain contains consensus sequences for phosphorylation, proteolytic cleavage and binding by different protein modulators and ATP, integrating different cellular signaling pathways or metabolic states with the IP_3R functionality (Zampese E. and Pizzo P., 2011).

All these structure-function relationships have been thoroughly investigated, and several molecules - such as homer, protein phosphatases (PP1, PP2A), RACK1, chromogranin, Na^+/K^+-ATPase, carbonic anhydrase-related protein (CARP) and IRBIT - interact with the IP_3R and modulate its activity, suggesting that the receptor can form multi-molecular complexes, different from cell type to cell type, and function as a center for signaling cascades (Mikoshiba K., 2007).

The other major Ca^{2+}-releasing channel in the ER membranes is the RyR. RyRs, the largest known ion channels (Takeshima et al. 1989), are large conductance channels capable of creating rapid transient increases of cytosolic Ca^{2+}.

The channel is formed by homo-tetramers, reaching a molecular mass of ~2 MDa (each subunit is ~550 kDa). RyRs have a mushroom shape with 4-fold symmetry. Most of the mass of RyR forms a large cytoplasmic assembly that is connected to the transmembrane region by a stalk-like structure. The cytoplasmic region is strikingly empty with numerous distinctive structural domains and intervening cavities that appear suitable for interaction with modulators that bind within the N-terminal regions of RyR (Fig. 7). The clamp-shaped regions, located at the corners of the cytoplasmic assembly, are likely regions for the inter-digitation of neighboring RyRs seen *in situ* or for interaction with modulators. The clamp-shaped regions are interconnected to form a continuous network

between the central rim and the cytoplasmic stalk-like structure via several bridging densities (S.L. Hamilton and I.I. Serysheva, 2008).

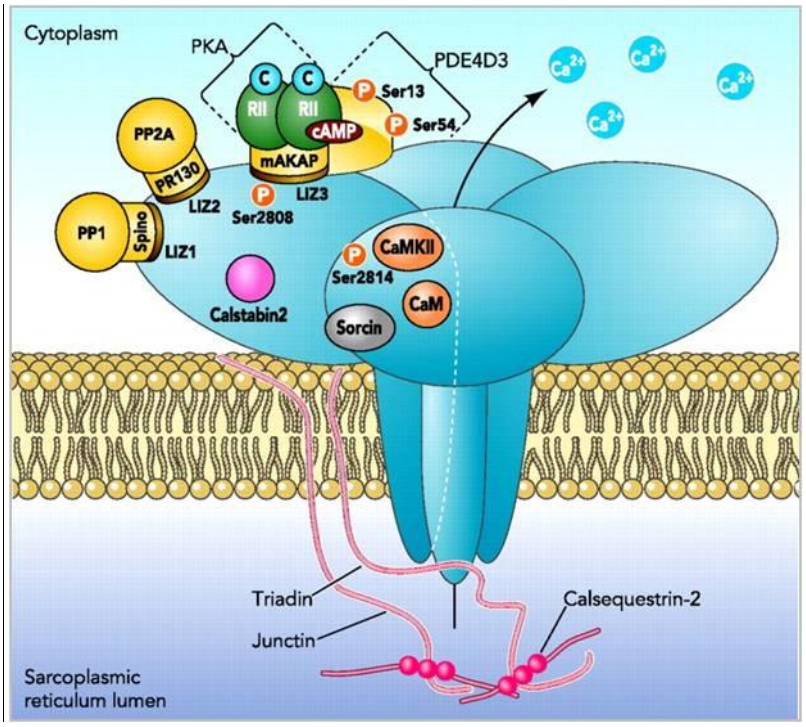

Fig.7: The RyR macromolecular signaling complex

The pore is thought to be composed of six to eight TM segments (Du G.G. et al., 2002).

While in skeletal muscle RyR1 opening is primarily (or exclusively) due to the electromechanical coupling with dihydropyridine receptor type voltage-dependent calcium channels (DHPR), the major gating mechanism of RyR2 and RyR3 is the Ca^{2+} induced Ca^{2+} release (CICR): in this case, the opening of RyRs is due to the local Ca^{2+} increase occurring in the proximity of plasma membrane Ca^{2+} channels, as initially demonstrated for cardiac muscle cells (Fill M. and Copello J.A., 2002); CICR can be also induced by Ca^{2+} release from neighboring ER channels, such as IP_3Rs or RyRs, in a regenerative wave.

1.1.2 The Golgi Apparatus (GA) as an intracellular Ca^{2+} store

The GA represents the central sorting and processing station along the secretory pathway, ensuring that cargo proteins, which are synthesized in the ER, are properly modified (e.g. glycosylated, processed and packaged

into carrier vesicles) and eventually directed to their final destination within the cell (P. Pizzo et al., 2011).

In high eukaryotes, the GA can be schematically viewed as being composed by three main compartments: *cis*-, medial- and *trans*-Golgi and consists of multiple flattened membranous cisternae arranged in close apposition to each other to form stacks. Stacks are indeed polarized, consisting of a *cis*-side associated with a tubular reticular network of membranes (*cis*-Golgi network, CGN), a medial area of disc-shaped flattened cisternae, and a *trans*-side associated with another tubular reticular membrane network (*trans*-Golgi network, TGN) (fig. 8) (P. Pizzo et al., 2011).

Traditionally, the GA was thought to be a stable, independent structure able to exchange components with other intracellular organelles, but it is actually a highly dynamic structure. Indeed, the steady-state structure of Golgi stacks depends on the balance of anterograde and retrograde transport through the different cisternae, between ER and the GA and between this latter and the other cellular compartments (P. Pizzo et al., 2011).

Functionally, the GA serves mainly as a cell 'factory' for the post-translational modification of proteins and lipids (primarily, but not only, glycosylation). Thus, the GA contains numerous glycosyl-transferases, glycosidases, sulphatases and pro-protein convertases (like furin) that cleave protein precursors into their mature forms (Schafer W. et al., 1995).

The polarized GA morphology parallels a specific functionality since the majority of GA glycosyl-transferases act sequentially and, in general, enzymes acting early in glycanbiosynthetic pathways are known to be localized in *cis*- and medial compartments of the GA, whereas enzymes acting later in the biosynthetic pathway tend to reside within the *trans*-Golgi cisternae and the TGN (Breton C. et al., 2001).

In the last two decades, numerous direct and indirect evidence supported the idea that the GA also plays a key role as intracellular Ca^{2+} store: (i) using ion microscopy, Chandra et al. showed that the GA can store up to 5% of the total cellular Ca^{2+} and that it is substantially more resistant to Ca^{2+} depletion than other cellular organelles (Chandra S. et al., 1991); (ii) using the electron energy loss spectroscopy technique in cryosections of

mammalian cells, it was reported a strong Ca^{2+} labelling extending across the entire *cis/trans* axis of the GA (Pezzati R. et al., 1991); (iii) processing enzymes located in the GA and/or TGN show a strong Ca^{2+} dependency of their activity (Oda K., 1992); (iv) finally, retrograde membrane traffic from the Golgi to the ER and selective aggregation of regulated secretory proteins in the TGN (Chanat E. and Huttner W.B., 1991) were also critically depended on GA Ca^{2+} content. Thus, the idea that variations of the $[Ca^{2+}]$ within the GA could affect cell functions in a variety of ways was generally accepted, though based on indirect approaches as no methodology were available to monitor directly the free Ca^{2+} concentration in the GA lumen of living cells.

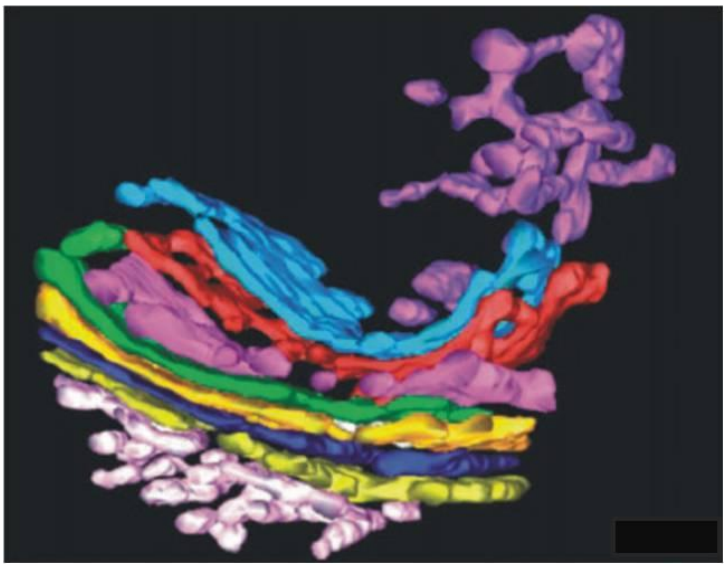

Fig. 8: Three-dimensional tomographic reconstruction of the Golgi complex. The cis-Golgi network (white) and the stack with the terminal three trans-Golgi cisternae (pink, red and cyan) are shown. The *trans*-Golgi network (violet) appears as a tubular network that emerges from the lateral part of the last *trans*-cisterna (cyan) (P. Pizzo et al., 2011)

The first direct demonstration that indeed the GA is a dynamic Ca^{2+} storing organelle capable of releasing Ca^{2+} into the cytosol upon cell activation came only when a new aequorin based Ca^{2+} probe specifically localized within the GA lumen was developed (Pinton P. et al., 1998). With this tool, obtained by adding to the aequorin sequence the first 69AA of the GA resident protein sialyl-transferase, it was shown that a high $[Ca^{2+}]$ is maintained in the GA lumen in steady state; Ca^{2+} uptake in the GA appeared to depend on the combined activity of a typical ER Ca^{2+} ATPase (SERCA) and of another Ca^{2+} pump, with distinct pharmacological

properties, the secretory pathway Ca^{2+} ATPase1, SPCA1. Furthermore, the Ca^{2+} content of the GA could be discharged rapidly and extensively following stimulation with an IP_3-generating agonist. Taken together these studies revealed that the GA could be regarded as a *bona fide* IP_3-sensitive, rapidly mobilizable, intracellular Ca^{2+} store and, for its specific perinuclear location within the cell, of potential strategic importance for the generation of local cytosolic Ca^{2+} signals.

Subsequently it has been suggested that Ca^{2+} handling within the GA is heterogeneous: in particular, it has been showed that the SPCA1-containing Ca^{2+} sub-compartment was insensitive (or mildly sensitive) to IP_3-generating agonist stimulation and therefore not involved in setting up cytosolic Ca^{2+} signals (Vanoevelen J. et al., 2004). Furthermore, the kinetics of Ca^{2+} release from the GA appeared to be somewhat different from those of the ER: in particular, while the latencies and initial rates of Ca^{2+} release were similar for the two organelles, Ca^{2+} release from the GA terminated faster than that from the ER (Missiaen L. et al., 2004). Altogether these data suggest that the GA could be heterogeneous in terms of Ca^{2+} handling properties, with distinct Ca^{2+} sub-compartments endowed with different molecular components.

As far as the molecular Ca^{2+} tool-kit is concerned, the GA contains several Ca^{2+} handling proteins known to be expressed in the ER. As mentioned above, SERCA2 pumps and IP_3Rs have been extensively demonstrated to be present and functional at the GA level (Pizzo P. et al., 2011). In addition to IP_3Rs also the other major intracellular Ca^{2+} releasing channel, the ryanodine receptor, RyR, has been shown to be expressed in the GA (Cifuentes F. et al., 2001).

As to the Ca^{2+} uptake mechanisms, data from different laboratories clearly indicate that, in addition to SERCA, another ATP-dependent Ca^{2+} pumping mechanism (not expressed at significant level within the ER) characterizes this cell compartment: the secretory-pathway Ca^{2+}-ATPases (SPCAs) (Pizzo P. et al., 2011). The relative contribution of each of the two types of Ca^{2+}-ATPases, SERCAs and SPCAs, to the total uptake of Ca^{2+} into the GA is apparently different in various cell types: in keratinocytes, for example, SPCA1 knock-down leads to a 67% of reduction in the average Golgi Ca^{2+} uptake (as measured with aequorin),

while in HeLa cells (using the same method) the effect of reducing SPCA1 level on the Golgi Ca^{2+} is modest (VanBaelen K. et al., 2003).

The secretory-pathway Ca^{2+}-ATPases (SPCAs) represent a recently recognized family of phosphorylation-type ATPases that supply the lumen of the Golgi apparatus with Ca^{2+} and Mn^{2+} needed for the normal functioning of this structure.

The knowledge of the SPCAs is much more limited than that of the well characterized SERCA (L. Missiaen et al., 2007).

SPCAs are single subunit integral membrane proteins with a large cytosolic head containing an actuator (A), nucleotide-binding (N), and phosphorylation (P) domain, and with 10 hydrophobic helices (M1–M10) displaying membrane-spanning propensity.

The SPCAs contain the typical SDKTGTLT sequence of phosphorylation-type ATPases with a highly conserved aspartyl residue that is transiently phosphorylated during the reaction cycle (L. Missiaen et al., 2007).

The transmembrane region of SPCA pumps only have one Ca^{2+}-binding site and indeed the Hill coefficients obtained from the Ca^{2+} dependence of ATP hydrolysis and phosphorylation of human SPCAs are close to 1, also suggesting that the pump transports only one Ca^{2+} or Mn^{2+} ion per each hydrolyzed ATP (Dode L. et al., 2006).

In human cells, two different genes encoding for SPCA have been cloned: ATP2C1 (on chromosome 3), that, by alternative processing at the 3'-end, results in 4 SPCA1 proteins with C-termini differing in length and specific amino acid sequence (Hu Z. et al., 2000), and ATP2C2 (on chromosome 16) encoding for a second human SPCA isoform, called SPCA2. As far as SPCAs distribution and localization is concerned, while SPCA1 is a housekeeping enzyme with a widespread expression in all cells and particularly high in human epidermal keratinocytes (Hu Z. et al., 2000), the tissue and cellular expression of SPCA2 appears to be more restricted (Vangheluwe P. et al., 2009), suggesting a more specialized function for this type of pump.

Similarly to the ER, the GA is also equipped with luminal Ca^{2+}-binding proteins. Notably, the Ca^{2+} binding proteins of the GA are not found (with one exception) in the ER lumen and, *viceversa*, the typical ER Ca^{2+} binding proteins are not found in the GA. The most abundant and better characterized of the GA Ca^{2+} binding proteins is CALNUC, an EF-hand,

Ca^{2+}-binding peripheral membrane protein tightly associated with the luminal surface of the *cis*-Golgi Network (CGN) and *cis*-Golgi cisternae (Lin P. et al., 1998).

The other two Ca^{2+}-binding proteins present in the GA lumen are p54/NEFA and calumenin. The first is a luminal protein strongly associated to GA membranes that shares significant sequence identity (62%) with CALNUC and, by immunofluorescence and immunoelectron microscopy, seems to be localized in the medial-Golgi cisternae (Morel-Huaux V.M. et al., 2002). The second one, calumenin, belongs to the family of multiple EF-hand proteins and shows a localization not confined to the Golgi, but also to the ER and throughout the secretory pathway (Yabe D. et al., 1997).

The GA is thus equipped with all the molecular components necessary for its function as a Ca^{2+} store: Ca^{2+} pumps, Ca^{2+} channels and luminal Ca^{2+}-binding proteins. The heterogeneity of these molecules, in part paralleled by their differential distribution within GA cisternae, suggests, however, that the GA Ca^{2+} store does not behave uniformly in terms of Ca^{2+} handling.

Recently, this problem has been directly addressed in our lab by the generation of a novel genetically encoded fluorescent Ca^{2+} indicator specifically targeted to the *trans*-Golgi lumen (Lissandron V. et al., 2010). This novel probe allowed the quantitative and dynamic measurement of luminal [Ca^{2+}] in this compartment at the single cell level and revealed that indeed the various GA compartments behave very differently in term of Ca^{2+} homeostasis.

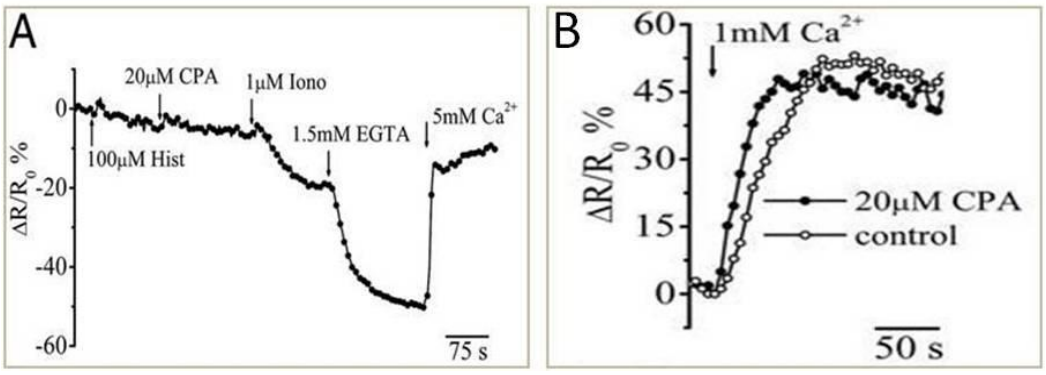

Fig.9: A representative transGo-D1cpv FRET changes in response to different stimuli (panel A) and a representative Ca^{2+} refilling kinetic of the trans-Go (panel B) in HeLa cells (V. Lissandron et al., 2010)

In particular, it has been demonstrated that the trans-Golgi takes up Ca^{2+} almost exclusively via SPCA1 (and not by SERCA) and does not release Ca^{2+} in response to IP_3 generation; rather the trans-Golgi accumulates the cation as a consequence of the cytoplasmic Ca^{2+} rises that follow this latter event (fig. 9).
Moreover, in cells endowed with high expression of RyRs (as neonatal primary cardiomyocytes), the *trans*-Golgi releases Ca^{2+} upon activation of these latter channels by caffeine or Ca^{2+} induced Ca^{2+} release, CICR (fig. 10).
From these finding, therefore, the *trans*-Golgi appears an intracellular Ca^{2+} store quite distinct from the ER and the other GA sub-compartments.

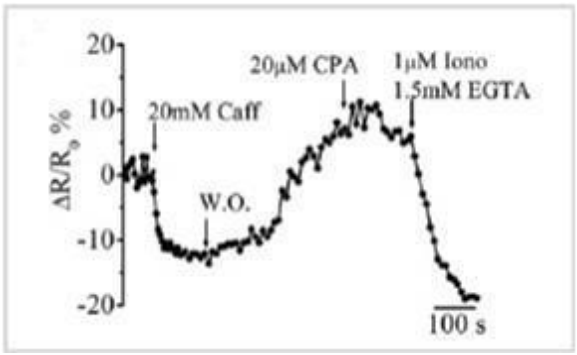

Fig.10: *trans*-Golgi Ca^{2+} response in cardiac myocytes upon ryanodine receptor stimulation (Lissandron V. et al., 2010).

In cells that do not express RyRs, the trans-Golgi behaves simply as a Ca^{2+} sink, taking up Ca^{2+} by SPCA1 when cytosolic Ca^{2+} is increased upon mobilization from the ER (and from other GA sub-compartments), while it represents a mobilizable Ca^{2+} store when the RyRs are functionally present, for example in cardiomyocytes (Lissandron V. et al., 2010).
The Ca^{2+} concentration within the *trans*-Golgi, calculated in HeLa cells is 130μM (Lissandron V. et al., 2010), a value somewhat lower than the average [Ca^{2+}] measured with aequorin (that is trapped in all the GA compartments) of the same cell type (i.e.2–300μM) (Pinton P. et al., 1998).
Overall, based on the Ca^{2+} values calculated for the various intracellular organelles, as obtained by several groups in different cell and by diverse probes, it appears that there is a decrease in the luminal Ca^{2+} concentration down the secretory pathway, ER (3–400μM) > overall GA (2–

300µM) > trans-Golgi(130µM) > secretory vesicles (80µM) (fig. 11) (Pizzo P. et al., 2011).

The complexity of the GA morphology, the *cis*-, medial- and *trans*-Golgi, and their specific enzymatic repertoire is paralleled by different mechanisms of the Ca^{2+} handling machinery in each compartment (in terms of Ca^{2+} pumps, channels and buffering proteins). The information on the *cis*- and medial-Golgi is still based on indirect data and one of the aim of my work has been to develop and set up specific targeted Ca^{2+} probes for these two sub-compartments, in order to characterized them in term of Ca^{2+} handling.

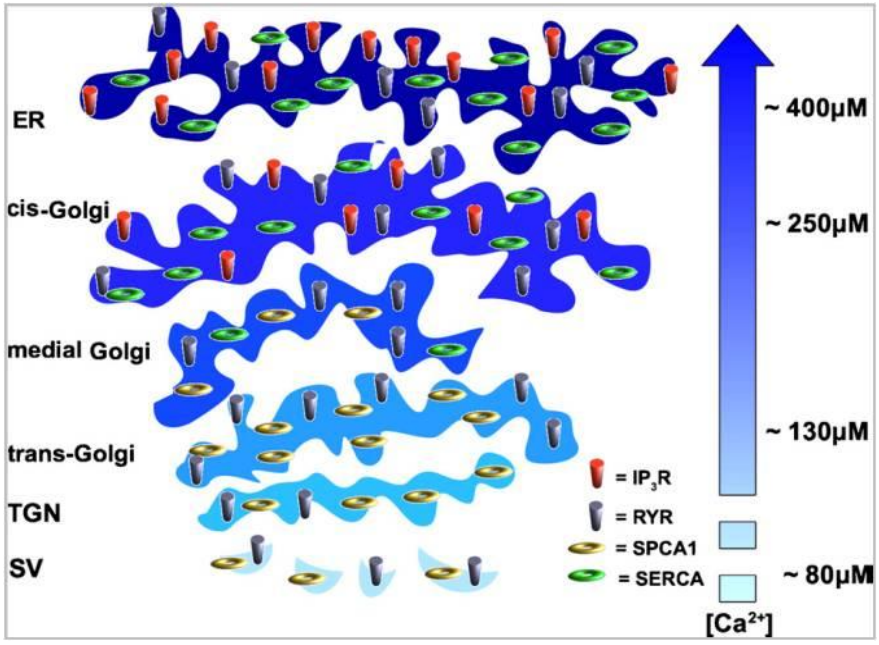

Fig. 11: Ca^{2+} concentration and molecular tool-kit gradient through the secretory pathway (P. Pizzo et al., 2011)

1.1.3. Peroxisomes, mithocondria and endolysosomal compartments in intracellular Ca^{2+} dynamics

1.1.3.1 Mithocondria

Mitochondria, the cellular organelles responsible primarily for energy generation, are also intracellular Ca^{2+} stores. Within the matrix of mitochondria, Ca^{2+} is stored not bound to Ca^{2+} buffering proteins but instead precipitated out as an insoluble salt, $CaPO_4$. The handling of Ca_{2+} by mitochondria is very complex , but one aspect worth highlighting is how

mitochondria communicate with the ER with respect to Ca^{2+} fluxes (Prins D. and Michalak M., 2011).
Release of Ca^{2+} from the ER results in elevated cytoplasmic Ca^{2+} levels, after which mitochondria take up Ca^{2+} resulting in elevated matrix Ca^{2+} levels (Rizzuto R. et al., 1992). ER and mitochondria are often tightly apposed in regions known as mitochondria-associated membranes (MAM); the interactions between these two organelles are regulated by cytoplasmic Ca^{2+} levels (Wang H.J., et al. 2000). Interestingly, resting cytoplasmic Ca^{2+} levels promote dissociation of the two organelles whereas higher Ca^{2+} levels enhance their association, suggesting that mitochondria may act as buffers to soak up Ca^{2+} released from the ER lumen (Wang et al., 2000).

1.1.3.2 Peroxisomes

Recent results indicate that peroxisomes are capable of taking up and storing Ca^{2+} within their lumen at concentrations much higher than those found in the cytoplasm (Raychaudhury B. et al. 2006; Drago I. et al. 2008). However, it is not yet known how Ca^{2+} is stored within these organelles and whether there exist specific peroxisomal Ca^{2+} buffering proteins (D. Prins and M. Michalak, 2011).

1.1.3.3 Endolysosomal compartments

Recent results show that nicotinic acid adenine dinucleotide phosphate (NAADP) acts as a second messenger to mobilize intracellular Ca^{2+} stores through actions on two-pore channels (TPCs) in endosomal membranes (Calcraft P.J. et al. 2009). Endosomes and lysosomes may thus be considered to be Ca^{2+} storage organelles; however, the mechanism of lysosomal Ca^{2+} buffering has not yet been described (D. Prins and M. Michalak, 2011).

1.2 Ca^{2+} entry from the extracellular space

1.2.1 Voltage-operated Ca^{2+} enty

Ca^{2+} channels in many different excitable cell types activate on membrane depolarization and mediate Ca^{2+} influx in response to action potentials and sub-threshold depolarizing signals.
Ca^{2+} entering the cell through voltage-gated Ca^{2+} channels serves as the second messenger of electrical signaling, initiating many different cellular events (fig. 12).

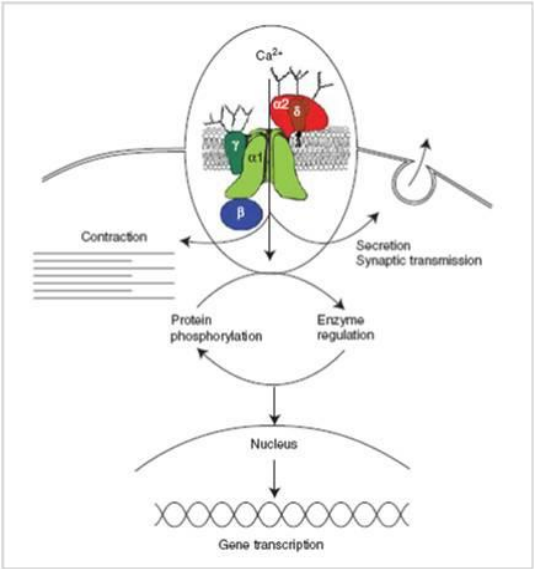

Fig.12: Signal transduction by voltage-gated Ca^{2+} channels.

In cardiac and smooth muscle cells, activation of Ca^{2+} channels initiates contraction directly by increasing cytosolic Ca^{2+} concentration and indirectly by activating calcium-dependent calcium release by ryanodine-sensitive Ca^{2+} release channels in the sarcoplasmic reticulum (W.A. Catterall, 2011). In skeletal muscle cells, voltage-gated Ca^{2+} channels in the transverse tubule membranes interact directly with ryanodine-sensitive Ca^{2+} release channels in the sarcoplasmic reticulum and activate them to initiate rapid contraction (Catterall W.A., 1991).
In endocrine cells, voltage-gated Ca^{2+} channels mediate Ca^{2+} entry that initiates secretion of hormones (Yang S.N. and Berggren P.O., 2006).
In neurons, voltage-gated Ca^{2+} channels initiate synaptic transmission.

In many different cell types, Ca^{2+} entering the cytosol via voltage-gated Ca^{2+} channels regulates enzyme activity, gene expression and other biochemical processes (W.A. Catterall, 2011).
Thus, voltage-gated Ca^{2+} channels are the key signal transducers of electrical excitability, converting the electrical signal of the action potential in the cell surface membrane to an intracellular Ca^{2+} transient. Signal transduction in different cell types involves different molecular subtypes of voltage-gated Ca^{2+} channels, which mediate voltage-gated Ca^{2+} currents with different physiological, pharmacological and regulatory properties (W.A. Catterall, 2011).
Since the first recordings of Ca^{2+} currents in cardiac myocytes, it has become apparent that there are multiple types of Ca^{2+} currents (table 1) as defined by physiological and pharmacological criteria (Tsien R.W. et al., 1988).
In cardiac, smooth, and skeletal muscle, the major Ca^{2+} currents are distinguished by high voltage of activation, large single channel conductance, slow voltage-dependent inactivation, marked up-regulation by cAMP-dependent protein phosphorylation pathways, and specific inhibition by Ca^{2+} antagonist drugs including dihydropyridines, phenylalkylamines and benzothiazepines.
These Ca^{2+} currents have been designated L-type, as they have slow voltage dependent inactivation and therefore are long lasting when Ba^{2+} is the current carrier and there is no Ca^{2+}-dependent inactivation (Tsien R.W. et al., 1988).
Electrophysiological studies of Ca^{2+} currents in starfish eggs (Hagiwara S. et al. 1975) first revealed Ca^{2+} currents with different properties from L-type, and these were subsequently characterized in detail in voltage-clamped dorsal root ganglion neurons (Carbone E. and Lux H.D., 1984). In comparison to L-type, these novel Ca^{2+} currents activated at much more negative membrane potentials, inactivated rapidly, deactivated slowly, had small single channel conductance and were insensitive to conventional Ca^{2+} antagonist drugs available at that time. They were designated low-voltage activated Ca^{2+} currents for their negative voltage dependence (Carbone E.and Lux H.D., 1984) or T-type Ca^{2+} currents for their transient openings (Nowycky M.C. et al. 1985).

Ca^{2+} current type	α1 Subunits	Specific blocker	Principal physiological functions	Inherited diseases
L	$Ca_v1.1$	DHPs	Excitation-contraction coupling in skeletal muscle, regulation of transcription	Hypokalemic periodic paralysis
	$Ca_v1.2$	DHPs	Excitation-contraction coupling in cardiac and smooth muscle, endocrine secretion, neuronal Ca^{2+} transients in cell bodies and dendrites, regulation of enzyme activity, regulation of transcription	Timothy syndrome: cardiac arrhythmia with developmental abnormalites and autism spectrum disorders
	$Ca_v1.3$	DHPs	Endocrine secretion, cardiac pacemaking, neuronal Ca^{2+} transients in cell bodies and dendrites, auditory transduction	
	$Ca_v1.4$	DHPs	Visual transduction	Stationary night blindness
N	$Ca_v2.1$	ω-CTx-GVIA	Neurotransmitter release, Dendritic Ca^{2+} transients	
P/Q	$Ca_v2.2$	ω-Agatoxin	Neurotransmitter release, Dendritic Ca^{2+} transients	Familial hemiplegic migraine, cerebellar ataxia
R	$Ca_v2.3$	SNX-482	Neurotransmitter release, Dendritic Ca^{2+} transients	
T	$Ca_v3.1$	None	Pacemaking and repetitive firing	
	$Ca_v3.2$		Pacemaking and repetitive firing	Absence seizures
	$Ca_v3.3$			

Abbreviations: DHP, dihydropyridine; ω-CTx-GVIA, ω-conotoxin GVIA from the cone snail *Conus geographus*; SNX-482, a synthetic version of a peptide toxin from the tarantula *Hysterocrates gigas*.

Table 1: Subunit composition and function of Ca^{2+} channel types

Whole-cell voltage clamp and single channel recording from dissociated dorsal root ganglion neurons revealed an additional Ca^{2+} current, N-type. N-type Ca^{2+} currents were initially distinguished by their intermediate voltage dependence and rate of inactivation - more negative and faster than L-type but more positive and slower than T-type (Nowycky M.C. et al. 1985). They are insensitive to organic L-type Ca^{2+} channel blockers but blocked by the cone snail peptide v-conotoxin GVIA and related peptide toxins (Tsien R.W., 1988).

This pharmacological profile has become the primary method to distinguish N-type Ca^{2+} currents, because the voltage dependence and kinetics of N-type Ca^{2+} currents in different neurons vary considerably.

Analysis of the effects of other peptide toxins revealed three additional Ca^{2+} current types (Table 1). P-type Ca^{2+} currents, first recorded in Purkinje neurons (Llina´s R. and Yarom Y., 1981), are distinguished by high sensitivity to the spider toxin v-agatoxin IVA (Mintz I.M. et al. 1992). Q-type Ca^{2+} currents, first recorded in cerebellar granule neurons are blocked by v-agatoxin IVA with lower affinity. R-type Ca^{2+} currents in cerebellar granule neurons are resistant to most subtype-specific organic and peptide Ca^{2+} channel blockers and may include multiple channel subtypes (Randall A. and Tsien R.W., 1995).

Although L-type and T-type Ca^{2+} currents are recorded in a wide range of cell types, N-, P-, Q-, and R-type Ca^{2+} currents are most prominent in neurons (Catterall W.A., 2011).

Ca^{2+} channels purified from skeletal muscle transverse tubules are complexes of α_1, α_2, β, γ, and δ subunits (fig. 12).
Analysis of the biochemical properties, glycosylation, and hydrophobicity of these five subunits led to a model comprising a principal transmembrane $\alpha 1$ subunit of 190 kDa in association with a disulfide-linked $\alpha 2\delta$ dimer of 170 kDa, an intracellular phosphorylated β subunit of 55 kDa, and a transmembrane γ subunit of 33 kDa (fig. 12) (Takahashi M. et al. 1997).
Intensive studies of the structure and function of the related pore-forming subunits of Na^+, Ca^{2+}, and K^+ channels have led to identification of their principal functional domains (Catterall W.A., 2011). Each domain of the principal subunits consists of six transmembrane α helices (S1–S6) and a membrane-associated loop between S5 and S6 (Fig. 12). The S4 segments of each homologous domain serve as the voltage sensors for activation, moving outward and rotating under the influence of the electric field and initiating a conformational change that opens the pore.

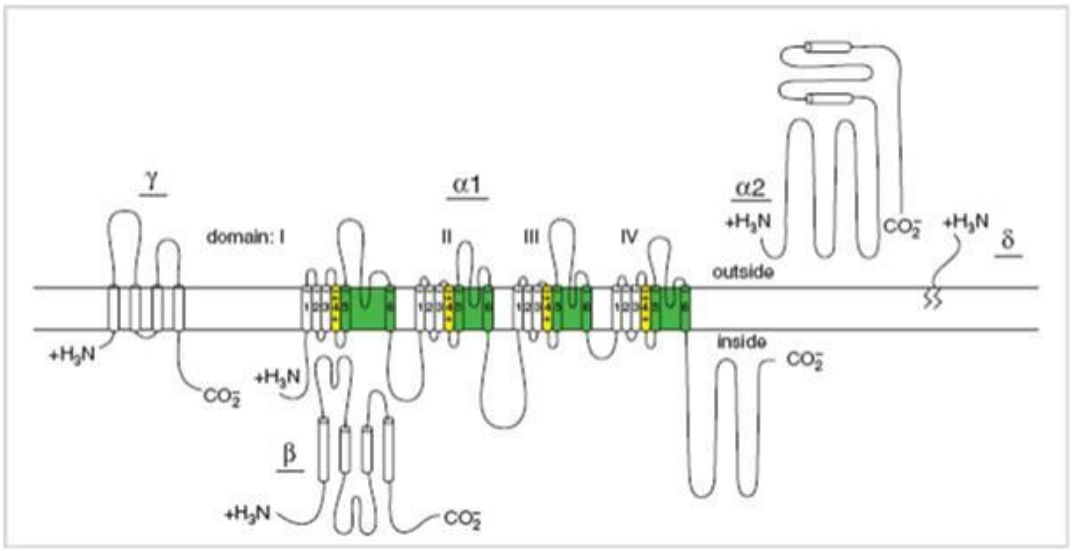

Fig. 13: Subunit structure of Ca^{2+} channels

The S5 and S6 segments and the membrane-associated pore loop between them form the pore lining of the voltage-gated ion channels. The narrow external end of the pore is lined by the pore loop, which contains a pair of glutamate residues in each domain that are required for Ca^{2+} selectivity, a structural feature that is unique to Ca^{2+} channels (Heinemann S.H. et al., 1992).

1.2.2 Store operated Ca^{2+} entry

Depletion of intracellular Ca^{2+} stores, via activation of G-protein-coupled receptors associated to the IP_3 cascade or by the blockade of SERCA, results in the activation of Ca^{2+} influx via the so-called store-operated channels (SOCs) (Vaca L., 2010). Replenishing the Ca^{2+} stores shuts down SOC and resets the system.

It has long been thought that the main function of store-operated Ca^{2+} entry was the replenishment of intracellular Ca^{2+} stores following their discharge during intracellular Ca^{2+} signaling.

Recent results, however, suggest that the primary function of these channels may be to provide direct Ca^{2+} signals to recipients localized to spatially restricted areas close to the sites of Ca^{2+} entry in order to initiate specific signaling pathways (Putney J.W., 2011).

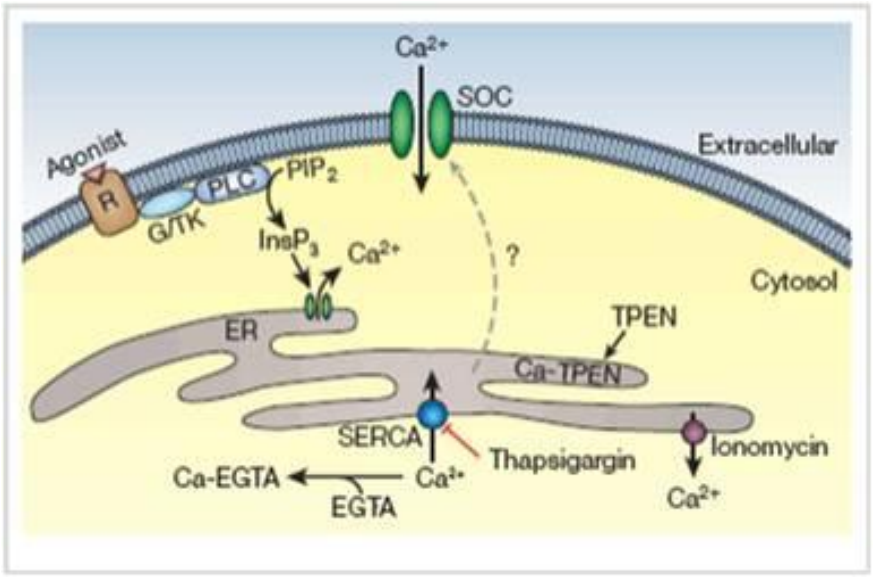

Fig. 14: Physiological pathway of SOC activation

It was just on 2005 that the modern era of research on store-operated calcium channels began with the first unequivocal discovery of a key molecular component of the pathway, the ER Ca^{2+} sensor (Putney J.W., 2011).

The key breakthroughs came from RNAi screening, which first identified STIM1 proteins as the molecular link from ER Ca^{2+} store depletion to SOC entry and Ca^{2+} release-activated Ca^{2+} (CRAC) channel activation in the

plasma membrane, and then identified Orai (CRACM) proteins that comprise the CRAC channel pore-forming subunit (Cahalan M.D., 2009).
STIM1, initially characterised as a phosphoprotein, includes a single transmembrane domain located in the ER in resting cells (fig. 15). The N-terminus of STIM1 stretches into the ER lumen, while the C-terminus extends into the cytosol. Within the former, a single EF-hand Ca^{2+}-binding motif acts as luminal Ca^{2+} sensor. A sterile-alpha motif (SAM), including two N-linked glycosylation sites, is followed by the transmembrane domain and a cytosolic C-terminus with two coiled-coil regions overlapping with an ezrin-radixin-moesin (ERM)-like domain. Subsequent glutamate-, serine/proline-, serine/threonine- and lysine-rich regions are additionally located at the C-terminus (fig. 15) (Liou J. et al., 2005).

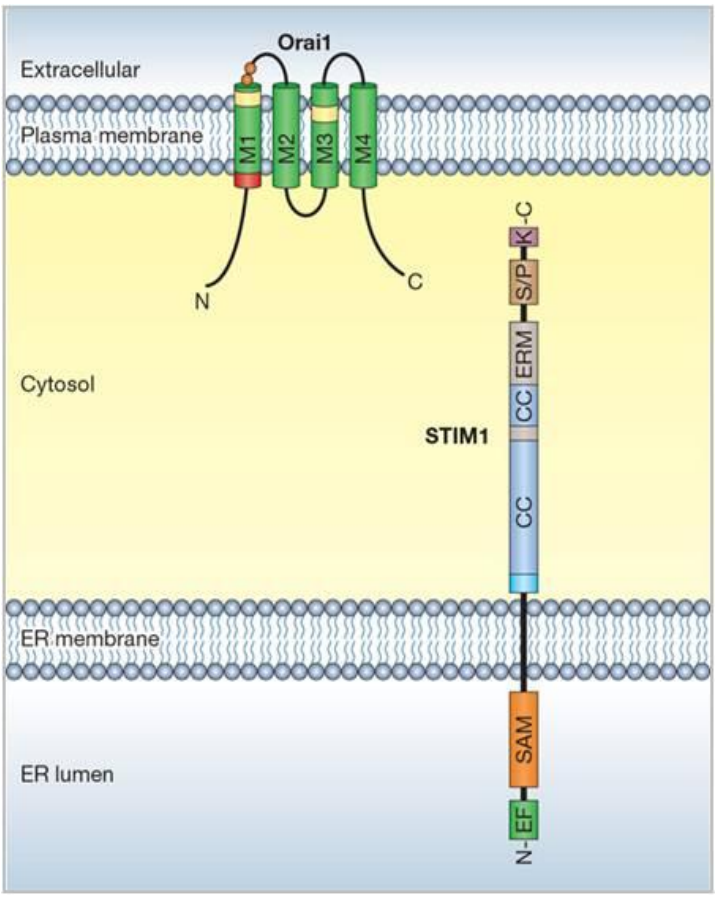

Fig. 15: STIM1 is localized primarily in the ER membrane and Orai1 is a plasma membrane protein with four membrane-spanning regions and intracellular N and C termini.

Orai1 contains four predicted transmembrane segments (fig. 15), form Ca^{2+} selective plasma membrane channels. Within the cytosolic strands,

the N-terminus of only Orai1 includes a proline/arginine-rich region. In their C-terminus Orai1 contains a putative coiled-coil domain. The extracellular loop of Orai1 between the third and fourth transmembrane segment comprises an N-glycosylation site (Cahalan M.D. et al., 2005).
STIM1 mediated robust Orai1 currents are initially stimulated by Ca^{2+} store-depletion sensed by the STIM1 luminal EF-hand (fig. 16).
In resting cells, STIM1 is uniformly distributed within the ER, displays tubular structures and binds to the microtubule-plus-end-tracking protein EB1 at those sites where microtubule ends come in contact with the ER (fig. 16) (Grigoriev I. et al, 2008).

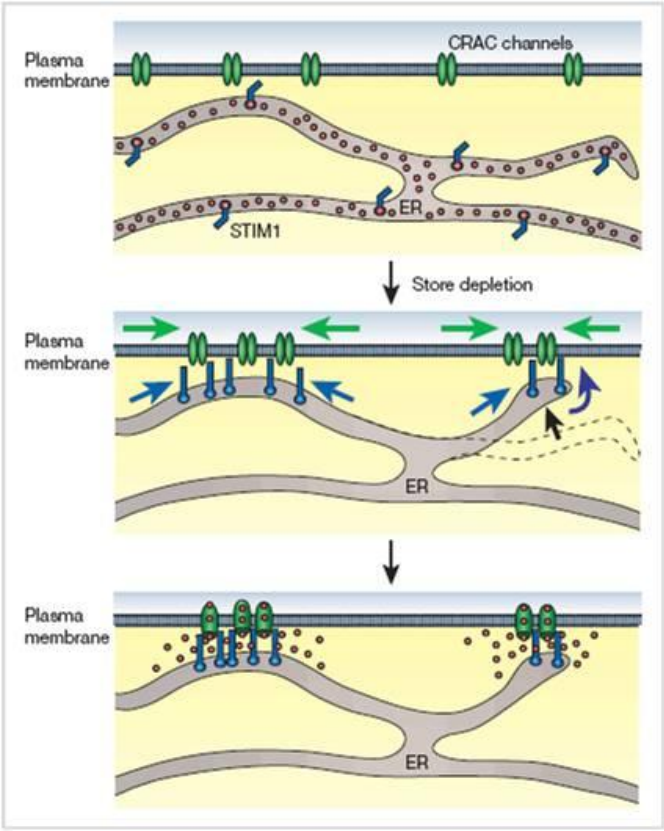

Fig. 16: The functional units of store-operated Ca^{2+} entry assemble in response to store depletion.

The STIM1 EF-hand is adequate to sense a decrease in the ER Ca^{2+} level that is approximately 300–500 μM at rest.
Subsequently, STIM1 forms oligomers before it redistributes into punctuate clusters close to the plasma-membrane (fig. 16) (Liou J. et al., 2005). It has recently been shown that oligomerisation of about four STIM1 proteins is the critical process transmitting ER store depletion to STIM1/Orai1 clusters thereby activating store-operated Ca^{2+} entry (fig.

16). In particular, four Orai1 molecules create the pore-forming subunit of CRAC that opens upon stimulation by STIM1, with the C-terminus of STIM1 and N-terminus of Orai1 participating in this process (fig. 16) (R.S. Lewis, 2007)

2. GENETICALLY ENCODED Ca^{2+} INDICATORS

Ca^{2+} is one of the most important and versatile second messengers in cell biology; consequently, there has been enormous effort devoted to developing tools to image Ca^{2+} in living cells.

Fluorescent indicators for Ca^{2+} allow the researcher to monitor Ca^{2+} signals in living cells and in real time, thus preserving temporal control of Ca^{2+} signaling.

Genetically encoded Ca^{2+} indicators (GECIs) are a subset of fluorescent indicators that offer the additional advantage of being able to monitor Ca^{2+} dynamics in specific sub-cellular locations, thereby maintaining spatial heterogeneity of Ca^{2+} transients (McCombs J.E. and Palmer A.E., 2008).

GECIs are defined as indicators that are produced by translation of a nucleic acid sequence. Therefore, these indicators are comprised solely of natural protein or peptide motifs. In order to convert a Ca^{2+} signal into an optical readout, GECIs consist of at least one light-emitting protein and a Ca^{2+} responsive element, such that Ca^{2+} binding changes the optical properties of the protein(s). These protein-based indicators are typically incorporated into cells by gene transfer techniques (McCombs J.E. and Palmer A.E., 2008).

There are three classes of GECIs that have been developed which differ in their overall architecture (fig. 17). The first class are bioluminescent reporters based on the aequorin photoprotein (Rizzuto R. et al., 1994). These probes are inherently different than the fluorescent protein-based probes as light is generated by a chemical reaction that requires reconstitution of the indicator with a co-factor.

The second class is based on single fluorescent proteins. These indicators are composed of Ca^{2+}-responsive elements, such as calmodulin (CaM) or portions there of that are inserted into a fluorescent protein, such that Ca^{2+} binding alters the protonation state, and hence spectral properties of the chromophore. These indicators include the camgaroos, G-CaMPs, pericams, "Case" sensors and grafted EF-hands (McCombs J.E. and Palmer A.E., 2008).

The last class of sensors are the "cameleon-type" in which Ca^{2+}-responsive elements are inserted between two fluorescent proteins so

that upon Ca^{2+} binding, an alteration in the efficiency of fluorescence resonance energy transfer (FRET) occurs (Miyawaki A. et al., 1997).

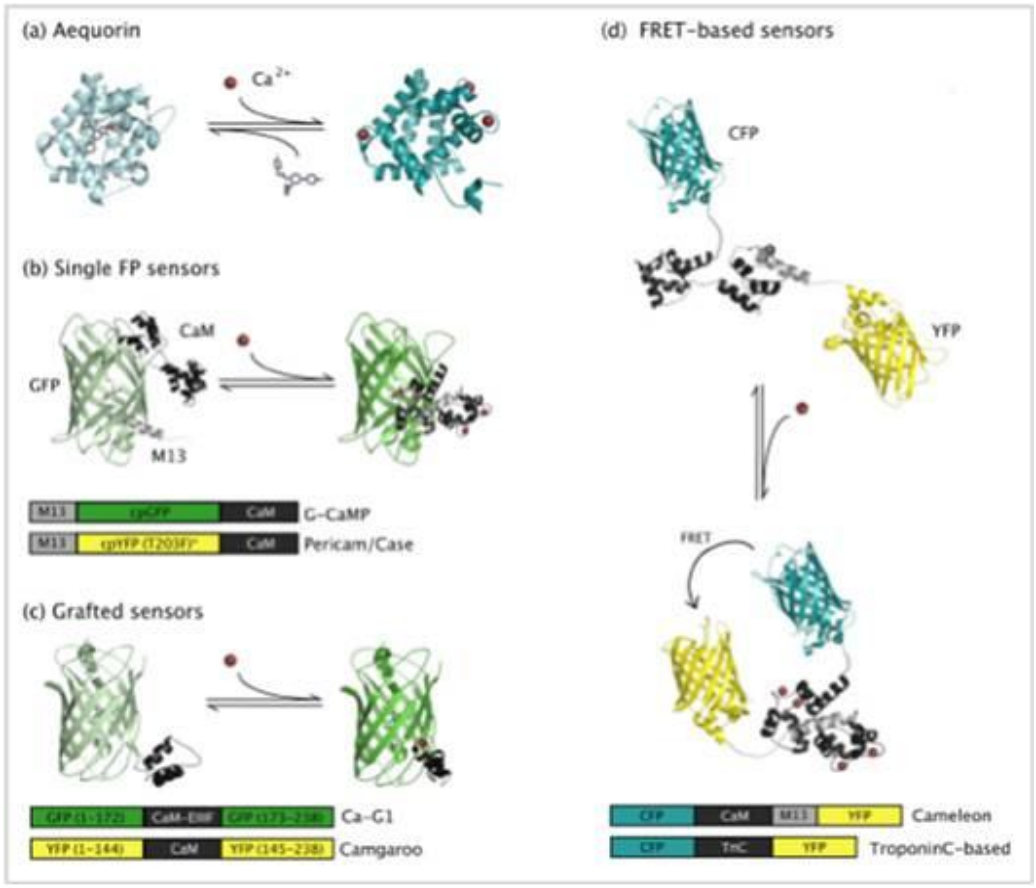

Fig. 17: Models of the three classes of GECIs. (a) The aequorin photoprotein is shown in complex with coelenterazine. Upon binding of Ca^{2+}, the aequorin undergoes a conformational change, releasing coelenteramide and emitting blue light. (b) Single FP sensors employing the Ca^{2+}-responsive element CaM and a CaM binding peptide attached to a circularly permutated FP. On binding Ca^{2+} , CaM executes a conformational change, interacting with the peptide and altering the protonation state of the chromophore thus changing the fluorescence intensity of the protein. (c) Grafted sensors utilizing EF hands or portions of CaM inserted into a fluorescent protein. Binding of Ca^{2+} causes a change in protein conformation and a shift in the protonation state of the chromophore. (d) FRET-based sensors having a Ca^{2+} binding domain located between two flurophorescent proteins. As Ca^{2+} binds, the Ca^{2+} binding domain undergoes a conformational change, interacting with its binding peptide. This brings the two FPs closer together, increasing the efficiency of FRET.

2.1 FRET-based cameleon probes

Cameleons (fig. 17) are tandem repeats of GFP mutants with overlapping excitation/emission spectra linked together by a Ca^{2+} sensor based on Calmodulin (CaM), a glycylglycine linker and the CaM binding peptide of myosin light chain kinase M13 (Miyawaki A. et al., 1997). In this design,

Ca^{2+} binding promotes the reversible association of CaM and M13, promoting fluorescence resonance energy transfer (FRET) between the two GFP variants (Demaurex N., 2005).

The first probes generated, yellow cameleons (YC), used cyan and yellow fluorescent proteins (CFP and YFP) as FRET donor and acceptors. The reversible changes in FRET can be detected as changes in the yellow over cyan emission fluorescence and the probes function as ratiometric emission Ca^{2+} indicators. The original YC comprised probes of different affinities, ranging from 1 to 300μM (YC2, YC3 and YC4), but all probes suffered from a poor dynamic range and were sensitive to pH and to chloride ions. YC were subsequently made pH resistant by YFP mutagenesis (YC2.1 and YC3.1) and brighter by replacing YFP with citrine (YC3.3) or with Venus, a YFP mutant with fast and efficient maturation (YC2.12 and VC6.1). Although these cameleons were greatly improved over the original design, they still displayed insufficient signal-to-noise ratio when targeted to organelles (Demaurex N., 2005).

To further increase the dynamic range of cameleons, Nagai et al. generated several circularly permuted YFP mutants in an attempt to optimize the relative orientation of the two FRET partners (Nagai T. et al., 2004). By introducing new termini into the surface exposed loop regions of the β-barrel of Venus, they generated several YC variants with improved dynamics. The best construct, YC 3.6, which contains a YFP circularly permutated at position 173 (173cpVenus), matures efficiently, is resistant to acidification, and displays a monophasic Ca^{2+} sensitivity with a Kd of 250 nM. The cp173Venus cameleon has much better dynamics than all previous cameleons when expressed in cells, with an impressive 5.6-fold increase in ratio between Rmin and Rmax. The expanded dynamic range of YC3.6 is a clear advantage to image Ca^{2+} dynamics in cells and tissues with adequate spatiotemporal resolution.

Moreover A.E. Palmer et al. generated a series of indicators that resist endogenous CaM and have varying Ca^{2+} affinities to be useful in monitoring Ca^{2+} in distinct sub-cellular locations as well as in micro-domains of high Ca^{2+} (Palmer A.E. et al., 2006). Their goal in redesigning the cameleon was to reengineer the binding interface between CaM and a target peptide to generate selective and specific binding pairs that could not be perturbed by wild-type (wt) CaM. They previously reversed the

salt bridge interactions between basic residues in the target peptide and acidic residues in CaM to generate a mutant calmodulin-peptide pair that was unaffected by large concentrations of excess CaM. This redesigned pair led to a Ca^{2+} indicator (D1) with a relatively weak affinity for Ca^{2+} (K_d = 60 μM) and has been used to monitor Ca^{2+} directly in the ER in individual living cells (Palmer A.E. et al., 2004).
Subsequently, they computationally designed steric bumps in the target peptide and complementary holes in CaM in order to generate a series of indicators (D2, D3, and D4) with varying Ca^{2+} affinities (fig. 18), including a high-affinity indicator that cannot be perturbed by excess CaM. These indicators show significant improvements in the ability to monitor Ca^{2+} in different sub-cellular locations such as the plasma membrane of neurons and the mitochondria (Palmet A.E. et al., 2006).

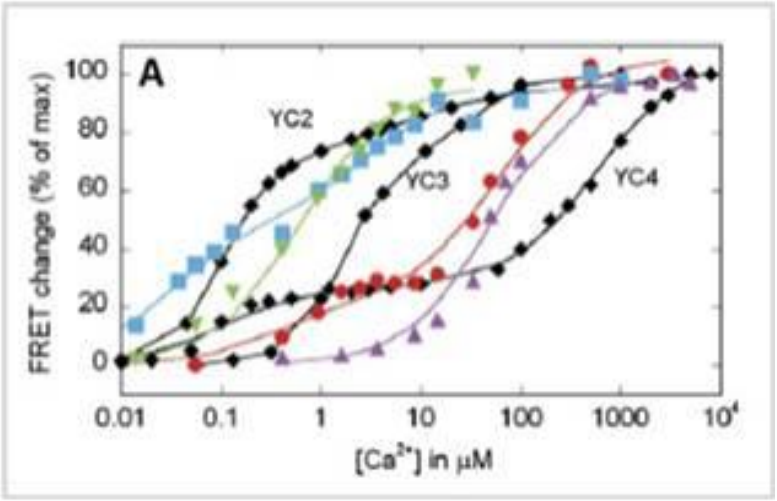

Fig. 18: *In Vitro* Characterization of the Redesigned Cameleons Ca^{2+} titration curves of original and redesigned cameleons. The original cameleons (YC2, YC3, and YC4; black diamonds) are labeled on the graph. The first redesign, D1, is presented as red circles, and the computational designs are presented as follows: D2cpv, blue squares; D3cpv, green, upside-down triangles; D4cpv, purple triangles.

To date, cameleons have been expressed in the cytosol (D1cpv probe) (Leite M.F. et al., 2003), targeted to the ER (ER-D1 probe) and the nucleoplasm (H2BD1cpv probe) (Leite M.F. et al., 2003), to the mitochondria (4mt-D1cpv probe) (Giacomello M., et al., 2010), to the trans-Golgi (Go-D1cpv probe) (V. Lissandron et al., 2010), to the peroxisomal matrix (KVK-SKL-D3cpv probe) (Drago I., et al., 2008).
All these probes have been successfully used to monitor Ca^{2+} dynamics in their specific sub-cellular compartments.

3. ALZHEIMER'S DISEASE

Alzheimer's disease (AD) was first described little more than 100 years ago. It is the most common cause of dementia with an estimated prevalence of 30 million people worldwide, a number that is expected to quadruple in 40 years.
In the 105 years since Alzheimer's original case report and particularly in the past 3 decades, much has been learned about AD. However, there currently is no effective treatment that delays the onset or slows the progression of the disease (Holtzman D.M. et al., 2011).

3.1 Clinical and pathological features of AD

Dementia is an acquired syndrome characterized by a loss or decline in memory and other cognitive abilities. It represents a decline from a person's previously established level of intellectual function that is sufficient to interfere with the everyday performance of that individual. AD is the most common cause of dementia, estimated to contribute to about 60–70% of cases (Barker W.W. et al., 2002).
The essential feature of AD, intra-individual decline in cognitive abilities, has an insidious onset over several months with subsequent gradual but relentless progression though successive stages of dementia severity. The time course of AD dementia averages 7–10 years and inevitably the illness culminates in death. Impaired recent memory usually is an initial symptom of AD but other cognitive deficits, such as executive dysfunction manifested by changes in attention and problem solving abilities, are typically also present. As dementia progresses, language dysfunction, visuospatial difficulty, loss of insight, and personality changes (withdrawal, decreased initiative, occasionally depression) frequently are apparent. There also is impaired ability to function at routine tasks at home, such that even basic activities of daily living (e.g., dressing, bathing, grooming) require supervision or assistance. In the severe stage of Alzheimer dementia, individuals are totally dependent on caregivers for all activities of daily living and, in advanced disease, often become mute, non-ambulatory and unable to swallow or control bladder and bowel function (Holtzman D.M. et al., 2011).

The key neuropathological elements of AD were described by Alois Alzheimer in 1906 and at about the same time by Oskar Fischer (Goedert M., 2009). At the macroscopic level, there is gross atrophy of the brain (Figure 19).

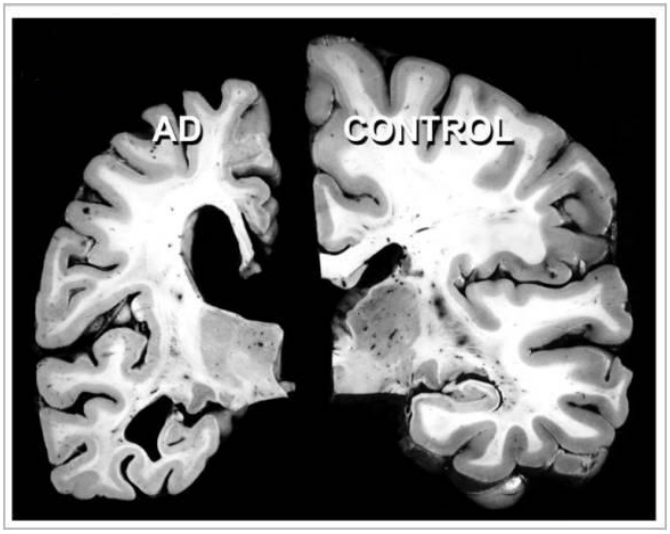

Fig. 19: Postmortem brain section from an AD case (left) compared with that of a cognitively normal individual (right)

At the microscopic level, the hallmarks of the disease are amyloid plaques, neurofibrillary tangles (fig. 20) and extensive neuronal loss.
Amyloid plaques are accumulations of molecules in the extracellular space of the brain (fig. 20). The principal proteinaceous component of plaques is the amyloid-β (Aβ) peptide, a 38–43 amino acid peptide derived from a much larger protein, the amyloid precursor protein (APP). Within plaques, Aβ is present in aggregated (insoluble) forms including fibrils as well as oligomers (Kayed R. et al., 2003).

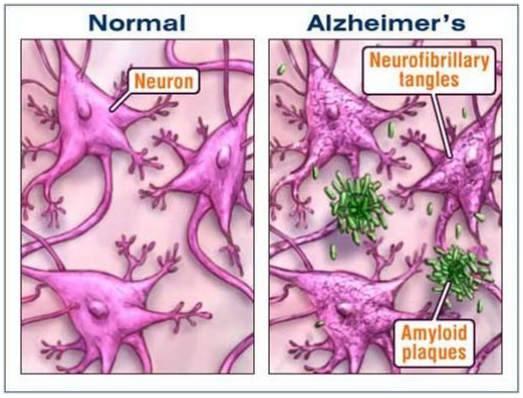

Fig. 20: The neurofibrillary tangles and tha amyloid plaques depositions in AD brain

These "neuritic" plaques are surrounded by swollen, degenerating neurites (axons and dendrites). In areas surrounding neuritic plaques, there is also "gliosis" with hypertrophy and an alteration of the morphology as well as the proliferation of astrocytes and microglia (immune cells of the CNS). It is likely that this inflammatory response contributes to brain injury although there is evidence that glial cells also play a protective role (Lucin K.M. and Wyss-Coray T., 2009) (fig. 21).

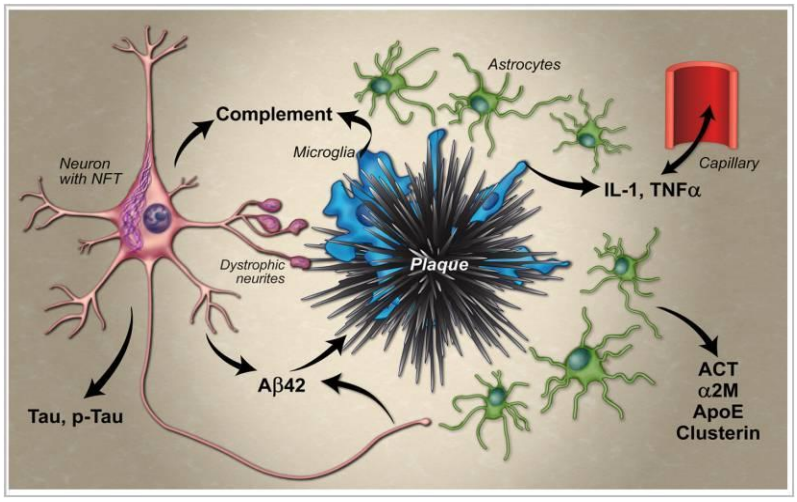

Fig. 21: Diagram illustrating aspects of the neuropathology of AD.

In addition to the deposition of Aβ in plaques in AD, nerve cell bodies as well as their processes in specific brain regions develop neurofibrillary tangles (NFTs) (fig. 20), neuropil threads and neuritic dystrophy (Braak H., and Braak E., 1997). NFTs (present in neuronal cell bodies) and neuropil threads (present in neuronal processes) are intracellular structures composed predominantly of a hyperphosphorylated, aggregated form of the microtubule binding protein, tau. Tau is synthesized and produced in all neurons and is also present in glia. The normal function of tau is to bind to tubulin and stabilize microtubules. However, in AD, tau becomes hyperphosphorylated and this form of tau disassociates from microtubules and has a tendency to self-aggregate forming NFTs in cell bodies and dystrophic neurites.

Data strongly suggest that neurofibrillary pathology contributes to neuronal dysfunction and correlates with the clinical progression of AD (Holtzman D.M., 2011).

Clinically, most cases of symptomatic AD begin after age 65 years with incidence increasing with age. These cases are often referred to as

"sporadic" or "late-onset" AD (LOAD). This form of AD accounts for >99% of all cases. In addition to LOAD, a very small percentage (<1%) of AD occurs within families and is inherited in an autosomal dominant fashion and are termed Familial AD (FAD). In these families, dementia onset is usually between the ages of 30–60 years. APP was identified as the first gene in which mutations in the coding sequence cause FAD (Levy E. et al., 1990). These mutations within the APP gene provided an important clue regarding the likely mechanism leading to increased Aβ accumulation in FAD brains.

In addition to APP, mutations in 2 other genes have been identified in which specific mutations result in the rare, autosomal dominant forms of FAD: presenilin-1 (PSEN1) (Levy-Lahad E. et al., 1995) and presenilin-2 (PSEN2) (Sherrington R. et al., 1990). These genes encode highly homologous transmembrane proteins in which multiple mutations have been identified in FAD families. Mutations in PSEN1 are the most common identified cause of FAD.

A molecular connection between presenilins and Aβ production was uncovered in the late 1990s. A normal function of presenilins is to form a γ-secretase complex with 3 other proteins, APH-1, PEN2, and nicastrin (Takasugi N. et al., 2003). The γ-secretase complex directly cleaves the transmembrane protein Notch, APP and other substrates, and its activity is required for Aβ formation (Holtzman M.D., 2011).

Thus, AD is thought to be a disorder of protein aggregation in which the aggregation and accumulation in the brain of Aβ and tau are key players in AD pathophysiology. However, there are many additional cellular pathways, processes and molecules involved in AD pathogenesis that have emerged and will continue to be discovered, that play important roles in the disease (Holtzman D.M., 2011).

3.2. The molecular pathogenesis of AD

The pathogenesis of AD is complex and involves many molecular, cellular and physiological phenomenon, firstly the accumulation of β amyloid and the hyperphosphorilation of tau. Although for many years 'Aβ-centric' hypotheses dominated AD research (Pritchard S.M. et al., 2011), the importance of tau in the pathogenesis of AD is now much more

appreciated (Small S.A. and Duff K., 2008) and seems to increase as new findings emerge. In addition, the calcium hypothesis support the proposal of an early, central role of calcium dysregulation in the pathogenesis of AD.

3.2.1 The amyloid hypothesis

The amyloid plaques associated with AD were first purified and found to consist of multimeric aggregates of Aβ polypeptide containing about 40 amino acid residues in the mid-1980s (Glenner G.G. and Wong C.W., 1984). Cloning of the complementary DNA (cDNA) of Aβ revealed that Aβ is derived from a larger precursor protein (Tanzi R.E. et al. 1987). The full-length cDNA of the amyloid precursor protein (APP) was later isolated and sequenced and APP was predicted to be a glycosylated integral membrane cell surface receptor protein with 695 amino acids (Kang J. et al., 1987).
The Aβ peptide was found to be a cleavage product derived from the transmembrane domain of this large precursor protein, the APP.
The APP protein is a type I integral membrane protein with a large extracellular portion, a hydrophobic transmembrane domain, and a short C-terminus designated the APP intracellular domain (AICD).
APP undergoes post-translational processing, involving several different secretases and proteases, via two major pathways. In the non-amyloidogenic pathway, APP is sequentially cleaved by α-secretase and γ-secretase. α-cleavage, which cuts APP at the 17th amino acid inside the Aβ peptide sequence (fig. 22), releases a large secreted extracellular domain (sAPP-α) and a membrane-associated C-terminal fragment consisting of 83 amino acids (C83). APP C83 is further cleaved by γ-secretase to release a P3 peptide and the AICD, both of which are degraded rapidly (Zhang H. et al., 2012).
In the amyloidogenic pathway, APP is primarily processed by β-secretase at the first residue or at the 11th residue (so called β' site) of the Aβ peptide sequence (fig. 22), shedding sAPPβ and generating a membrane associated C-terminal fragment consisting of 99 amino acids (C99) (Sarah C. and Robert V., 2007). γ-Secretase further cleaves C99 to release

AICD and the amyloidogenic Aβ peptide which aggregates and fibrillates to form amyloid plaques in the brain.

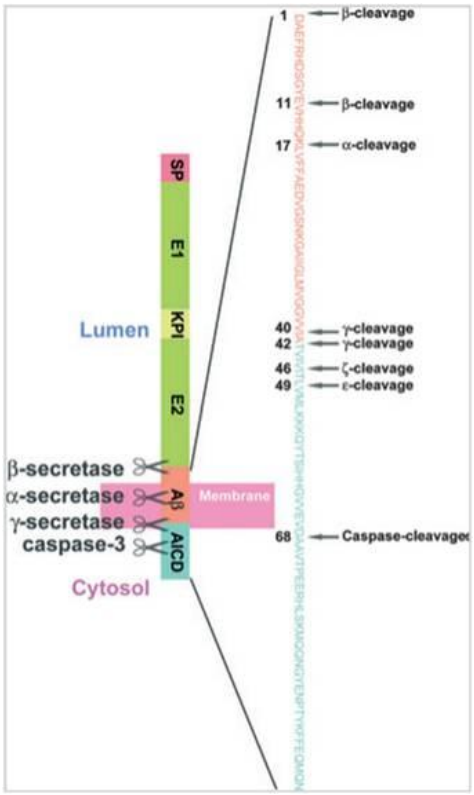

Fig. 22: Proteolytic processing of APP

3.2.1.1 α-secretase and α-cleavage

As APP was found to be constitutively cleaved at the α-site to yield sAPP-α, three members of the α disintegrin and metalloproteinase (ADAMs), ADAM-10, ADAM-17 and ADAM-9 have been proposed as the α-secretase (Koike H. et al. 1999).

ADAMs are type I integral membrane proteins that belong to the zinc protease super family and have been implicated in the control of cytokine and growth factor shedding.

ADAM10 is widely expressed in the brain and in other tissues and a several fold increase in sAPP-α levels in cell lines overexpressing ADAM10 can be observed (Kojro E. et al. 2001).

Moderate neuronal over-expression of human ADAM10 increases sAPP-α production while reducing Aβ generation/plaque formation in mice carrying the human APP V717I mutation, while expression of a catalytically-inactive form of the ADAM10 mutation increases the size

and number of amyloid plaques in mouse brains (Postina R. et al. 2004). These findings suggest that ADAM10 may be responsible for constitutive α-cleavage activity. However, although sAPP-α generation is not affected in ADAM9/17 knock-down cell lines nor in mice carrying deficient ADAM9/17 genes, over-expression of ADAM9/17 does increase the level of sAPP-α under some conditions, suggesting that ADAM9 and ADAM17 are more likely involved in the regulated α-cleavage of APP rather than in constitutive α-cleavage (Zhang H. et al, 2012).

3.2.1.2 β-Secretase and β-cleavage

Aβ generation is initiated by β-cleavage at the ectodomain of APP, resulting in the generation of an sAPP-β domain and the membrane associated APP C-terminal fragment C99.
The putative β-secretase, β-site APP cleaving enzyme 1 (BACE1), was first identified and characterized in 1999 (Sinha S. et al., 1999). BACE1 is a type I transmembrane aspartyl protease with its active site on the luminal side of the membrane. The originally identified full length BACE1 has 501 amino acids (BACE1-501) and is predominantly expressed in perinuclear post-Golgi membranes, vesicular structures throughout the cytoplasm, as well as on the cell surface (Ehehalt R. et al., 2002).
Knocking out the BACE1 gene prevents Aβ generation and completely abolishes Aβ pathology in mice expressing the Swedish mutation of human APP (Cai H. et al. 2001). The expression level and activity of BACE1 were also found to be elevated in AD patients (Holsinger R.M. et al. 2002).

3.2.1.3 γ-Secretase and γ-cleavage

Both α-cleavage and β-cleavage generate short APP C-terminal fragments that are further processed by γ-secretase.
Distinct from α-/β-secretases, γ-activity involves a large proteinase complex (fig. 23) consisting of at least four major protein components (Presenilin1 or Presenilin2, Presenilin enhancer 2 (PEN2), Anterior pharynx-defective1 (APH1) and Nicastrin) (Vetrivel K.S. et al. 2006).

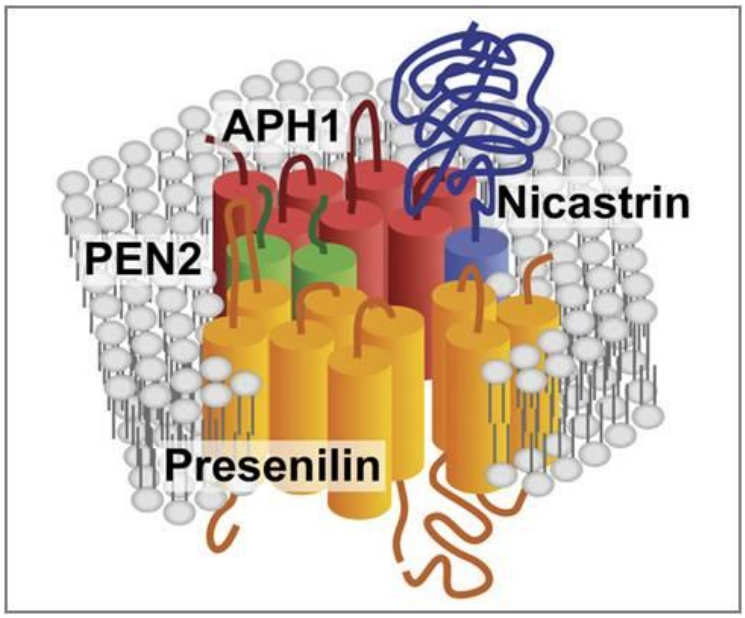

Fig. 23: The γ-secretase complex

Presenilins (PSs) were identified and cloned in the mid-1990s (Levy-Lahad E. et al., 1995; Sherrington R. et al., 1995). Genetic mutations of PSs are found in a large portion of FAD cases, indicating its crucial role in AD. Although other proteins are required for the γ-secretase complex, PSs are believed to contain the actual protease activity (Zhang H., 2012).

PSs (fig. 24) are multi-transmembrane proteins and can be cleaved at the cytoplasmic loop between the sixth and seventh transmembrane regions to generate an N-terminal and a C-terminal fragment during post-translational maturation (Thinakaran G. et al., 1996). The two fragments interact with each other after the cleavage and they are both necessary for γ-secretase activity.

Nicastrin, identified as a protein that interacts with PS in 2000 (Yu G. et al., 2000), is a type I membrane glycoprotein with a large ectodomain. Nicastrin undergoes a glycosylation/maturation process that causes a conformation change in its ectodomain, which is crucial for the assembly and maturation of the γ-secretase complex and γ-activity. Mature nicastrin can bind to the ectodomain of APP C-terminal fragments derived through α-/β-secretase cleavage and may act as a substrate receptor of γ-secretase (Shirotani K. et al. 2003).

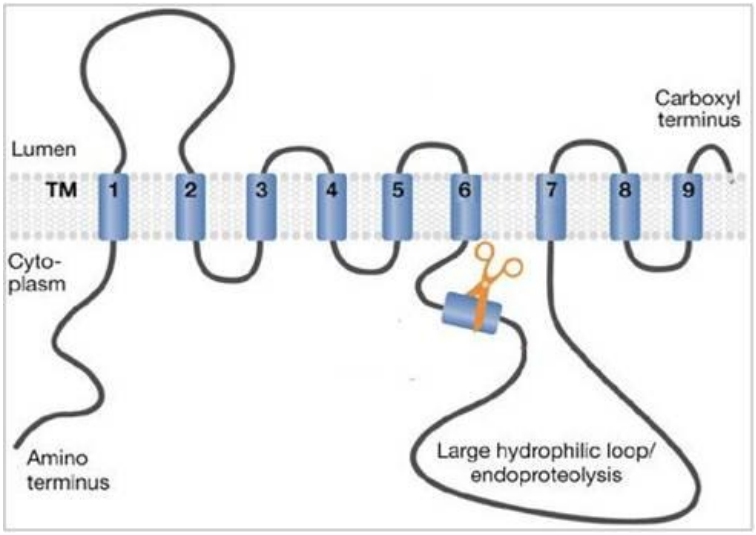

Fig. 24: Schematic representation of Presenilin

PEN2 and APH1 are another two γ-secretase complex components that were originally identified as the enhancers of PSs (Francis R. et al., 2002).

APH1 is a multiple transmembrane protein with seven transmembrane domains and a cytosolic C terminus. APH1 interacts with immature nicastrin and PS to form a relatively stable pre-complex which is then translocated to the trans-Golgi from the ER/cis-Golgi for further maturation (Lee S.F. et al., 2002).

PEN2 is a hairpin-like protein with two transmembrane domains and with both ends in the lumen. PEN2 is found to mediate the endoproteolysis of PS (Luo W.J. et al., 2003).

γ-Secretase cleaves APP at multiple sites and in sequential steps to generate Aβ peptides of different lengths (fig. 22). The majority of Aβ peptides produced are 40 amino acids long, however, peptides ranging from 38 to 43 amino acids are found *in vivo*. Besides the dominant γ-cleavage site at 40 and 42 residues, ξ-cleavage at 46 and e-cleavage at 49 residues are also thought to be mediated by γ-secretase. Accordingly, various AICDs (C50, C53, C57 and C59) can be generated during these multi-site cleavages executed by γ-secretase. However, all of the endogenous AICD forms are rarely detected, probably because of their very rapid degradation (Zhang H., 2012).

Strong evidence suggests that the γ-secretase complex resides primarily in the ER, Golgi/TGN, endocytic and intermediate compartments – most of which (except the TGN) are not major subcellular localizations for APP

(Cupers P. et al., 2001). In addition to cleaving APP, γ-secretase cleaves a series of functionally important transmembrane proteins, including Notch, cadherin, tyrosinase, ErbB4, CD44, etc (Zhang Y. et al., 2011).
The cleavage of various substrates appears to be dependent on the sub-cellular compartment; APP is mainly cleaved in the TGN and early endosomal domains whereas Notch is primarily cleaved at the plasma membrane (Tarassishin L. et al., 2004). Thus a disturbance in the localization of the γ-secretase complex may play some role in abnormal Aβ generation and AD pathogenesis (Zhang Y. et al., 2011).

3.2.2 The hyperphosphorylated tau hypothesis

AD belongs to a group of neurodegenerative diseases collectively designated as "tauopathies", because they are characterized by the aggregation of abnormally phosphorylated tau protein. The mechanisms responsible for tau aggregation and its contribution to neurodegeneration are still unknown. Thereby, understanding the modes of regulation of tau is of high interest in the determination of the possible causes at the origin of the formation of tau aggregates and to elaborate protection strategies to cope with these pathological lesions (Martin L. et al., 2011).
Tau protein (tubulin-associated unit) was identified in 1975 (Weingarten M.D. et al., 1975). Tau is a microtubule-associated protein highly conserved and exclusively found in higher eukaryotes. Tau is mainly expressed in neuron and its primary role, by interacting with microtubules, is to stabilize neuronal cytoskeleton.
Tau protein is subdivided into four regions (fig. 25): (1) an acidic region in the N-terminal part; (2) a proline-rich region; (3) a region responsible for tau binding with microtubules that contains four repeat domains R1, R2, R3 and R4 also called MBDs (microtubule-binding domains); and (4) a C-terminal region. Each repeat domain contains a conserved consensus motif KXGS, which can be phosphorylated at serine (Ozer R.S. and Halpain S., 2000). Serine phosphorylation at KXGS motifs, belonging to MBD region, decreases tau affinity for microtubules and consequently prevents its binding to microtubules which results in the destabilization of the neuronal cytoskeleton (Sengupta A. et al., 1998).

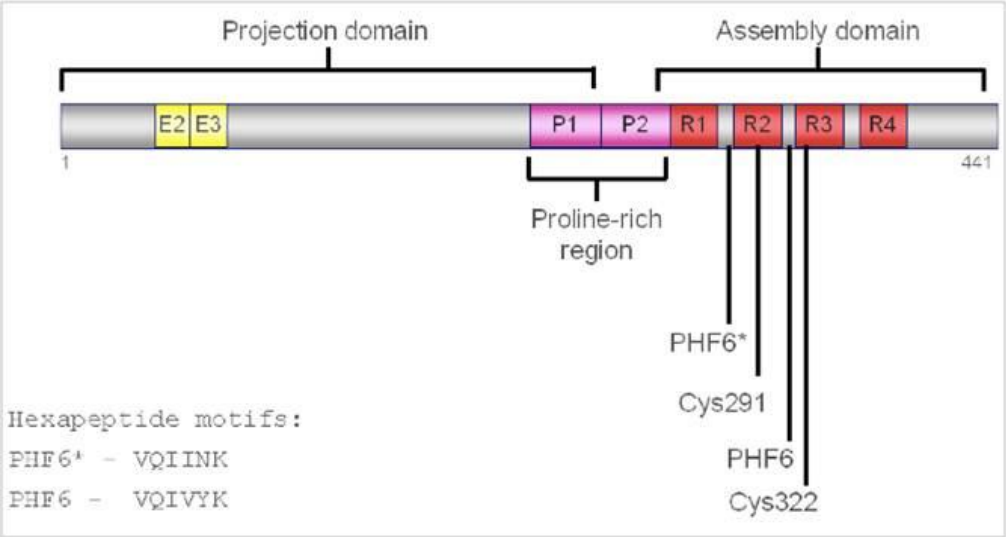

Fig. 25: Tau protein

Cytoskeleton destabilization is well known to cause disruption of tau-dependent cellular functions including axonal growth, vesicle and organelle transport as well as nervous signal propagation along the nerve network formed by microtubules (LaPointe N.E. et al., 2009).

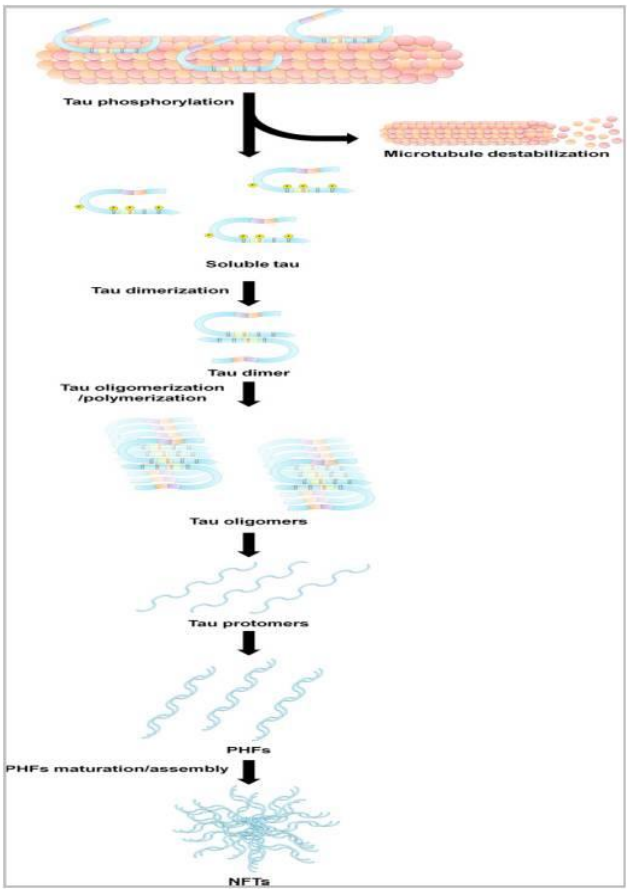

Fig. 26: Model for multistep process of tau aggregation

Phosphorylation specifically modulates tau aggregation by disrupting its binding to microtubules and subsequently by promoting tau self-aggregation (fig. 26) (Martin L. et al., 2011).
Various kinases and phosphatases regulate tau phosphorylation. Each tau phosphorylation site is subjected to the action of one or more protein kinase. Tau kinases are grouped into three classes: protein kinases PDPKs (proline-directed protein kinases), protein kinases non-PDPKs and protein kinases specific for tyrosines. Alterations in the expression and/or the activity of tau kinases such as GSK3β, CDK5, DYRK1A, p38 and CK1 have been reported in the brains of AD patients, suggesting that one or several of them could be involved in the tau hyperphosphorylation (Chung S.H., 2009).

3.2.3 The Ca^{2+} hypothesis

A perturbed Ca^{2+} homeostasis has been demonstrated in AD and, in particular, mutations in PSs have variably been correlated to alteration of Ca^{2+} signaling and different molecular targets have been identified, suggesting a physiological role for these proteins in multiple intracellular Ca^{2+} pathway (Zampese E. et al., 2009).
PS, present as two homologous proteins PS1 and PS1, is an essential component of the APP cleaving enzymes γ-secretase. As an integral membrane protein, it is abundantly expressed with markers of ER, GA, endo-exocytic vesicles and only a minor fraction is present at the plasma membrane level (Vetrivel K.S. et al., 2004).
Both PS1 and PS2 are however regarded as a multi-faceted proteins whose roles can be functionally distinguished and independent of their enzymatic activity. In particular, several lines of evidence suggest that PS is also involved in the regulation of cellular Ca^{2+} homeostasis (E. Zampese et al., 2009). Since their discovery, different FAD-linked PS mutants were reported to induce alterations of cellular Ca^{2+} handling in several cell models and, in particular, it was observed that the FAD-mutant PS1-L286V, when expressed in PC12 cells, causes an increased Ca^{2+} release upon different stimulation (Furukawa K. et al., 1998). Then, other two FAD mutations in PS1 (A246E and M146V) were described to cause larger Ca^{2+} release from intracellular stores and increase excitotoxicity in

neurons from transgenic (Tg) mice expressing the mutant protein (Stutzmann G.E. et al., 2006). The idea that FAD-linked PS mutations are somehow correlated to altered Ca^{2+} signaling was further supported by the fact that these mutations could modify the sensitivity (or expression) of ER Ca^{2+} release channels (RyR and IP_3R) in different cell models, in neurons from tg AD mice as well as in isolated brain microsomes.

According to the popular "Ca^{2+} overload" hypothesis, PS mutations increase Ca^{2+} content of the ER, thus sensitizing neurons to excitotoxicity and progressive dementia (Zampese E. et al., 2009).

However, different studies reported either no alteration or a reduced store Ca^{2+} content in cells expressing wt or FAD-mutant PSs. In particular, it was demonstrated that the FAD-linked PS2 mutations M239I and T122R reduce rather than increase Ca^{2+} release in fibroblasts from FAD patients and in cell lines stably or transiently expressing the PS2 mutants (Zatti G. et al., 2004; Giacomello M. et al., 2005;). In addition, an extended investigation of other FAD-linked PS mutants by directly monitoring the ER and the Golgi Ca^{2+} content in different cell lines confirmed that the FAD-linked PS2 mutations cause a reduction in the Ca^{2+} level of these organelles and none of the PS1 mutations cause an increase (Zatti G. et al., 2006). Similar results have been obtained in rat cortical neurons transiently expressing FAD-mutant PSs (Zatti G. et al., 2006) and in neurons from transgenic mice expressing mutant presenilin 2 (Kipanyula M.J., et al., 2012).

The absence of elevated ER [Ca^{2+}] in these models suggests that the enhanced Ca^{2+} release observed by other groups, upon expression of various FAD-linked PS mutants, might depend on different mechanisms, not necessarily due to an increased amount of Ca^{2+} within the stores (Zampese E. et al., 2009).

A dysregulation of store Ca^{2+} handling seems however the common feature of a heterogeneous group of FAD-linked PS mutants.

The hypothetical mechanisms through which PS mutants exert their effect on Ca^{2+} homeostasis are numerous. For instance, a model that was suggested in accordance with the Ca^{2+} overload supports the idea that PSs represent one of the molecular components of the elusive Ca^{2+} leak channel of the ER membrane and the FAD-linked PS mutants, by reducing

the leak, increase the ER Ca^{2+} content (Zampese E., et al., 2009). Moreover, in addition to the ER Ca^{2+} release channel and modulation of CCE, other mechanisms have been implicated, on the basis of either physical or functional interactions with proteins involved in cellular Ca^{2+} handling, such as sorcin (Pack-Chung E. et al., 2000), calsenilin (Buxbaum J.D. et al., 1998), calcindin (Guo Q. et al., 1998). In particular, recent data by our lab have demonstrated that PS2 mutations linked to FAD reduce ER and GA Ca^{2+} levels by inhibiting SERCA pump (Zatti et al., 2006 and Brunello et al., 2009). Moreover, endogenous PS seems to interact with SERCA and modulate SERCA function; SERCA pumping is impaired in the absence of both PSs (Green K.N. et al., 2008).

Materials and Methods

Constructs

The first 32 N-terminal amino acids of the resident Golgi enzyme 1,6 N-acetyl glucosaminyl transferase (C2gnT) (MIHTNLKKKFSCCVLVFLLFAVICVWKEKKK GSYYDSFKLQTKEFQVLKSLGKLAMGSDSQSVFSSSTQ), was introduced before the start codon of the D1cpv cDNA (kindly provided by Dr. R. Tsien) in the HindIII - BamHI restriction sites, after its isolation from the GFP fused construct kindly provided by Dr. A. El-Battari (Zerfaoui et al., 2002).

Cell culture and transfection

SH-SY5Y cells and fibroblasts were grown in DMEM containing 10% (20% for fibroblasts) FCS, supplemented with L-glutamine (2 mM), penicillin (100 U/ml), and streptomycin (100 μg/ml), in a humidified atmosphere containing 5% CO_2. Cells were seeded onto glass coverslips (18-mm diameter) and transfection was performed at 60% confluence using Lipofectamine™ 2000 Transfection Reagent (Life Technologies) with 2 μg of DNA (0.5 μg of cameleon codifying DNAs and 1.5 μg of pcDNA3 or PSs codifying DNAs); fibroblasts were transfected by electroporetion, using the Neon Transfection System (MPK500, Invitrogen). FRET measurements have been usually performed 24 h after transfection.

SPCA1 siRNA transfection in SH-SY5Y cells and Western Blot

The day before transfection, SH-SY5Y cells were plated in order to ensure 50% confluence on the day of transfection. Functionally validated Stealth™ RNA directed against SPCA1 CATCGAGAAGTAACATTGCCTTTA (SPCA1 Oligo 1) and Stealth™ RNA negative control were from Invitrogen. SPCA1 siRNAs (100 nM each) or control siRNA were transfected using Lipofectamine™ 2000 Transfection Reagent (Life Technologies).

Proteins were resolved by SDS-PAGE, blotted onto a PVDF membrane and probed with selected antibodies (mouse monoclonal anti-ATP2C1, Sigma-Aldrich); mouse monoclonal anti-β-actin (Sigma-Aldrich).

Cell imaging

Cells expressing the fluorescent probes were analyzed using a DM6000 inverted microscope (Leica, Wetzlar, Germany) with a 40X oil objective (HCX Plan Apo, NA 1.25). Excitation light produced by a 410nm LED (Led Engin #LZ1-00UA00 LED) was filtered at the appropriate wavelength (425 nm) through a band pass filter, and the emitted light was collected through a beamsplitter (OES s.r.l., Padua, Italy) (emission filters HQ 480/40M (for CFP) and HQ 535/30M (for cpv-YFP) and a dichroic mirror 515 DCXR). The beamsplitter permits the collection of the two emitted wavelengths at the same time, thus preventing any artefact due to movement of the organelles. All filters and dichroics were from Chroma Technologies (Bellow Falls, VT, USA). Images were acquired using an IM 1.4C cool camera (Jenoptik Optical Systems) attached to a 12-bit frame grabber. Synchronization of the excitation source and cool camera was performed through a control unit ran by a custom-made software package, Roboscope (developed by Catalin Cubotaru at VIMM, Padua, Italy); this software was also used for image analysis. Exposure time and frequency of image capture varied from 200 ms to 400 ms, depending on the intensity of the fluorescent signal of the cells analyzed and on the speed of fluorescence changes.

Cells were mounted into an open-topped chamber and maintained in an extracellular medium (modified Krebs-Ringer Buffer). Classical experiments started in 1 mM $CaCl_2$; after perfusion with 300 μM EGTA, cells were stimulated by applying bradykinin (BK, 100nM) and/or CPA (20 μM); thereafter, the Ca^{2+} ionophore ionomycin (1 μM) was applied to completely discharge the stores; finally digitonin (50 μM, to obtain plasma membrane permeabilization) in Ca^{2+}-free medium and then a saturating $CaCl_2$ concentration (3 mM) were applied, in order to verify the dynamic range of the probe.

An intracellular-like medium was used for pH determination [130 mM KCl, 10 mM NaCl, 1 mM $MgCl_2$, 2 mM succinic acid and 20 mM Pipes at different pH, at 37°C] and for experiments in permeabilized cells for NAADP response and medialGo-D1cpv calibration [130 mM KCl, 10 mM NaCl, 1mM KH_2PO_4, 1 mM $MgSO_4$, 2 mM succinic acid, 300 μM EGTA

and 20 mM Hepes, pH 7.05, at 37 °C] to which different concentrations of $CaCl_2$ were added.
For Ca^{2+} pumping experiments a Ca^{2+}-buffer solution was prepared by adding to the intracellular medium: H-EDTA, pyruvic acid and $MgCl_2$ (1 mM each), EGTA (2 mM) and $CaCl_2$ (350 μM). ATP-Na (100 μM) was added to this Ca^{2+}-buffered solution. The free [Ca^{2+}] (0.1 μM) was estimated by MaxChelator2.5 and checked by fluorimetric measurements with fura-2.
All media were perfused through a temperature controller (Warner Instruments, TC-324B) set to have a constant temperature of 37°C in the chamber.

Immunocytochemistry
Cells decorated with anti-GM130 (BD Bioscience Pharmigen, San Jose CA, USA), anti-TGN46 anti-Giantin (AbCam, Cambridge UK) and anti-PS2 (Santa Cruz Biotechnology, Dallas Texas, USA) antibodies were fixed in Phosphate Buffered Saline (PBS) containing 4% paraformaldehyde for 15 min, incubated with 50mM NH_4Cl for 20 min, permeabilized with 0.1% Triton X-100 in PBS 3 min and then blocked with 2% BSA and 0,2% gelatine for 30 min; anti-GM130 (1:1000) and anti-Giantin (1:300) were added for 1 hour at room temperature, anti-TGN46 (1:200) and anti-PS2 (1:500) were added for 2h at 37°C. Samples were treated with Alexa Fluor 488 (555, 568 or 647) conjugated goat anti-mouse, anti-rabbit or rabbit anti-goat IgG (Molecular Probes Invitrogen, Eugene OR) for 1 hour at room temperature and mounted with Mowiol (Sigma-Aldrich Saint Louis, MI). Images were collected at Leica TCS-SP5-II confocal system, equipped with a PlanApo 100×/1.4 numerical aperture objective. For all images, pinhole was set to 1 Airy unit. The Argon laser line (488 nm) was used to excite the Cameleon sensors or AlexaFluor488 the He/Ne 543 nm laser was used to excite the AlexaFluor555/568 and the AlexaFluor647 was excited by the HeNe 633nm laser line. Video microscopy was performed at 1024×1024 pixels per image, with a 100Hz acquisition rate. Images were elaborated with ImageJ program (Wayne Rasband, Bethesda,USA). Z-stacks were acquired with a step of 0.42 μm.

Materials

Restriction and modification enzymes were purchase from NEB Inc. (Ipswich, MA). CPA, digitonin, BK, caffeine were purchased from SIGMA-Aldrich; ionomycin from Calbiochem and NAADP from Tocris. All other materials were analytical or highest available grade.

Statistical analysis

Off-line analysis of FRET experiments was performed with ImageJ software (Wayne Rasband, Bethesda, USA). Cpv-YFP and CFP images were subtracted of background signals and distinctly analyzed after selecting proper regions of interest (ROIs) on each cell; subsequently, a ratio between cpv-YFP and CFP emissions was calculated (R=F530/F480). Data are presented as a normalized $\Delta R/R_0$ %, where R is the R value at each time (t) of the experiment and R_0 is the R value at the beginning of the experiment (t_0), or as % of FRET.

All the data are representative of at least five different experiments. Data were analyzed by Origin 7.5 SR5 (OriginLab Corporation). Averages are expressed as mean ± s.e.m. (n = number of independent experiments; * = $p < 0.05$, ** = $p < 0.01$, *** = $p < 0.001$, unpaired Student's t test).

Results

2. CHARACTERIZATION OF Ca^{2+} HANDLING BY THE CIS/MEDIAL-GOLGI

In order to study in details and at the single cells level the effects of FAD-mutants PS2, we firstly characterized, in terms of Ca^{2+} handling, the cis/medial-Golgi subcompartement by taking advantage of a newly created Cameleon Ca^{2+} probe specifically targeted to the cis/medial-Golgi region.

1.1 A new Cameleon Ca^{2+} probe specifically targeted to cis/medial-Golgi

1.1.1 Creation of the new Cameleon Ca^{2+} probe

In order to specifically monitor the Ca^{2+} levels in the cis/medial part of the Golgi Apparatus, we generated a new Ca^{2+} probe, taking advantage of the first 32 N-terminal amino acids of the resident Golgi enzyme 1,6 N-acetyl glucosaminyl transferase (C2gnT), that have been shown to represent the minimal cis- to medial-Golgi targeting determinant when fused to a GFP (Zerfaoui et al., 2002). This sequence was cloned upstream of the cDNA coding for the cameleon D1cpv (Fig. 27A) and the obtained construct was then transiently transfected in the human neuroblastoma cell line SH-SY5Y.

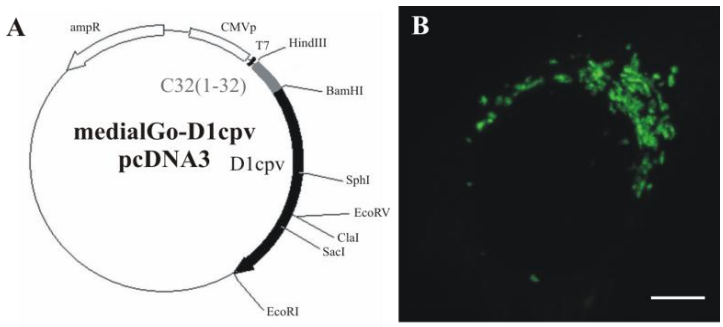

Fig. 27: (A) The first 32 N-terminal AA of the Golgi enzyme 1,6 N-acetylglucosaminyltransferase, C32(1-32), were cloned upstream of the cDNA coding for the cameleon D1cpv. (B) Z-projection confocal image (10 sections) of a SH-SY5Y cell expressing the new Golgi Ca^{2+} sensor excited at 488 nm. Scale bar, 5 µm

Figure 27B shows that the expressed probe localized in a perinuclear region that appears composed of cysternae and small vesicles, thus resembling the Golgi complex.

1.1.2 Localization of the new probe

Figure 28 shows that, when probe-expressing cells (panels A, D, G) were fixed and immunolabeled with bona fide markers of the cis- (GM130; panel B), cis/medial- (Giantin; panel E) and trans- (TGN46; panel H) GA compartments, there was a good overlap of the probe's fluorescence with that of the cis/medial-Golgi marker (panel F) while a partial separation was observed between the signals of GM130 (panel C) and TGN46 (panel I) and that of the novel probe (although a partial overlapping of the signals was however evident).

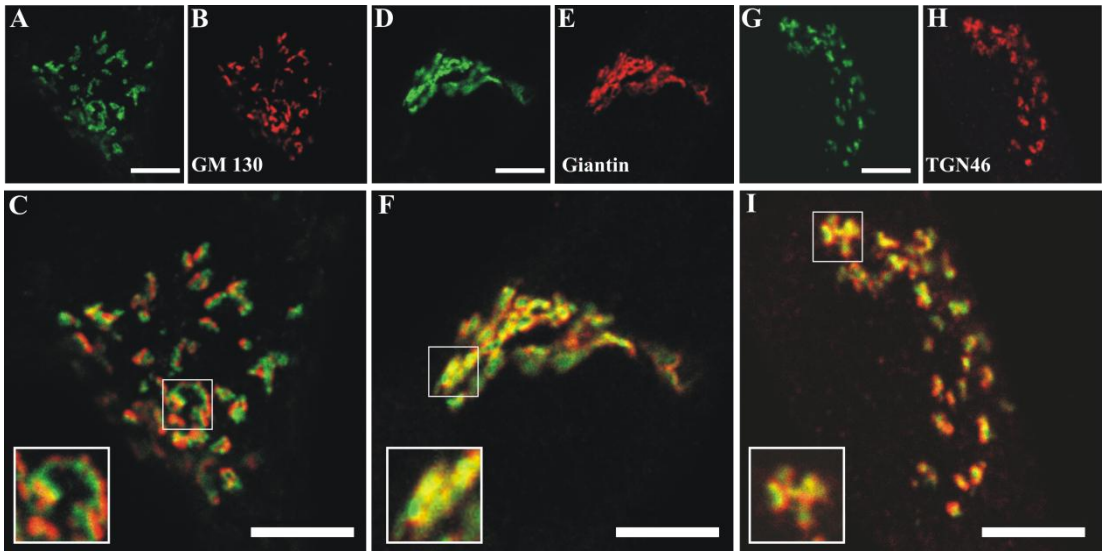

Fig. 28: Confocal fluorescence images corresponding to Ca^{2+} probe expressing SH-SY5Y cells either excited at 488 nm (A, D, G) or decorated with antibody against the cis-Golgi marker GM130 (B), the medial-Golgi marker Giantin (E) and the trans-Golgi marker TGN46 (H), and excited at 543 nm. (C, F, I) Merging of the two previous images; the yellow colour indicates overlapping of the green and red signals. Insets in each panel show magnifications of selected cisternae. Bar, 10 μm.

Confocal Z-stacks of cells labelled as above were statistically analyzed (by ImageJ) to quantify the signal co-localizations of the new probe versus the three markers (Fig. 29, panel A): the Pearson's coefficient (an index of signal co-localization that varies from -1, no co-localization, to +1,

complete overlapping; Adler J. and Parmryd I., 2010) was lowest for the probe and the cis-Golgi GM130 marker and larger for the cis/medial (Giantin) and trans- (TGN46) Golgi markers, indicating a stronger overlap of the probe with the last two proteins.

The spatial resolution of confocal microscopy is about 0.4 μm on the X/Y-axis, but only 1 μm, at the best, on the Z-axis. Given that the diameter of the GA cysternae can be significantly smaller than these values, the question is whether the co-localization of the new probe with the different markers is real or only apparent.

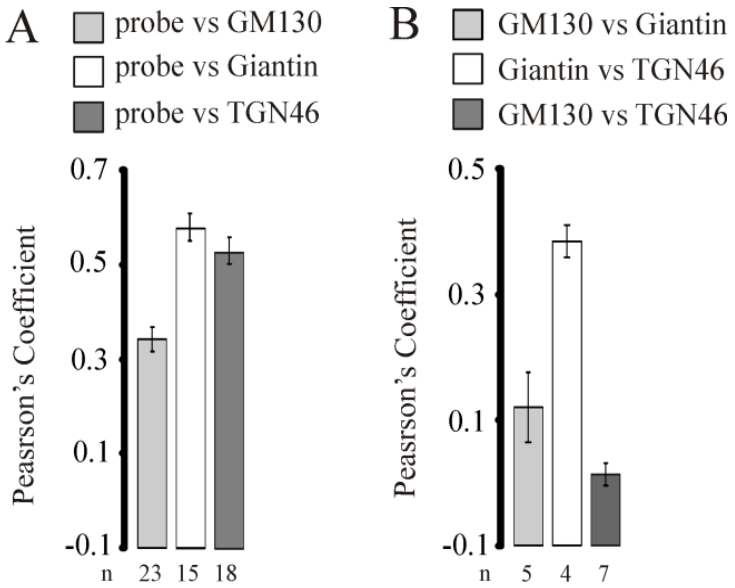

Fig. 29: Pearson's coefficients for signal co-localization between (A) the new probe and the three Golgi markers GM130, Giantin and TGN46, or (B) between the three markers for different Golgi compartments. The values were calculated from Z-axis confocal stacks by the Image-J JACoP plug-in; mean ± SEM; n, number of cells.

Indeed, when the cells were immunolabeled for the three endogenous Golgi marker proteins (GM130, Giantin, TGN46), although it is known that they are localized in distinct GA sub-compartments, a high co-localization index between the cis/medial- and the trans-GA marker was found, while the signals coming from the cis- and the trans-compartment of the GA (and from the cis- and the medial-) appeared better separated (Fig. 29, panel B), though, again, some apparent overlap was observed.

To investigate more precisely the localization within the GA of the new probe, the cells were thus treated with the microtubule depolymerizing agent nocodazole (which results in the accumulation of dispersed individual Golgi stacks in the cytoplasm). Under these conditions, the distinction, by

confocal microscopy, of the different GA sub-compartments should be facilitated (Thyberg J and Moskalewski S., 1999). In figure 30A, the cells were thus first treated with nocodazole, fixed and then triple-immunolabeled for GM130, Giantin and TGN46. In this case, the localization of the three endogenous markers appears more distinct and, particularly when the vesicles were image en face, a typical 3 colour staining was often evident, with the Giantin signal closer to that of partially overlapped to that of TGN46, while the GM130 signal was more clearly separated from the other two.

Cells expressing the probe were thus similarly treated, fixed and immunolabelled with the same two antibodies towards the cis- and the trans-GA marker (fig. 30, panel B). In some structures, the spatial separation among the three signals was striking evident. On the contrary, if the same protocol was applied, but the cells were immunolabelled with antibodies against GM130 and Giantin (fig. 30, panel C), the probe signal appears almost completely separated from the first marker, but completely largely overlapped with the second.

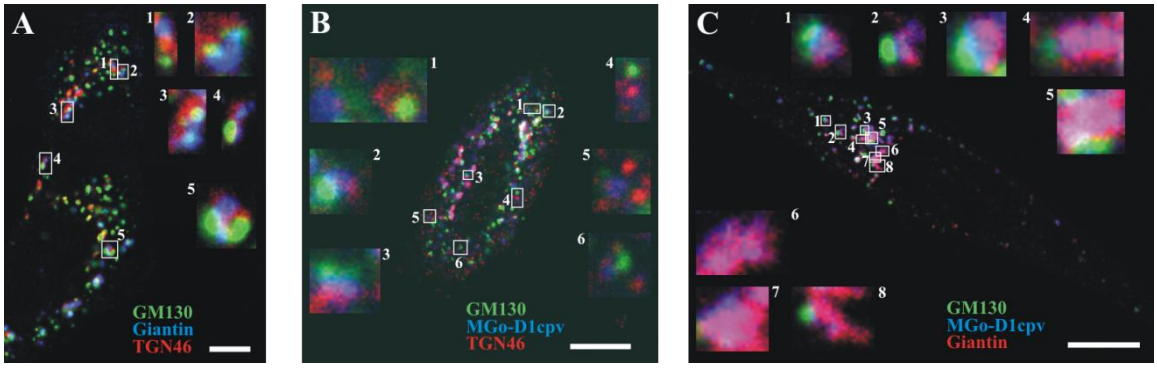

Fig. 30: Confocal fluorescence images corresponding to SH-SY5Y cells treated with nocodazole and expressing the new Ca^{2+} probe (and excited at 488 nm; B and C, blue). Cells were decorated with antibody against the cis-Golgi marker GM130 (and excited at 647 nm; A, B, C, green), the medial-Golgi marker Giantin (and excited at 488 nm; A, blue; or at 543 nm; C, red) and the trans-Golgi marker TGN46 (and excited at 543 nm; A and B, red). Insets in each panel show magnifications of en face vesicles. Bar, 10 μm.

In conclusion, the new probe appears to be almost completely excluded from the compartment containing primarily localized halfway between the TGN46- and GM130-positive structures while and well overlapped the best overlapping was observed with the vesicles to that containing Giantin. A partial overlapping between the probe distribution and TGN46 was observed,

similar to that between the trans-GA marker and Giantin. Accordingly, for simplicity, the new probe from now on is named medialGo-D1cpv (mGo-D1cpv).

1.1.3 Calibration of the new mGo-D1cpv

In order to determine the absolute value of [Ca^{2+}] within the medial-GA compartment, the calibration of the probe was carried out, performing passive Ca^{2+} loading experiments, permeabilizing the cells with digitonin in an intracellular-like medium containing different Ca^{2+} concentrations and no energy source (fig. 31, panels A and B).

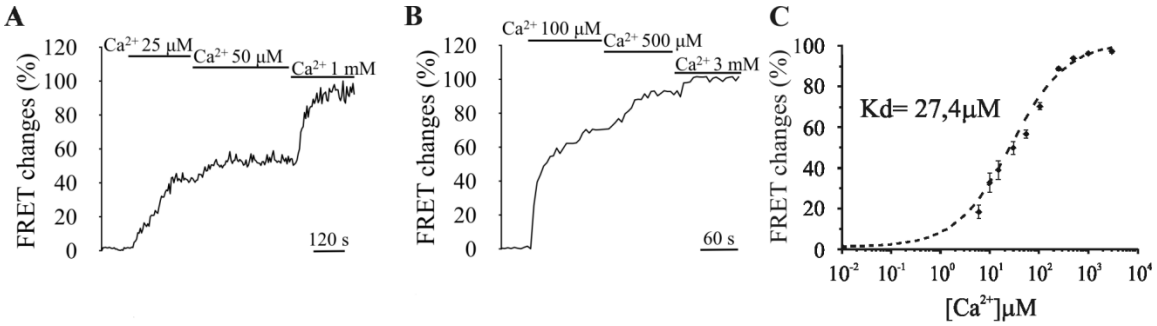

Fig. 31: (A-B) Representative kinetics of the FRET changes (% of maximal) in permeabilized SH-SY5Y cells transiently transfected with mGo D1cpv. Where indicated, digitonin-permeabilized cells were bathed with the an intracellular-like medium without energy source and containing different [Ca^{2+}]; 3mM $CaCl_2$ was finally added to reach the maximum value. (C) In situ calibration curve for the mGo D1cpv, obtained perfusing the cells with different [Ca^{2+}]-containing intracellular-like medium as described in A. Mean ± s.e.m., n ≥ 3 for each Ca^{2+} concentration.

The calculated apparent Kd for the new probe is 27.4 µM (fig. 31, panel C) and the mean Ca^{2+} level that matched the cpv YFP/CFP fluorescence emission ratio of SH-SY5Y cells at rest before permeabilization was 235 ± 30 µM (mean ± s.e.m., n = 24).

1.2 Ca^{2+} handling in the medial-Golgi

Functional experiments were then carried out in living SH-SY5Y cells transiently transfected with the cDNA encoding mGo-D1cpv. Dcpv-probes are FRET-based and FRET occours between two mutants of GFP (the CFP and YFP). It is caused by the interaction between Ca^{2+} activated Calmodulin (CaM) and its target peptide M13. Variations in Ca^{2+} concentration can be followed as variations in the ratio between YFP and CFP fluorescence.

Changes in [Ca^{2+}] can be conveniently expressed as $\Delta R/R_0$. A drop in $\Delta R/R_0$ indicates a decrease of [Ca^{2+}] within the lumen.

Figure 32 shows typical $\Delta R/R_0$ changes in medialGo-D1cpv expressing SH-SY5Y cells after addition of different stimuli. Perfusion, in a Ca^{2+}-free (EGTA supplemented) medium, of an IP_3-generating stimulus, such as bradikinin (BK; Fig. 32 B), results typically in small decreases (a drop of 10 ± 0.4%, mean ± s.e.m., n = 14; Fig. 32 E) of the average $\Delta R/R_0$ value within the GA region. The following addition of the Ca^{2+} ionophore ionomycin causes a rapid and large decrease (a drop of 70 ± 2.1%, mean ± s.e.m., n = 37; Fig. 32 E) of the Golgi $\Delta R/R_0$ down to a level that was not significantly affected by the subsequent permeabilization of the plasma membrane with digitonin.

We then tested the effect on medial-Golgi Ca^{2+} handling of the SERCA inhibitor cyclopiazonic acid (CPA), added alone (Fig. 32 C) or in combination with BK (Fig. 32 D): the SERCA inhibitor alone resulted in a slow decrease of $\Delta R/R_0$ down to a new steady state value approximately halfway between the value at rest and the minimum obtained after cell permeabilization with digitonin in Ca^{2+}-free, EGTA-containing medium (-40 ± 3.4%, mean ± s.e.m., n = 21; Fig. 4 E); however, when the addition of the SERCA inhibitor was rapidly followed by BK, the slow CPA-induced $\Delta R/R_0$ decrease was strongly accelerated (Fig. 32 D) until a new steady-state value, similar to that reached upon CPA addition alone was reached (-40 ± 1%, mean ± s.e.m., n = 9; Fig. 31 E). Addition of ionomycin, after CPA, induced, in both cases, a further large drop in the $\Delta R/R_0$ signal (Fig. 32 C and D). In Fig. 32 E, the averaged decreases in $\Delta R/R_0$ values obtained in SH-SY5Y cells expressing the mGo-D1cpv upon different stimulations are reported.

The partial depletion of medial-Golgi by SERCA inhibitors suggests that this Golgi compartment is endowed with two mechanism of Ca^{2+} uptake, only one of which sensitive to the drugs. The existence in the medial-Golgi of a Ca^{2+} uptake mechanism other than the SERCA was then investigated. First, cells expressing the mGo-D1cpv were treated (in Ca^{2+} free, EGTA-containing medium) with ionomycin to completely deplete Ca^{2+} from the lumen; ionomycin was then washed away, cells were treated with the irreversible SERCA inhibitor thapsigargin (Tg, 1 μM) and finally 1mM $CaCl_2$ was added to the medium. For comparison, the same procedure was employed in parallel cells expressing an ER targeted Ca^{2+} probe, ER-D4.

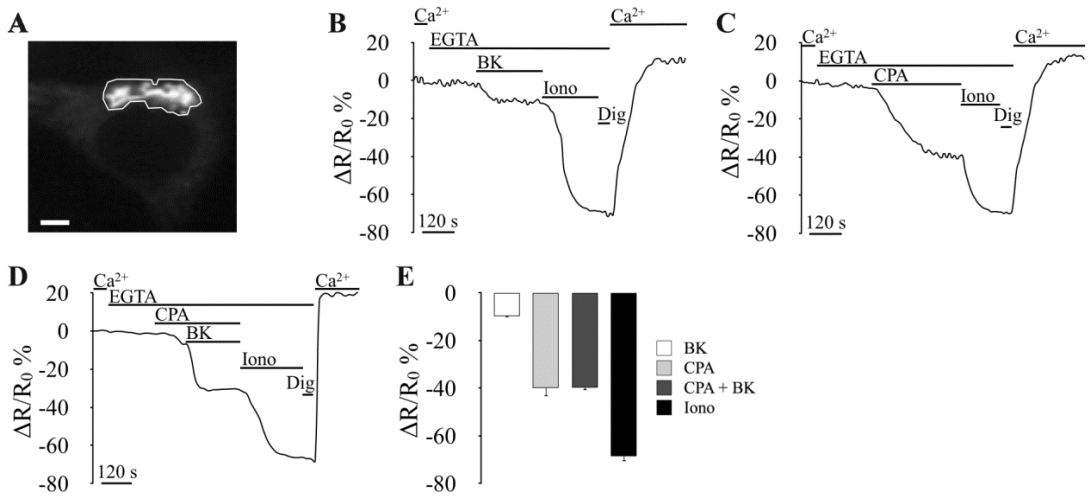

Fig. 32: (A): Image of a SH-SY5Y cell expressing the mGo-D1cpv probe. Bar, 10 μm.
(B-C-D) Representative $\Delta R/R_0$ variations in medialGo-D1cpv expressing SH-SY5Y cells in response to different stimuli. Where indicated 1 mM $CaCl_2$, 300 μM EGTA, 100 nM bradikinin (BK), 20 μM cyclopiazonic acid (CPA), 1 μM ionomycin (Iono), 50 μM digitonin (Dig) were perfused.
(E) Statistical medial-Golgi $\Delta R/R_0$reduction in SH-SY5Y cells upon different stimulation (mean ± s.e.m.; n ≥ 9).

Figure 33, panel A, shows that, while a substantial reuptake of Ca^{2+} was observed, in these conditions, in the medial-Golgi (black trace), no Ca^{2+} refilling was observed in cells expressing the ER Ca^{2+} sensor (grey trace). Similar results were obtained when refilling of pre-emptied stores was followed in cells permeabilized with digitonin and perfused with an intracellular-like medium at fixed [Ca^{2+}] (Fig. 33, panel B).

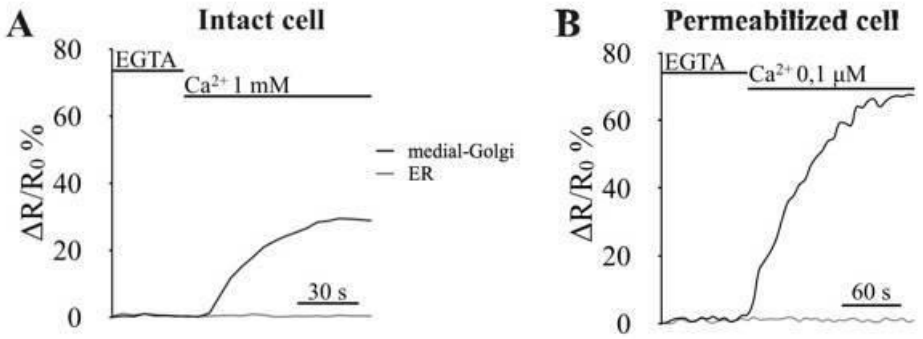

Fig. 33: (A) Representative medial-GA (black trace) and ER (grey trace) Ca^{2+} refilling kinetics in pre-emptied intact SH-SY5Y cells treated with thapsigargin (1 μM). Where indicated, Ca^{2+}-free, EGTA (300 μM)-containing medium was changed with the mKRB containing 1mM $CaCl_2$.
(B) Representative medial-GA (black trace) and ER (grey trace) Ca^{2+} refilling kinetics in pre-emptied, digitonin-permeabilized SH-SY5Y cells treated with thapsigargin (1 μM). Where indicated, intracellular-like, Ca^{2+}-free, EGTA (300 μM)-containing medium was changed with an intracellular-like medium at fixed [Ca^{2+}] (0.1 μM).

We thus hypothesized that the medial-Golgi is equipped by both the SERCA and the SPCA-1 pumps. To further investigate this Ca^{2+} uptake mechanisms in these Golgi subcompartment, we verified the effect in SH-SY5Y cells expressing the medial-Golgi probe of SPCA1 knock-down (Fig. 34). SH-SY5Y cells treated with specific siRNA against SPCA1 and expressing medialGo-D1cpv were analyzed by Western blotting with an anti-SPCA1 antibody: a reduction in the total SPCA1 protein level of 54 ± 9% (n=3) was revealed in interfered cells, compared to control scramble siRNA-transfected cells (Fig. 34A). Taken into consideration the transfection efficiency in these cells (~70%), this should correspond to a reduction of about 70% of SPCA1 level in the transfected cells.

The effects of SPCA1 down-regulation were then tested on medial-GA Ca^{2+} handling. Fig. 34B shows that SPCA1 knockdown caused a lower steady-state FRET level with the medial-Golgi at rest and a bigger ΔFRET change upon CPA addition, compared to controls (Fig. 34C); accordingly, the additional drop induced by ionomycin was larger in controls compared to SPCA1 knocked-down cells (Fig. 34C).

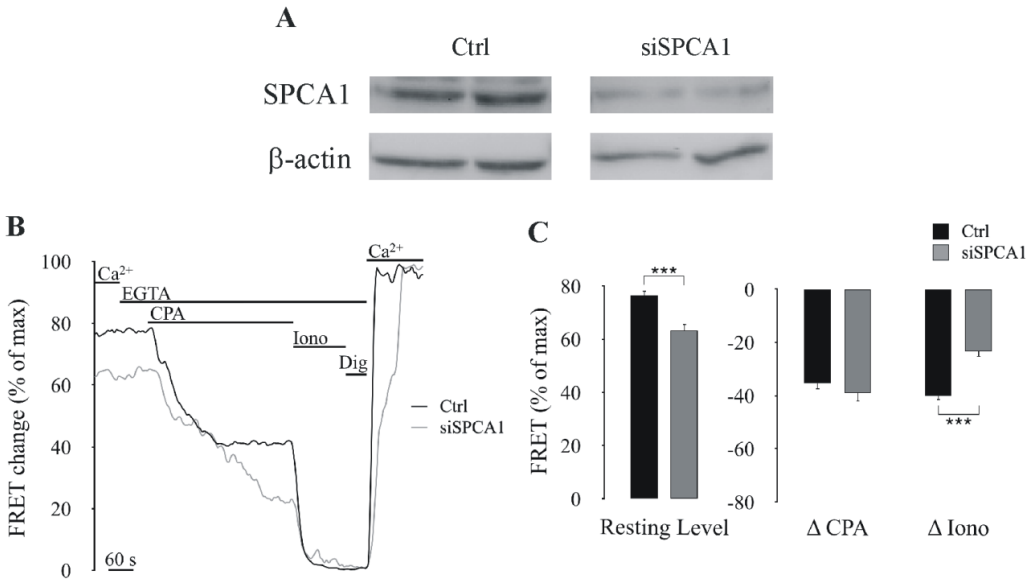

Fig. 34: (A) Western blot of control (Ctrl, scrambe siRNA-trasfected) and interfered (siSPCA1-transfected) SH-SY5Y cell extracts visualized with anti SPCA1 and a-actin antibodies. A significant reduction in the level of SPCA1 was observed in interfered cells (-54 ± 9%, mean ± s.e.m., n = 3). (B) Representative FRET changes (% of maximal) in medialGo-D1cpv expressing control (grey trace) and interfered (black trace) SH-SY5Y cells in response to the addition of different stimuli. Where indicated, 1 mM $CaCl_2$, 300 μM EGTA, 20 μM CPA, 1 μM ionomycin (Iono) were perfused. (C) Statistical medial-Golgi FRET variations in SH-SY5Y cells treated as in B.
(mean ± s.e.m., n = 25; = $p < 0.05$; *** = $p < 0.001$).

Concluding, medial-Golgi subcompartment seems to be equipped by IP_3R and Ca^{2+} uptake can be mediated by both SERCA and SPCA1 pumps.

2. EFFECTS OF THE FAMILIAL ALZHEIMER'S DISEASE LINKED-PRESENILIN 2-T122R MUTANT ON Ca^{2+} HOMEOSTASIS IN THE GOLGI APPARATUS SUBCOMPARTMENTS.

To study in details the effects of FAD-linked PS2 mutations in both medial- and trans- subcompartments I transfected cells from human neuroblastoma cell line with the trans or the medialGo targeted cameleon probes and PS2 T122R mutated form or a void vector as control. Upon different protocol, Ca^{2+} measurements were performed.

2.1 Intracellular localization of PS2 in SH-SY5Y cells

In order to study the effect of transient over-expression of PS2 (wt or T122R) on Golgi-Apparatus Ca^{2+} handling in SH-SY5Y cells, we firstly checked where they localized intracellularly together with the two cameleon probes used for Ca^{2+} measurements.
We thus decorated cells over-expressing PS2 (wt or T122R) and mGo-D1cpv or tGo-D1cpv with an antibody against PS2 (fig. 9) and we found a good co-localization between the signal coming from the two fluorescent probes and those from the antibody, thus suggesting that PS2, both mutated and wt, localized both in the cis/medial- and in the trans-Golgi.

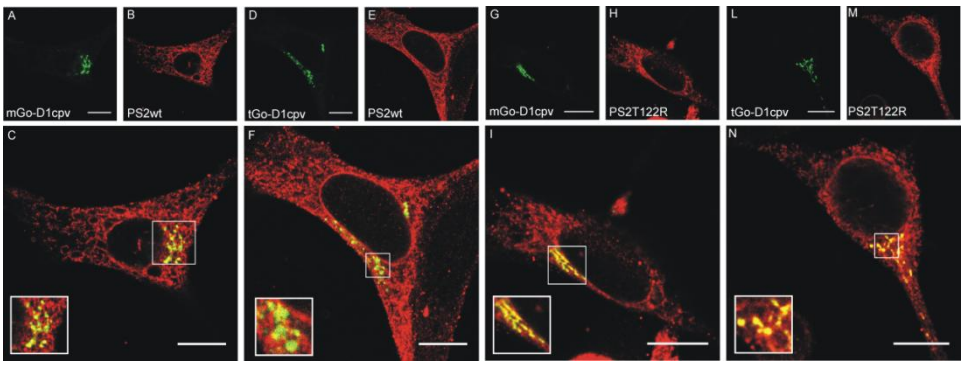

Fig. 35: Confocal fluorescence images corresponding to SH-SY5Y cells expressing the two Ca^{2+} probes either excited at 488 nm (A, D, G, L) or decorated with antibody against PS2 (B, E, H, M) and excited at 543 nm. (C, F, I, N) Merging of the two previous images; the yellow colour indicates overlapping of the green and red signals. Insets in each panel show magnifications of selected ROIs. Bar, 10 μm.

2.1 Both FAD-linked PS2 and PS1 mutants strongly affect the Ca^{2+} level of the medial-Golgi apparatus but do not affect the Ca^{2+} level of the trans-Golgi apparatus

In order to study the effect of FAD-linked PS2 on Ca^{2+} handling in Golgi Apparatus subcompartments, Ca^{2+} measurements were performed in SH-SY5Y cells transiently transfected with the cDNAs coding for mGo-D1cpv or tGo-D1cpv and the different PS mutants or wild type (wt) or a void vector as control.
First of all, we monitored the Golgi Apparatus subcompartments Ca^{2+} content at steady state (fig. 36).

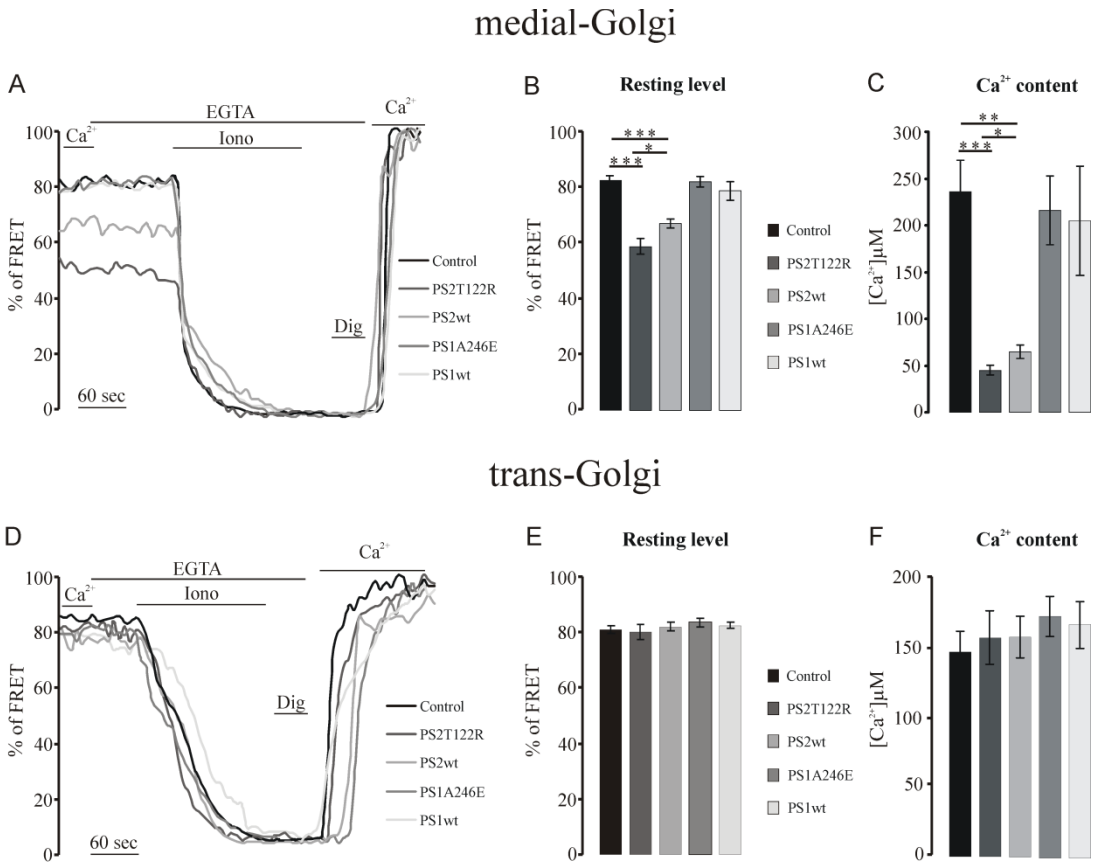

Fig. 36: (A and D) Representative % of FRET variations in medialGo-D1cpv (A) or trans-Golgi-D1cpv (D) and PS2T122R, PS2wt, PS1A246E or PS1wt expressing SH-SY5Y cells in response to different stimuli. Where indicated 1 mM $CaCl_2$, 300 µM EGTA, 1 µM ionomycin (Iono), 50 µM digitonin (Dig) and 3mM $CaCl_2$ were perfused. (B and D) Statistical medial-Golgi (B) and trans-Golgi (E) % of FRET at resting level in PS2T122R, PS2wt, PS1A246E or PS1wt expressing SH-SY5Y cells (mean ± s.e.m.; n ≥ 10). (C and F) Statistical Ca^{2+} concentration at the steady state of medial-Golgi (C) and trans-Golgi (F) at resting level in PS2T122R, PS2wt, PS1A246E or PS1wt expressing SH-SY5Y cells (mean ± s.e.m.; n ≥ 10). * = p < 0.05, ** = p < 0.01, *** = p < 0,0001

We found that the overexpression of FAD-linked PS2T122R but not PS1A246E affects the Ca^{2+} level of the medial-Golgi apparatus that appears to be strongly reduced.
In term of FRET (fig. 36, panel B), the effect of PS2T122R over-expression is from about 82 ± 1.5 % (mean ± s.e.m., n = 24) of FRET in control cells to about 58 ± 3 % (mean ± s.e.m., n = 15) in PS2T122R expression cells that in terms of Ca^{2+} (fig. 36, panel C) reflects a reduction from about 235 ± 30 μM (mean ± s.e.m., n = 24) of control cells to about 45 ± 6 μM (mean ± s.e.m., n = 15) of PS2T122R expressing cells. This effect is mimicked, in a weaker manner, by the over-expression of wt PS2, that reduces medial-Golgi Ca^{2+} content to 64 ± 7 μM (mean ± s.e.m., n = 10) but not wt PS1 (fig. 36, panels A, B, C).
No differences in Ca^{2+} content between cells expressing mutated PS1 or PS2 and control cells has been found in trans-Golgi apparatus, whose Ca^{2+} content at the steady state were about 146 ± 15 μM (mean ± s.e.m., n = 16) for control cells, 156 ± 19 μM (mean ± s.e.m., n = 15) for PS2T122R expressing cells, 157 ± 14 μM (mean ± s.e.m., n = 17) for PS2wt expressing cells, 173 ± 15 μM (mean ± s.e.m., n = 12) for PS1A246E expressing cells and 167 ± 17 μM (mean ± s.e.m., n = 12) for wt PS1 expressing cells (fig. 36, panels D, E, F).
Similar results have been obtain in fibroblasts from FAD patients transiently transfected with mGo-D1cpv (fig. 37, panel A) or tGo-D1cpv (fig. 37, panel B), whose cells carrying PS2 N141I mutation showed a reduced Ca^{2+} content in the medial-Golgi (fig. 37, panels C, D, E) with control cells showing a % of FRET of about 87 ± 1 % (mean ± s.e.m., n = 12) and PS2N141I cells a % of FRET of about 69 ± 3 % (mean ± s.e.m., n = 10) at the steady state in the medial-Golgi. In terms of Ca^{2+} content, control fibroblasts showed a medial-Golgi Ca^{2+} content of about 298 ± 30 μM (mean ± s.e.m., n = 12) whereas PS2N141I fibroblasts showed a medial-Golgi Ca^{2+} content of about 84 ± 12 μM (mean ± s.e.m., n = 10).
No alterations in trans-Go Ca^{2+} content as respect to fibroblasts from healthy patients have been found in PS2N141I fibroblasts (fig. 37, panels F, G, H). Control and PS2N141I fibroblasts showed respectively a trans-Golgi Ca^{2+} content at the steady state of about 105 ± 7 μM (mean ± s.e.m., n = 10) and 110 ± 12 μM (mean ± s.e.m., n = 10).

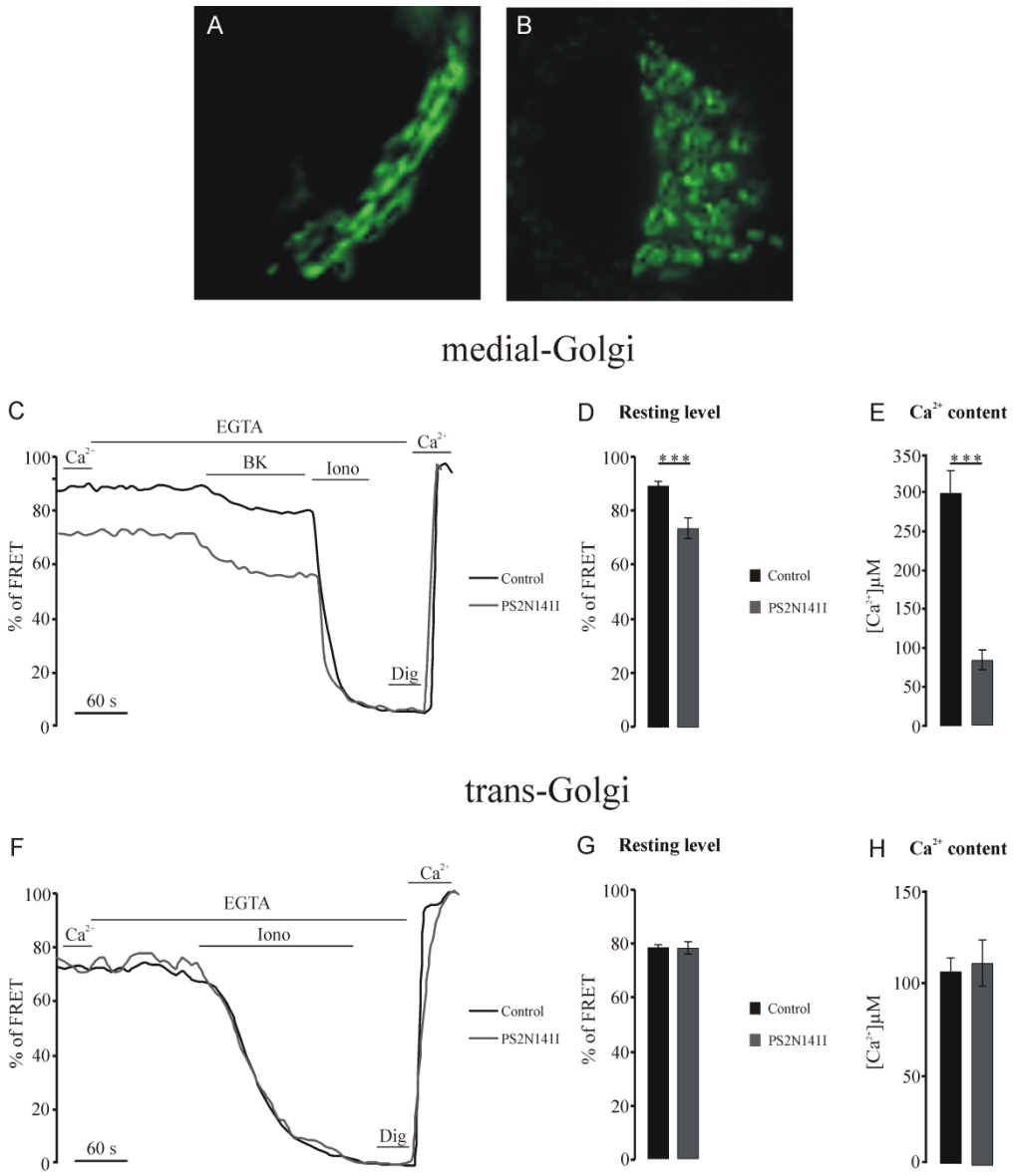

Fig. 37: (*A* and B) Fluorescence images of fibroblasts expressing the mGo-D1cpv (*A*) and tGo-D1cpv (B) excited at 488 nm.

(*C* and F) Representative % of FRET variations in medialGo-D1cpv (*C*) or trans-Golgi-D1cpv (F) control and PS2N141I fibroblasts in response to different stimuli. Where indicated 1 mM $CaCl_2$, 300 µM EGTA, 100nM Bradikinin (BK), 1 µM ionomycin (Iono), 50 µM digitonin (Dig) and 3mM $CaCl_2$ were perfused.

(D and *G*) Statistical medial-Golgi (D) and trans-Golgi (*G*) % of FRET at resting level in control and PS2N141I fibroblasts (mean ± s.e.m.; n ≥ 10).

(E and H) Statistical Ca^{2+} concentration at the steady state of medial-Golgi (E) and trans-Golgi (H) at resting level in control and PS2N141I fibroblasts (mean ± s.e.m.; n ≥ 10). *** = p < 0,0001

2.2 FAD-linked PS2 reduced medial-Golgi Ca^{2+} uptake by inhibiting SERCA pump activity

To investigate how PS2 affects Ca^{2+} homeostasis in medial-Golgi subcompartments, we carried out an analysis in permeabilized SH-SY5Y cells

transiently transfected with cDNA coding for mGo-D1cpv and the PS2T122R or wild type (wt) and a void vector as control.
Permeabilized cells were incubated in an EGTA containing medium for 10 min to induce Ca^{2+} stores depletion and then Ca^{2+} uptake was measured at 100nM of free [Ca^{2+}] in presence of ATP (fig. 38, panels A-E). In cells transiently expressing mGo-D1cpv, the expression of PS2-T122R significantly reduced the initial uptake rate (fig. 38, panel B) from 1.64 ± 0.35 Δ FRET/s % (mean ± s.e.m., n = 13) in control cells to 0.63 ± 0.06 Δ FRET/s % (mean ± s.e.m., n = 15) in PS2T122R expressing cells and the plateau reached after refilling (fig. 38, panel D) from 148 ± 20 μM (mean ± s.e.m., n = 13) in control cells to 35 ± 6 μM (mean ± s.e.m., n = 15).
Medial-Golgi Ca^{2+} uptake were also affected upon over-expression of wt PS2 even if its effect is weaker than the FAD-mutant effect (fig. 38) with an the initial uptake rate (fig. 38, panel B) of 0.85 ± 0.07 Δ FRET/s % (mean ± s.e.m., n = 13) and a plateau reached after refilling (fig. 38, panel D) corresponding to 54 ± 5 μM (mean ± s.e.m., n = 13).
Similar experiments were then performed in SH-SY5Y cells treated with the SERCA inhibitor CPA. In this case, Ca^{2+} uptake were mediated only by SPCA-1 pump and no effect of PS2-T122R and wt PS2 over-expression was found (fig. 38, panels D, E and F). All samples showed a similar initial uptake rate (fig. 38, panel F): 1 ± 0.1 Δ FRET/s % (mean ± s.e.m., n = 9) for control cells, 0.9 ± 0.1 Δ FRET/s % (mean ± s.e.m., n = 10) for PS2T122R expressing cells and 1.1 ± 0.06 Δ FRET/s % (mean ± s.e.m., n = 9) for wt PS2 expressing cells and respectively a plateau reached after refilling (fig. 38, panel H) corresponding to 52 ± 6 μM (mean ± s.e.m., n = 9), 49 ± 7 μM (mean ± s.e.m., n = 10) and 49 ± 4 μM (mean ± s.e.m., n = 9).
In order to investigate whether PS2 affect also trans-Golgi Ca^{2+} uptake, we carried out an analysis in permeabilized SH-SY5Y cells transiently transfected with cDNA coding for tGo-D1cpv and the PS2T122R, wt PS2 or a void vector as control. Ca^{2+} uptake was then measured at 100nM of free [Ca^{2+}] (fig. 38, panels I-O). Expression of PS2-T122R, and also PS2 wt, does not alter neither the initial uptake rate (fig. 38, panel L), with 1.4 ± 0.16 Δ FRET/s % (mean ± s.e.m., n = 10) for control cells, 1.4 ± 0.12 Δ FRET/s % (mean ± s.e.m., n = 10) for PS2T122R expressing cells and 1.4 ± 0.16 Δ FRET/s % (mean ± s.e.m., n = 10) for wt PS2 expressing cells neither the plateau reached after refilling (fig. 38, panel O) with Ca^{2+} level of 28 ± 5 μM (mean ±

s.e.m., n = 10) for control cells, 30 ± 7 µM (mean ± s.e.m., n = 10) for PS2T122R expressing cells and 27 ± 5 µM (mean ± s.e.m., n = 10) for wt PS2 expressing cells.

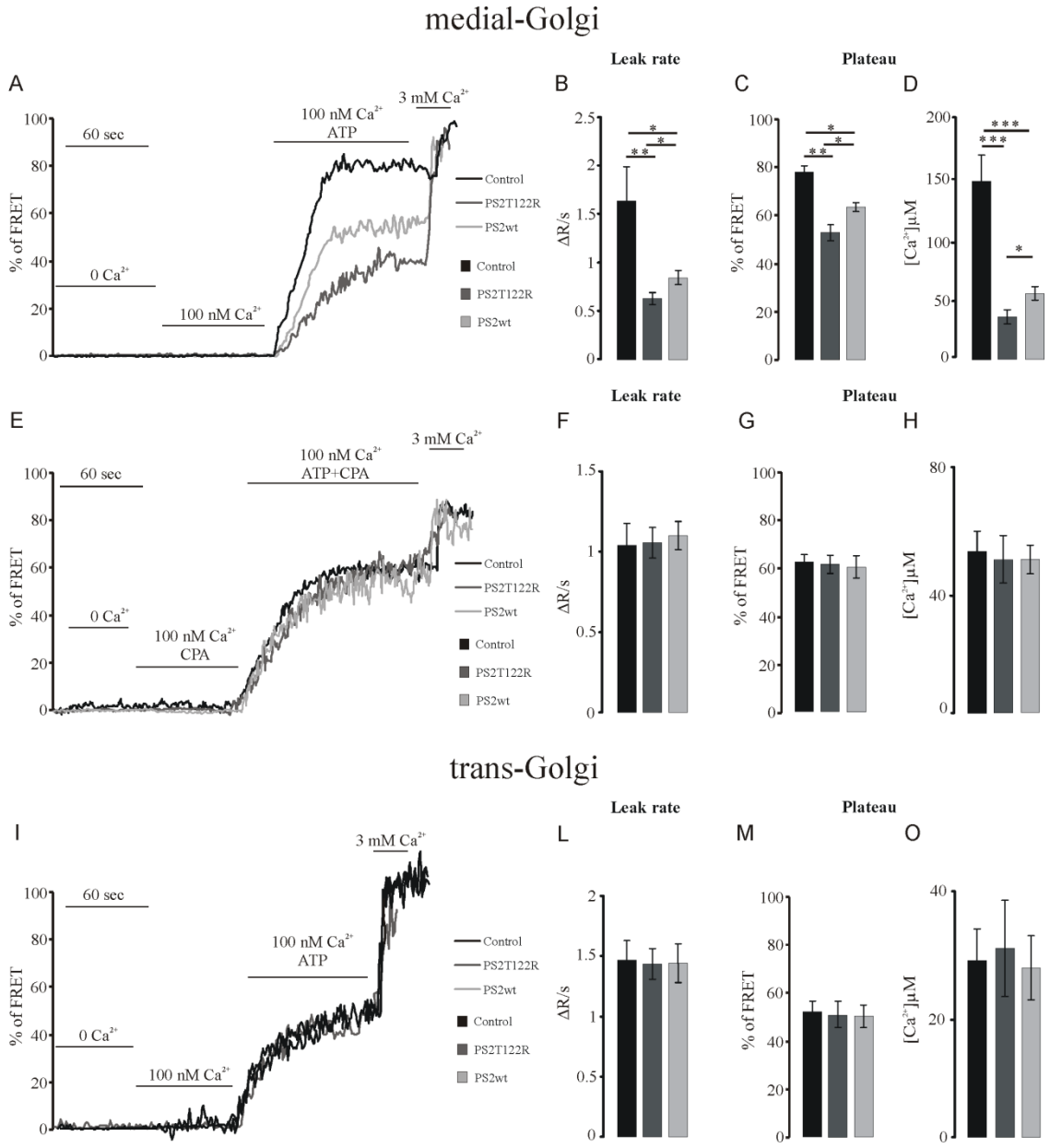

Fig. 38: (A, E and I) Representative % of FRET variations in mGo-D1cpv (A and E) or tGo-D1cpv (I) and PS2-T122R or PS2wt expressing SH-SY5Y cells, in response to different stimuli. Where indicated ICB 0 Ca^{2+}, ICB 100nM Ca^{2+}, ICB 100nM Ca^{2+} and 200µM ATP with (E) or without (A and I) CPA and 3mM $CaCl_2$ were perfused. (B, F and L) Statistical medial-Golgi (B and F) and trans-Golgi (L) ΔR/s % for the first 10 s of Ca^{2+} uptake level in PS2-T122R, or PS2wt, expressing SH-SY5Y cells (mean ± s.e.m.; n ≥ 10). (C, G and M) Statistical medial-Golgi (C and G) and trans-Golgi (M) % of FRET reached after refilling in PS2-T122R, PS2wt expressing or control SH-SY5Y cells (mean ± s.e.m.; n ≥ 9). (D, H and O) Statistical medial-Golgi (D and H) and trans-Golgi (O) Ca^{2+} concentration reached after refilling in PS2-T122R, PS2wt expressing or control SH-SY5Y cells (mean ± s.e.m.; n ≥ 9). *= p* < ** = p**0.05.

These results thus suggested that the over-expression of FAD-linked PS2-T122R (and similarly wt PS2) decreases medial-Golgi Ca^{2+} content by inhibiting SERCA pump activity whereas it doesn't affect SPCA1 activity and consequently trans-Golgi Apparatus Ca^{2+} content is not altered.

2.3 FAD-linked PS2 increases medial-Golgi Ca^{2+} leak

In order to study if other Ca^{2+} handling mechanisms were altered by the over-expression of FAD-linked PS2 mutants, we monitored passive Ca^{2+}leak from the medial-Golgi.

In order to eliminate any differences due to the differential Ca^{2+}content between control cells and cells over-expressing PS2-T122R, or PS2wt, control cells and wt PS2 expressing cells were pre-treated by incubating them in an EGTA-containing media, respectively at 4 C° for about 20 minutes and 5 min at room temperature before starting Ca^{2+} measurement, to match the Ca^{2+}content of PS2T122R-expressing cells (fig. 39, panel B). In this way, control cells showed an initial Ca^{2+} content of about of 45 ± 4 μM (mean ± s.e.m., n = 9), PS2T122R expressing cells showed an initial Ca^{2+} content of about of 44 ± 4 μM (mean ± s.e.m., n = 10) and wt PS2 expressing cells showed an initial Ca^{2+} content of about of 47 ± 5 μM (mean ± s.e.m., n = 10) (fig. 39, panel C).

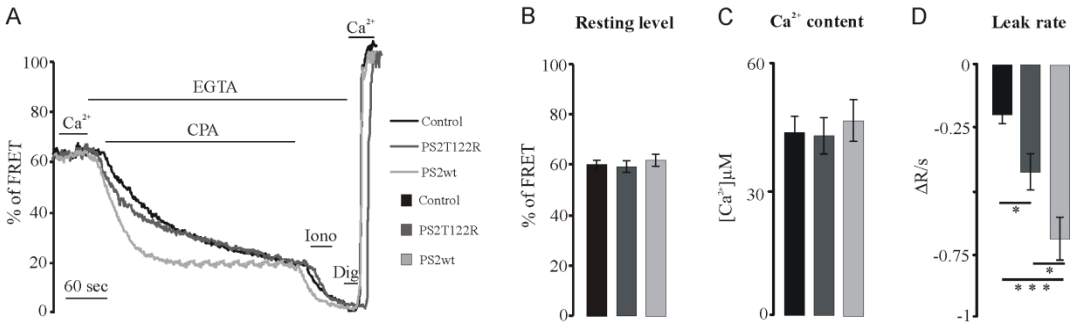

Fig. 39: (A) Representative % of FRET variations in mGo-D1cpv and PS2-T122R, or PS2wt, expressing SH-SY5Y cells in response to different stimuli. Where indicated 1 mM $CaCl_2$, 300 μM EGTA, 20 μM cyclopiazonic acid (CPA), 1 μM ionomycin (Iono), 50 μM digitonin (Dig) and 3mM $CaCl_2$ were perfused. (B) Statistical medial-Golgi % of FRET at resting level in PS2-T122R, PS2wt expressing SH-SY5Y cells and controls. (C) Statistical Ca^{2+} concentration at the steady state of medial-Golgi in control, PS2T122R and wt PS2 expressing SH-SY5Y cells. (D) ΔR/s% for the first 10 s of Ca^{2+} leak in PS2-T122R or PS2wt expressing SH-SY5Y cells and controls.
(mean ± s.e.m.; n ≥ 9). *= $p < 0.05$, *** = $p < 0.001$

Figure 39, panel D, shows that the over-expression of PS2wt increases spontaneous Ca^{2+} leak from the medial-Golgi treated with CPA in an EGTA-containing media to visualize it (fig. 39, panel A). A similar, but weaker effect seemed to be caused by the over-expression of PS2T122R. Infact, the initial leak rate were about -0.2 ± 0.03 Δ FRET/s % (mean ± s.e.m., n = 9) for control cells, about -0.4 ± 0.07 Δ FRET/s % (mean ± s.e.m., n = 10) for PS2T122R expressing cells and -0.7 ± 0.08 Δ FRET/s % (mean ± s.e.m., n = 11) for wt PS2 expressing cells.

2.4 FAD-linked PS2 increase IP_3 sensitivity of medial-Golgi Apparatus

We finally evaluated if FAD-linked PS2 mutants affected also the medial-Golgi sensitivity to the Ca^{2+} releasing second messenger IP_3.
SH-SY5Y transiently transfected with mGo-D1cpv and PS2 (T122R or wt), or a void vector as control, were treated with the IP_3-generating stimulus BK and the induced drop were measured (Fig. 40, panels A-F). Figure 40 shows that over-expression of PS2T122R and also PS2wt, increased Ca^{2+} release due to IP_3 generation. Indeed, in terms of FRET changes, BK induced-drop is measured in control cells about -12 ± 1.6 Δ FRET % (fig. 40, panel C) from 82 ± 3 FRET % at the steady state to 69 ± 3 FRET % after BK (fig. 40, panel B), in PS2T122R expressing cells about -24 ± 1.8 Δ FRET % (fig. 40, panel C) from 61 ± 2 FRET % at the steady state to 36 ± 1.5 FRET % after BK (fig. 40, panel B) and in wt PS2 expressing cells about -24 ± 1.9 Δ FRET % (fig. 40, panel C) from 68 ± 3 FRET % at the steady state to 45 ± 13 FRET % after BK (fig. 40, panel B). Even if the FRET drops were translated in term of Ca^{2+} (fig. 40, panels D-E), the increased IP_3 sensitivity seemed to be induced in both PS2T122R and wt PS2 expressing cells, where the 71 ± 3 % (mean ± s.e.m., n = 12), in PS2T122R expressing cells, and the 73 ± 3 % (mean ± s.e.m., n = 9), in wt PS2 expressing cells, of the Ca^{2+} store seemed to be sensitive to IP_3, versus the 58 ± 6 % (mean ± s.e.m., n = 10) in control cells (fig. 40, panel F).

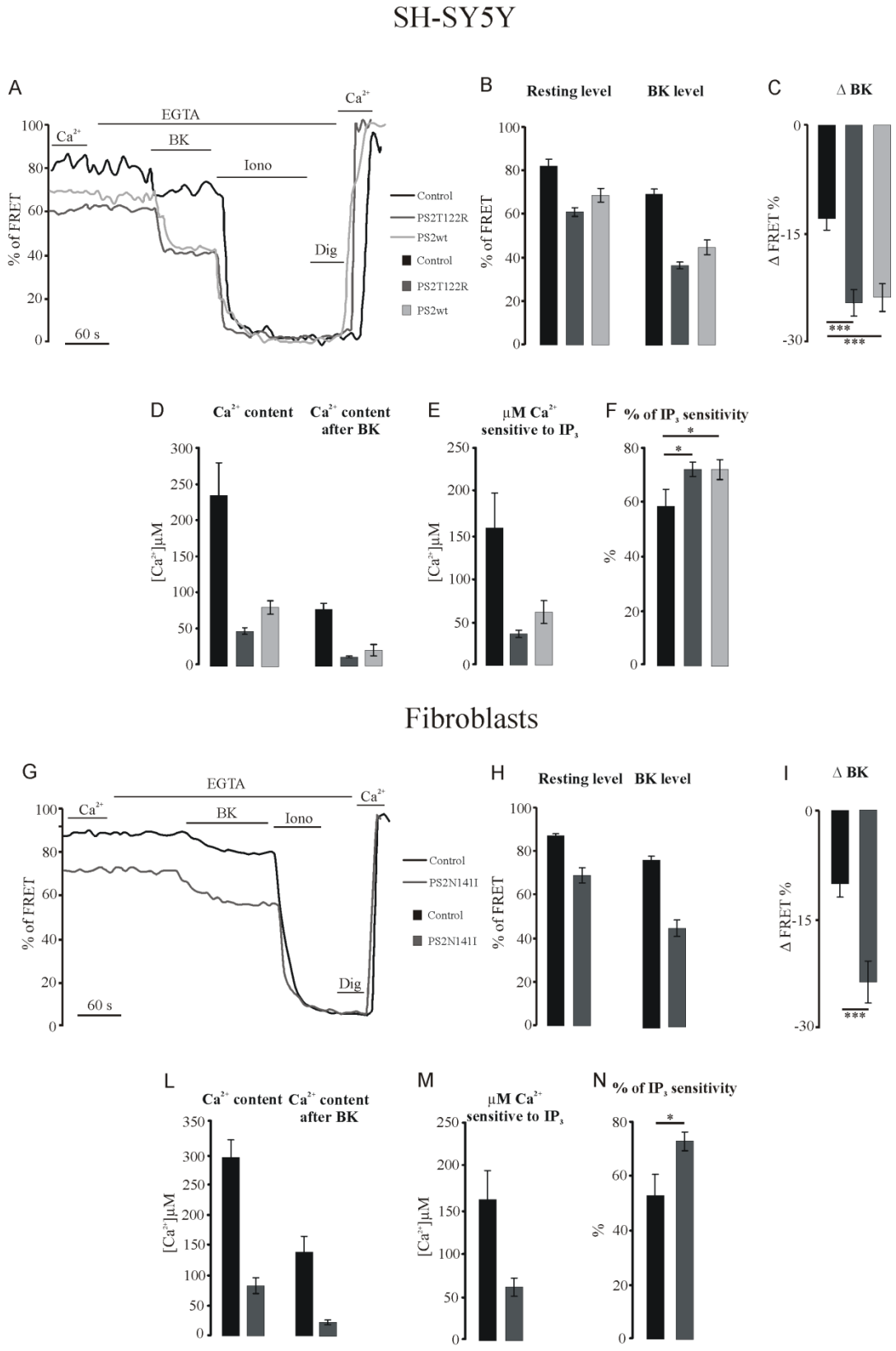

Fig. 40: (A-G) Representative % of FRET variations in medialGo-D1cpv and PS2-T122R, or PS2wt, expressing and control SH-SY5Y cells (A) and in mGo-D1cpv expressing FAD-PS2-N141I or control human fibroblasts, in response to different stimuli. Where indicated 1 mM $CaCl_2$, 300 µM EGTA, 100nM Bradikinin (BK), 1 µM ionomycin (Iono), 50 µM digitonin (Dig) and 3mM $CaCl_2$ were perfused.

(B-H) Statistical medial-Golgi % of FRET at resting level in PS2-T122R, PS2wt expressing and control SH-SY5Y cells (B) nad in FAD-PS2 and control fibroblasts (H). (C and I) Statistical medial-Golgi Δ FRET % between resting level and the plateau reached after BK-induced drop in PS2-T122R, PS2wt expressing and control SH-SY5Y cells (C) and FAD-PS2 or control fibroblasts (I).
(D and L) Statistical Ca^{2+} concentration at the steady state and at the plateau reached after BK-induced drop of medial-Golgi in control, PS2T122R and wt PS2 expressing SH-SY5Y cells (D) and in FAD-PS2 and control fibroblasts (L). (E and M) μM Ca^{2+} released in response to IP_3 generation in PS2-T122R, PS2wt expressing and control SH-SY5Y cells (E) and FAD-PS2 or control fibroblasts (M).
(F and N) % of medial-Golgi Ca^{2+} content released in response to IP_3 generation in PS2-T122R, PS2wt expressing and control SH-SY5Y cells (E) and FAD-PS2 or control fibroblasts (M).
(mean ± s.e.m.; n ≥ 9) *= p < 0.05, *** = p < 0.001.

Similar results have been obtained in human fibroblasts (fig. 40, panels G-N). In control cells, the BK induced-drop is measured about -10 ± 1.8 Δ FRET % (fig. 40, panel I) from 87 ± 1 FRET % at the steady state to 77 ± 1.8 FRET % after BK (fig. 40, panel H) whereas in PS2N141I fibroblasts, the BK induced-drop is measured (fig. 40, panel I) about -24 ± 3 Δ FRET % from 69 ± 3 FRET % at the steady state to 45 ± 3.7 FRET % after BK (fig. 40, panel H). These data are confirmed also after Ca^{2+} translation (fig. 40, panels L-N), with the 71 ± 3 % (mean ± s.e.m., n = 10) of Ca^{2+} store sensitive to IP_3 in PS2N141I (fig. 40, panel N) compared to controls cells with a 51 ± 8 % (mean ± s.e.m., n = 12) of Ca^{2+} store sensitive to IP_3. (Fig. 40, panel N).

Discussion and conclusions

Direct information on the Ca^{2+} homeostatic mechanisms in the GA of living cells has been obtained for the first time only in 90's, using an aequorin chimeric construct localized in the organelle lumen (Pinton P. et al., 1998). It was demonstrated that GA Ca^{2+} handling (as a whole) resembles that of the ER. Subsequently it has been suggested that Ca^{2+} handling within the GA is heterogeneous: in particular it has been showed that the SPCA1-containing Ca^{2+} sub-compartment was insensitive (or mildly sensitive) to IP_3-generating agonist stimulation and therefore not involved in setting up cytosolic Ca^{2+} signals (Vanoevelen J. et al., 2004).

More recently, using a novel GFP-based Ca^{2+} probe, tGo-D1cpv, selectively localized in the trans-Golgi, also our laboratory have demonstrated that this GA sub-compartment is endowed with unique characteristics that differ completely from those of the ER (only SPCA1 and not SERCA equipped and IP_3 insensitive store) (Lissandron V. et al., 2010).

During my PhD, we generated another Ca^{2+} probe aimed at measuring the $[Ca^{2+}]$ in the cis/medial-GA that reveals additional complexities in the Ca^{2+} handling characteristics of the organelle. In fact, unlike the trans-Golgi that utilizes solely SPCA1 for Ca^{2+} uptake, the medial compartment appears to accumulate Ca^{2+} within its lumen taking advantage of both SPCA1 and SERCA. Moreover, the medial-Golgi, but not the trans-Golgi, seems to be sensitive to IP_3.

Thus, in a space of a few microns, and despite its continuous inter-mixing dynamics, the Golgi-Apparatus appears to be formed by separate functional entities with clearly distinct Ca^{2+} handling mechanisms.

The differences between the two GA sub-compartments are confirmed by the specific effect on Ca^{2+} homeostasis of the expression of Familial Alzheimer's Disease-linked Presenilin-2 mutants. Cells expressing a FAD mutated form of the protein show a decreased Ca^{2+} content in the cis/medial-Golgi, but no effects on trans-Golgi Ca^{2+} homeostasis: PS2 mutants decrease Ca^{2+} uptake in the cis/medial-Golgi by inhibiting SERCA pump activity while do not affect Ca^{2+} uptake, mediated by SPCA1, in the trans-Golgi.

Also the over-expression of PS2wt seems to alter Ca^{2+} handling in the medial-compartment but in a different way: while the decreased Ca^{2+} content

induced by FAD-linked PS2 mutants is primarily due to SERCA inhibition, the effect mediated by the over-expression of the wt protein seems to be more aspecific and caused by the increased passive Ca^{2+} leak from the organelle. One of the proposed functions of presenilin is indeed to act as a calcium leak channel and this function could be exaggerated in PS over-expressing cells.
Finally, we demonstrated that FAD-linked mutants increase medial-Golgi IP_3 sensitivity. It has been reported that FAD mutant PS can interact with, and increase the open probability of IP_3R, causing an abnormally exaggerated calcium signals in cells.
Concluding, FAD-linked presenilin mutants cause dysregulation in medial-Golgi Ca^{2+} handling and because the cation regulates many neuronal functions, this abnormality may contribute to the pathogenesis of the Alzheimer's disease.
Calcium in cells is precisely regulated and chronic abnormal calcium dysregulation, as a result of mutations in presenilin, may therefore cause cellular toxicity and eventually cell death. Presenilin-2 seems indeed to interact with important Ca^{2+} signaling proteins altering their function, and altered calcium signaling in turn could affect cell functionality.
These study should thus provide new insights into the molecular mechanisms of AD and into the development of novel targets for therapeutic interventions.

Abbreviations

Aβ, Amyloid-β

AD, Alzheimer's Disease

ADP, Adenosine Diphosphate

AICD, APP Intracellular Domain

APH1, Anterior Pharynx-defective 1

APP, Amyloid Precursor Protein

ATP, Adenosine-5'-triphosphate

BACE1, β-site APP Cleaving Enzyme 1

BK, Bradikin

CaM, calmodulin

CCE, Capacitative Calcium Entry

cDNA, complementary DNA

CFP, Cyan Fluorescent Protein

CIRC, Ca^{2+} induced Ca^{2+} release

CNG, cis-Golgi Network

CPA, Ciclopiazonic Acid

CRAC, Ca^{2+} release-activated Ca^{2+} channel

Dig, Digitonin

DNA, Desossiribonucleic Acid

EGTA, Ethylene Glycol Tetraacetic Acid

ER, Endoplasmic Reticulum

FAD, Familial Alzheiemer's Disease

FRET, Fluorescence Resonance Energy Transfer

GA, Golgi Apparatus

GECIs, Genetically Encoded Ca^{2+} Indicators

GFP, Green Fluorescent Protein

$InsP_3Rs$, Inositol 1,4,5-trisphosphate Receptors

Iono, Ionomycin

IP_3, Inositol Trisphosphate

LOAD, "late-onset" AD

MBDs, microtubule-binding domains

NAADP, nicotinic acid adenine dinucleotide phosphate

NFTs, neurofibrillary tangles

PEN2, Presenilin Enhancer 2

PS, Presenilin

PSEN1, Presenilin-1

PSEN2, Presenilin-2

R, Ratio

RyRs, Ryanodine Receptors

sAPP-α , Secreted Extracellular Domain

SERCA, Sarco/Endoplasmatic Reticulum Calcium ATPasi

siRNA, Small Interference Ribonucleic Acid

SOCs, Store-operated Channels

SPCA1, Secretory Pathway Ca^{2+}-ATPase isoform 1

Tau, Tubulin-associated Unit

tBHQ, 2,5-di(t-butyl)hydroquinone

Tg, Thapsigargin

TGN, Trans-Golgi Network

TPCs, Two-pore Channels

wt, wild type

YFP, Yellow Fluorescent Protein

References

Adler J. and Parmryd I., **Quantifying Colocalization by Correlation: The Pearson Correlation Coefficient is Superior to the Mander's Overlap Coefficient.** *Cytometry*, Vol. 77: 733-742, 2010.

Baird G.S., Zacharias D.A., Tsien R.Y., **Circular permutation and receptor insertion within green fluorescent proteins.** *Proc. Natl. Acad. Sci. U.S.A.*, Vol. 96: 11241–11246, 1999.

Barker W.W., Luis C.A., Kashuba A., Luis M., Harwood D.G., Loewenstein D., Waters C., Jimison P., Shepherd E., Sevush S., Graff-Radford N., Newland D., Todd M., Miller B., Gold M., Heilman K., Doty L., Goodman I., Robinson B., Pearl G., Dickson D., Duara R., **Relative frequencies of Alzheimer disease, Lewy body, vascular and frontotemporal dementia, and hippocampal sclerosis in the State of Florida Brain Bank.** *Alzheimer Dis. Assoc. Disord.*, Vol. 16:203–212, 2002.

Berridge M.J., Bootman M.D. and Roderick H.L., **Calcium signaling: dynamics, homeostasis and remodeling**, *Nature Review*, Vol. 4: 517-529, 2004.

Berridge M.J., **Inositol trisphosphate and calcium signalling.** *Nature*, Vol. 361: 315–325, 1993.

Boehning D., Mak D.O.D., Foskett J.K., Joseph S.K., **Molecular determinants of ion permeation and selectivity in inositol 1,4,5-trisphosphate receptor Ca^{2+} channels.** *J Biol Chem*, Vol. 276: 13509–13512, 2001.

Braak H., and Braak E., **Frequency of stages of Alzheimer-related lesions in different age categories.** *Neurobiol. Aging*, Vol. 18: 351–357, 1997.

Breton C., Mucha J., Jeanneau C., **Structural and functional features of glycosyl-transferases**. *Biochimie*, Vol. 83: 713–718, 2001.

Brini M. and Carafoli E., **Calcium Pumps in Health and Disease**, *Physiol Rev*, Vol. 89: 1341–1378, 2009.

Brunello L., Zampese E., Florean C., Pozzan T., Pizzo P., Fasolato C., **Presenilin-2 dampens intracellular Ca^{2+} stores by increasing Ca^{2+} leakage and reducing Ca^{2+} uptake.** *J. Cell. Mol. Med.*, Vol. 13: 3358-69, 2009.

Buxbaum J.D., Choi E.K., Luo Y., Lilliehook C., Crowley A.C., Merriam D.E., Wasco W., **Calsenilin: a calcium-binding protein that interacts with the presenilins and regulates the levels of a presenilin fragment.** *Nat. Med.*, Vol. 4: 1177-81, 1998.

Cahalan M.D., **STIMulating store-operated Ca^{2+} entry.**, *Nat Cell Biol.*, Vol. 11: 669–677, 2009.

Cahalan M.D., Zhang S.L., Yeromin A.V., et al. **Molecular basis of the CRAC channel.** *Cell Calcium*, Vol. 42: 133-144, 2007.

Cai H., Wang Y., McCarthy D., Wen H., Borchelt D.R., Price D.L. and Wong P.C., **BACE1 is the major beta-secretase for generation of Abeta peptides by neurons.** *Nat. Neurosci.*, Vol. 4: 233–234, 2001.

Calcraft P.J., Ruas M., Pan Z., Cheng X., Arredouani A., Hao X., Tang J., Rietdorf K., Teboul L., Chuang K.T., et al., **NAADP mobilizes calcium from acidic organelles through two-pore channels.** *Nature*, Vol. 459: 596–600, 2009.

Carbone E., Lux H.D., **A low voltage-activated, fully inactivating Ca channel in vertebrate sensory neurones.** *Nature*, Vol. 310: 501–502, 1984.

Catterall W.A., **Excitation-contraction coupling in vertebrate skeletal muscle: A tale of two calcium channels.** *Cell*, Vol. 64: 871–874, 1991.

Catterall W.A., **Voltage-Gated Calcium Channels**. *Cold Spring Harb. Perspect. Biol.*, Vol. 3: 3947-3960, 2011.

Chanat E. and Huttner W.B., **Milieu-induced,selective aggregation of regulated secretory proteins in the trans-Golgi network.** *J.Cell Biol.*, Vol. 115:1505–1519, 1991.

Chandra S., Kable E.P., Morrison G.H., Webb W.W., **Calcium sequestration in the Golgi apparatus of cultured mammalian cells revealed by laser scanning confocal microscopy and ion microscopy.** *J.CellSci.*, Vol. 100: 747–752, 1991.

Chung S.H., **Aberrant phosphorylation in the pathogenesis of Alzheimer's disease.** *BMB Rep.*, Vol. 42, 467–474, 2009.

Cifuentes F., Gonzalez C.E., Fiordelisio T., Guerrero G., Lai F.A., Hernandez-Cruz A., **A ryanodine fluorescent derivative reveals the presence of high-affinity ryanodine binding sites in the Golgi complex of rat sympathetic neurons, with possible functional roles in intracellular Ca^{2+} signaling.** *Cell Signal.*, Vol. 13: 353–362, 2001.

Coe H., Michalak M., **Calcium binding chaperones of the endoplasmic reticulum.** *Gen Physiol Biophys*, Vol. 28 Spec No Focus:F96–F103, 2009.

Csala M., Ba´nhegyi G., Benedetti A., **Endoplasmic reticulum: A metabolic compartment**, *FEBS Letters*, Vol. 580: 2160–2165, 2006.

Cupers P., Bentahir M., Craessaerts K., Orlans I., Vanderstichele H., Saftig P., De Strooper B., Annaert W., **The discrepancy between presenilin subcellular localization and gamma-secretase processing of amyloid precursor protein.** *J. Cell Biol.*, Vol. 154:731-740, 2001.

de Brito O.M. and Scorrano L., **Mitofusin2 tethers endoplasmic reticulum to mitochondria.** *Nature*, Vol. 456: 605–610, 2008.

Demaurex N., **Calcium measurements in organelles with Ca^{2+}-sensitive fluorescent proteins.** *Cell Calcium*, Vol. 38: 213–222, 2005.

Dode L., Andersen J.P., Vanoevelen J., et al., **Dissection of the functional differences between human secretory pathway Ca^{2+}/Mn^{2+}-ATPase (SPCA) 1 and 2 isoenzymes by steady-state and transient kinetic analyses.** *J. Biol. Chem.*, Vol. 281: 3182–3189, 2006.

Drago I., Giacomello M., Pizzo P., Pozzan T., **Calcium dynamics in the peroxisomal lumen of living cells.** *J. Biol. Chem.*, Vol. 283:14384-90, 2008.

Du G.G., Sandhu B., Khanna V.K., Guo X.H., and MacLennan D.H., **Topology of the Ca^{2+} release channel of skeletal muscle sarcoplasmic reticulum (RyR1).** *Proc. Natl. Acad. Sci. U.S.A.* Vol: 99, 16725–16730, 2002.

Ehehalt R., Michel B., De Pietri Tonelli D., Zacchetti D., Simons K. and Keller P., **Splice variants of the beta-site APP-cleaving enzyme BACE1 in human brain and pancreas.** *Biochem. Biophys. Res. Commun.*, Vol. 293, 30–37, 2002.

Fill M., Copello J.A., **Ryanodine receptor calcium release channels.** *Physiol Rev*, Vol. 82: 893–922, 2002.

Foskett J.K., White C., Cheung K., Mak D.D., **Inositol Trisphosphate Receptor Ca^{2+} Release Channels**. *Physiol Rev*, Vol. 87: 593–658, 2007;

Foskett J.K., White C., Cheung K.H., Mak D.O., **Inositol trisphosphate receptor Ca^{2+} release channels.** *Physiol Rev*, Vol. 87: 593–658, 2007.

Francis R., McGrath G., Zhang J. et al., **aph-1 and pen-2 are required for Notch pathway signaling, gamma-secretase cleavage of betaAPP, and presenilin protein accumulation.** *Dev. Cell*, Vol. 3: 85–97, 2002.

Furukawa K., Guo Q., Schellenberg G.D., Mattson M.P., **Presenilin-1 mutation alters NGF-induced neurite outgrowth, calcium homeostasis, and transcription factor (AP-1) activation in PC12 cells.** *J. Neurosci Res.*, Vol. 52: 618-24, 1998.

Giacomello M., Barbiero L., Zatti G., Squitti R., Binetti G., Pozzan T., Fasolato C., Ghidoni R., Pizzo P., **Reduction of Ca^{2+} stores and capacitative Ca^{2+} entry is associated with the familial Alzheimer's disease presenilin-2 T122R mutation and anticipates the onset of dementia.** *Neurobiol. Dis.*, Vol. 18: 638-48, 2005.

Giacomello M., Drago I., Bortolozzi M., Scorzeto M., Gianelle A., Pizzo P., Pozzan T., **Ca^{2+} hot spots on the mitochondrial surface are generated by Ca^{2+} mobilization from stores, but not by activation of store-operated Ca^{2+} channels.** *Mol Cell.*, Vol. 38: 280-90, 2010.

Glenner G.G. and Wong C.W., **Alzheimer's disease: initial report of the purification and characterization of a novel cerebrovascular amyloid protein.** *Biochem. Biophys. Res. Commun.* Vol. 120, 885–890, 1984.

Goedert M., **Oskar Fischer and the study of dementia.** *Brain*, Vol. 132: 1102–1111, 2009.

Green K.N., Demuro A., Akbari Y., Hitt B.D., Smith I.F., Parker I., LaFerla F.M., **SERCA pump activity is physiologically regulated by presenilin and regulates amyloid beta production.** *J. Gen. Physiol.*, Vol. 132, 2008.

Grigoriev I., Gouveia S.M., van der Vaart B., et al. **STIM1 is a MT-plus-end-tracking protein involved in remodeling of the ER.** *Curr. Biol.*, Vol. 18: 177-182, 2008.

Guo Q., Christakos S., Robinson N., Mattson M.P., **Calbindin D28k blocks the proapoptotic actions of mutant presenilin 1: reduced oxidative stress and preserved mitochondrial function.** *Proc. Natl. Acad. Sci. USA*, Vol. 95: 3227-32, 1998.

Hagiwara S., Ozawa S., Sand O, **Voltage clamp analysis of two inward current mechanisms in the egg cell membrane of a starfish.** *J. Gen. Physiol.*, Vol. 65: 617–644, 1975.

Hattori M., Suzuki A.Z., Higo T., Miyauchi H., Michikawa T., Nakamura T., Inoue T., Mikoshiba K., **Distinct roles ofinositol 1, 4, 5-trisphosphate receptor types 1 and 3 in Ca^{2+} signaling.** *J Biol Chem*, Vol. 279: 11967–11975, 2004.

Heinemann S.H., Terlau H., Stühmer W., Imoto K. Numa S., **Calcium channel characteristics conferred on the sodium channel by single mutations.** *Nature*, Vol. 356: 441–443, 1992.

Holsinger R.M., McLean C.A., Beyreuther K., Masters C.L. and Evin G., **Increased expression of the amyloid precursor beta-secretase in Alzheimer's disease.** *Ann. Neurol.*, Vol. 51, 783–786, 2002.

Holtzman D.M., Morris John C., and Goate A., **Alzheimer's Disease: The Challenge of the Second Century.** *Sci. Transl. Med.*, Vol. 6: 77-112, 2011;

Hu Z., Bonifas J.M., Beech J., Bench G., Shigihara T., Ogawa H., Ikeda S., Mauro T., EpsteinJr. E.H., **Mutations in ATP2C1, encoding a calcium pump, cause Hailey–Hailey disease.** *Nat. Genet.*, Vol. 24: 61–65, 2000.

Kang J., Lemaire H.G., Unterbeck A., Salbaum J.M., Masters C.L., Grzeschik K.H., Multhaup G., Beyreuther K. and Muller-Hill B., **The precursor of Alzheimer's disease amyloid A4 protein resembles a cell-surface receptor.** *Nature*, Vol. 325: 733–736, 1987.

Kayed R., Head E., Thompson J.L., McIntire T.M., Milton S.C., Cotman C.W., Glabe C.G., **Common structure of soluble amyloid oligomers implies common mechanism of pathogenesis.** *Science*, Vol. 300: 486–489, 2003.

Koike H., Tomioka S., Sorimachi H., Saido T.C., Maruyama K., OkuyamaA., Fujisawa-Sehara A., Ohno S., Suzuki K. and Ishiura S., **Membrane-anchored**

metalloprotease MDC9 has an alphasecretase activity responsible for processing the amyloid precursor protein. *Biochem. J.*, Vol. 343: 371–375, 1999.

Kojro E., Gimpl G., Lammich S., Marz W. and Fahrenholz F., **Low cholesterol stimulates the nonamyloidogenic pathway by its effect on the alpha-secretase ADAM 10**. *Proc. Natl Acad. Sci. USA*, Vol. 98: 5815–5820, 2001.

Kipanyula M.J., Contreras L., Zampese E., Lazzari C., Wong A.K., Pizzo P., Fasolato C., Pozzan T., **Ca^{2+} dysregulation in neurons from transgenic mice expressing mutant presenilin 2**. *Aging Cell*, Vol 11: 885-93, 2012.

LaPointe N.E., Morfini G., Pigino G., Gaisina I.N., Kozikowski A.P., Binder L.I., Brady S.T., **The amino terminus of tau inhibits kinesin-dependent axonal transport: implications for filament toxicity**. *J. Neurosci. Res.*, Vol. 87: 440–451, 2009.

Lee S.F., Shah S., Li H., Yu C., Han W. and Yu G., **Mammalian APH-1 interacts with presenilin and nicastrin and is required for intramembrane proteolysis of amyloid-beta precursor protein and Notch**. *J. Biol. Chem.*, Vol. 277: 45013–45019, 2002

Leite M.F., Thrower E.C., Echevarria W., Koulen P., Hirata K., Bennett A.M., Ehrlich B.E., Nathanson M.H., **Nuclear and Ca^{2+} homeostasis in sub-cellular compartments cytosolic calcium are regulated independently**. *Proc Natl Acad Sci USA*, Vol. 100: 2975–2980, 2003.

Levy E., Carman M.D., Fernandez M.I.J., Power M.D., Lieberburg I., van Duinen S.G., Bots G.T., Luyendijk W., Frangione B., **Mutation of the Alzheimer's disease amyloid gene in hereditary cerebral hemorrhage. Dutch type**. *Science*, Vol. 248: 1124–1126, 1990.

Levy-Lahad E., Wasco W., Poorkag P., Romano D.M., Oshima J., Pettingell W.H., Yu C-E., Jondor P.D., Schmidt S.D., Wang K., et al. **Candidate gene for the chromosome 1 familial Alzheimer's disease locus**. Science. 1995; 269:973–977.

Lin P., Le-Niculescu H., Hofmeister R., McCaffery J.M., Jin M., Hennemann H-, McQuistan T., DeVries L., Farquhar M.G., **The mammalian calcium-**

binding protein, nucleobindin (CALNUC) is a Golgi resident protein. *J. Cell Biol.*, Vol. 141: 1515–1527, 1998.

Liou J., Kim M.L., Heo W.D., et al., **STIM is a Ca^{2+} sensor essential for Ca^{2+}-store-depletion triggered Ca^{2+} influx.** *Curr. Biol.*, Vol. 15: 1235-1241, 2005.

Lissandron V., Podini P., Pizzo P. and Pozzan T., **Unique characteristics of Ca^{2+} homeostasis of the trans-Golgi compartment.** *Proc. Natl. Acad. Sci. U.S.A.*, Vol: 107, 9198–9203, 2010.

Llina´s R. and Yarom Y., **Electrophysiology of mammalian inferior olivary neurones in vitro. Different types of voltage-dependent ionic conductances.** *J. Physiol.* Vol. 315: 569–584, 1981.

Lucin K.M. and Wyss-Coray T., **Immune activation in brain aging and neurodegeneration: too much or too little?** *Neuron*, Vol. 64: 110–122, 2009.

Luo W.J., Wang H., Li H., Kim B.S., Shah S., Lee H.J., Thinakaran G., Kim T.W., Yu G. and Xu H., **PEN-2 and APH-1 coordinately regulate proteolytic processing of presenilin 1.** *J. Biol. Chem.*, Vol. 278: 7850–7854, 2003.

Maeda N., Kawasaki T., Nakade S., Yokota N., Taguchi T., Kasai M., Mikoshiba K., **Structural and functional characterization of inositol 1,4,5-trisphosphate receptor channel from mouse cerebellum.** *J Biol Chem*, Vol. 266: 1109–1116, 1991.

Mak D.O.D., McBride S., Foskett J.K., **Inositol 1,4,5-trisphosphate activation of inositol trisphosphate receptor Ca^{2+} channel by ligand tuning of Ca^{2+} inhibition.** *Proc Natl Acad Sci USA*, Vol. 95: 15821–15825, 1998.

Mak D.O.D., McBride S., Foskett J.K., **Regulation by Ca^{2+} and inositol 1,4,5-trisphosphate ($InsP_3$) of single recombinant type 3 $InsP_3$ receptor channels. Ca^{2+} activation uniquely distinguishes types 1 and 3 $InsP_3$ receptors.** *J Gen Physiol*, Vol. 117: 435–446, 2001.

Martin L., Latypova X., Terro F., **Post-translational modifications of tau protein: Implications for Alzheimer's disease.** *Neurochemistry International*, Vol. 58: 458–471, 2011.

McCombs J.E. and Palmer A.E., **Measuring calcium dynamics in living cells with Genetically Encodable Calcium Indicators.** *Methods*, Vol. 46: 152–159, 2008.

Meldolesi J. and Pozzan T., **The endoplasmic reticulum Ca^{2+} store: A view from the lumen**, *Trends Biochem. Sci.* Vol. 23: 10–14, 1998.

Michikawa T., Hamanaka H., Otsu H., Yamamoto A., Miyawaki A., Furuichi T., Tashiro Y., Mikoshiba K., **Transmembrane topology and sites of N-glycosylation of inositol 1,4,5 trisphosphate receptor.** *J Biol Chem*, Vol. 269: 9184–9189, 1994.

Mignery G.A., Newton C.L., Archer B.T., Sudhof T.C., **Structure and expression of the rat inositol 1,4,5-trisphosphate receptor.** *J Biol Chem*, Vol. 265: 12679–12685, 1990.

Mikoshiba K., **The IP_3 receptor/Ca^{2+} channel and its cellular function.** *Biochem Soc Symp*, Vol. 74:9–22, 2007.

Mintz I.M., Adams M.E., Bean B.P., **P-type calcium channels in rat central and peripheral neurons.** *Neuron*, Vol. 9: 85–95, 1992.

Missiaen L., Dode L., Vanoevelen J., Raeymaekers L., Wuytack F., **Calcium in the Golgi apparatus.** *Cell Calcium*, Vol. 41: 405–416, 2007.

Missiaen L., VanAcker K., VanBaelen K., Raeymaekers L., Wuytack F., Parys J.B., DeSmedt H., Vanoevelen J., Dode L., Rizzuto R., Callewaert G., **Calcium release from the Golgi apparatus and the endoplasmic reticulum in HeLa cells stably expressing targeted aequorin to these compartments.** *Cell Calcium*, Vol. 36: 479–487, 2004.

Miyawaki A., Llopis J., Heim R., McCaffery J.M., Adams J.A., Ikura M., Tsien R.Y., **Fluorescent indicators for Ca^{2+} based on green fluorescent proteins and calmodulin.** *Nature*, Vol. 388: 882–887, 1997.

Miyawaki A., Llopis J., Heim R., McCaffery J.M., Adams J.A., Ikura M., Tsien R.Y., **Fluorescent indicators for Ca^{2+} based on green fluorescent proteins and calmodulin.** *Nature*, Vol. 388: 882–887, 1997.

Moncoq K., Trieber C.A., Young H.S., **The molecular basis for cyclopiazonic acid inhibition of the sarcoplasmic reticulum calcium pump.** *J Biol Chem*, Vol. 282: 9748–9757, 2007.

Morel-Huaux V.M., Pypaert M., Wouters S., Tartakoff A.M., Jurgan U., Gevaert K., Courtoy P.J., **The calcium-binding protein p54/NEFA is a novel luminal resident of medial Golgi cisternae that traffics independently of mannosidase II.** *Eur. J. Cell Biol.*, Vol. 81: 87–100, 2002.

Nagai T., Yamada S., Tominaga T., Ichikawa M., Miyawaki A., **Expanded dynamic range of fluorescent indicators for $Ca^{(2+)}$ by circularly permuted yellow fluorescent proteins.** *Proc. Natl. Acad. Sci. USA*, Vol. 10: 10554–10559, 2004.

Nowycky M.C., Fox A.P., Tsien R.W., **Three types of neuronal calcium channel with different calcium agonist sensitivity.** *Nature*, Vol. 316: 440–443, 1985.

Oda K., **Calcium depletion blocks proteolytic cleavages of plasmaprotein precursors which occur at the Golgi and/or trans-Golgi network. Possible involvement of $Ca^{(2+)}$-dependent Golgi endo proteases.** *J.Biol.Chem.*, Vol. 267: 17465–17471, 1992.

Oldershaw K.A., Taylor C.W., **2,5-Di-(tert-butyl)-1,4-benzohydroquinone mobilizes inositol 1,4,5-trisphosphate-sensitive and –insensitive Ca^{2+} stores.** *FEBS Lett*, Vol. 274: 214–216, 1990.

Ozer R.S., Halpain S., **Phosphorylation-dependent localization of microtubule- associated protein MAP2c to the actin cytoskeleton.** *Mol. Biol. Cell*, Vol. 11, 3573–3587, 2000.

Pack-Chung E., Meyers M.B., Pettingell W.P., Moir R.D., Brownawell A.M., Cheng I., Tanzi R.E., Kim T.W., **Presenilin 2 interacts with sorcin, a modulator of the ryanodine receptor.** *J. Biol. Chem.*, Vol. 275: 14440-5, 2000.

Palmer A.E., Giacomello M., Kortemme T., Andrew Hires S., Lev-Ram V.,Baker D. and Tsien R.Y., **Ca^{2+} Indicators Based on Computationally Redesigned Calmodulin-Peptide Pairs.** *Chemistry & Biology*, Vol. 13: 521–530, 2006.

Palmer A.E., Jin C., Reed J.C. and Tsien R.Y., **Bcl-2-mediated alterations in endoplasmic reticulum Ca^{2+} analyzed with an improved genetically encoded fluorescent sensor.** *Proc. Natl. Acad. Sci. USA*, Vol. 101: 17404–17409, 2004.

Pezzati R., Bossi M. , Podini P., Meldolesi J., Grohovaz F., **High-resolution calcium mapping of the endoplasmic reticulum-Golgi-exocytic membrane system. Electron energy loss imaging analysis of quick frozen-freeze dried PC12cells.** *Mol. Biol.Cell*, Vol. 8: 1501–1512, 1991.

Pinton P., Pozzan T., Rizzuto R., **The Golgi apparatus is an inositol 1,4,5-trisphosphate-sensitive Ca^{2+} store, with functional properties distinct from those of the endoplasmic reticulum.** *EMBO J.*, Vol. 17: 5298–5308, 1998.

Pizzo P., Lissandron V., Capitanio P., Pozzan T., **Ca^{2+} signalling in the Golgi apparatus.** *Cell Calcium*, Vol. 50: 184-92, 2011.

Postina R., Schroeder A., Dewachter I. et al., **A disintegrin-metalloproteinase prevents amyloid plaque formation and hippocampal defects in an Alzheimer disease mouse model.** *J. Clin. Invest.*, Vol. 113, 1456–1464, 2004.

Pozzan T., Rizzuto R., Volpe P., Meldolesi J., **Molecular and cellular physiology of intracellular calcium stores**, *Physiol Rev July* Vol. 74: 595-636, 1994.

Prins D. and Michalak M., **Organellar Calcium Buffers**, *Cold Spring Harb Perspect Biol*, Vol. 3: 1-16, 2011.

Pritchard S.M., Dolan P.J., Vitkus A., Johnson G.V.W, **The toxicity of tau in Alzheimer disease: turnover, targets and potential therapeutics.** *J. Cell. Mol. Med.*, Vol. 15: 1621-1635, 2011.

Putney J.W., **The Physiological Function of Store-operated Calcium Entry.**, *Neurochem. Res.*, Vol. 36:1157–1165, 2011.

Ramos-Franco J., Galvan D., Mignery G.A., Fill M., **Location of the permeation pathway in the recombinant type 1 inositol 1,4,5-trisphosphate receptor.** *J Gen Physiol*, Vol. 114: 243–250, 1999.

Randall A., Tsien R.W., **Pharmacological dissection of multiple types of calcium channel currents in rat cerebellar granule neurons.** *J. Neurosci.* Vol. 15: 2995–3012, 1995.

Raychaudhury B., Gupta S., Banerjee S., Datta S.C., **Peroxisome is a reservoir of intracellular calcium.** *Biochim. Biophys. Acta*, Vol. 1760: 989–992, 2006.

Rizzuto R., Brini M., Pozzan T., **Targeting recombinant aequorin to specific intracellular organelles.** *Methods Cell. Biol.*, Vol. 40:339–358, 1994.

Rizzuto R., Simpson A.W., Brini M., Pozzan T., **Rapid changes of mitochondrial Ca^{2+} revealed by specifically targeted recombinant aequorin.** *Nature*, Vol. 358: 325–327, 1992.

S.L. Hamilton and I. Serysheva, **Ryanodine Receptor Structure: Progress and Challenges.** *J Biol Chem*, Vol. 284: 4047-4051, 2008.

Sagara Y., Fernandez-Belda F., de Meis L., Inesi G., **Characterization of the inhibition of intracellular Ca^{2+} transport ATPases by thapsigargin.** *J Biol Chem*, Vol. 267: 12606–12613, 1992.

Sagara Y., Inesi G., **Inhibition of the sarcoplasmic reticulum Ca^{2+}transport ATPase by thapsigargin at subnanomolar concentrations.** *J Biol Chem*, Vol. 266: 13503–13506, 1991.

Sarah C. and Robert V., **The Alzheimer's disease beta-secretase enzyme, BACE1.** *Mol. Neurodegener.*, Vol. 2: 22, 2007.

Schafer W., Stroh A., Berghofer S., Seiler J., Vey M. , Kruse M.L., Kern H.F., Klenk H.D., Garten W., **Two independent targeting signals in the cytoplasmic domain determine trans-Golgi network localization and endosomal trafficking of the proprotein convertase furin.** *EMBO J.*, Vol. 14: 2424–2435, 1995.

Schrader M. and Yoon Y., **Mitochondria and peroxisomes: are the 'big brother' and the 'little sister' closer than assumed? BioEssays : news and reviews in molecular.** *Cell. Dev. Biol.*, Vol. 29: 1105–1114, 2007.

Seidler N.W., Jona I., Vegh M., A. Martonos, **Cyclopiazonic acid is a specific inhibitor of the Ca^{2+}-ATPase of sarcoplasmic reticulum.** *J Biol Chem*, Vol. 264: 17816–17823, 1989.

Sengupta A., Kabat J., Novak M., Wu Q., Grundke-Iqbal I., Iqbal K., **Phosphorylation of tau at both Thr 231 and Ser 262 is required for maximal inhibition of its binding to microtubules.** *Arch. Biochem. Biophys.*, Vol. 357: 299–309, 1998.

Sherrington R., Rogaev E.I., Liang Y., Rogaeva E.A., Levesque G., Ikeda M., Chi H., Lin C., Li G., Holman K., Tsuda T., Mar L., Foncin J.F., Bruni A.C., Montesi M.P., Sorbi S., Rainero I., Pinessi L., Nee L., Chumakov I., Pollen D., Brookes A., Sanseau P., Polinsky R.J., Wasco W., Da Silva H.A.R., Haines J.L., Pericak-Vance M.A., Tanzi R.E., Roses A.D., Fraser P.E., Rommens J.M., St George-Hyslop P.H., **Cloning a gene bearing missense mutations in early-onset familial Alzheimer's disease.** *Nature,* Vol. 375: 754–760 (1990).

Shirotani K., Edbauer D., Capell A., Schmitz J., Steiner H. and Haass C., **Gamma-Secretase activity is associated with a conformational change of nicastrin.** *J. Biol. Chem.*, Vol. 278: 16474, 2003.

Sinha S., Anderson J.P., Barbour R. et al., **Purification and cloning of amyloid precursor protein beta-secretase from human brain.** *Nature*, Vol. 402: 537–540, 1999.

Small S.A. and Duff K., **Linking Abeta and tau in late-onset Alzheimer's disease: a dual pathway hypothesis.** *Neuron*, Vol. 60: 534–42, 2008.

Stutzmann G.E., Smith I., Caccamo A., Oddo S., Laferla F.M., Parker I., **Enhanced ryanodine receptor recruitment contributes to Ca^{2+} disruptions in young, adult, and aged Alzheimer's disease mice.** *J Neurosci.*, Vol. 26: 5180-9, 2006.

Supattapone S., Worley P.F., Baraban J.M., Snyder S.H., **Solubilization, purification, characterization of an inositol trisphosphate receptor.** *J Biol Chem*, Vol. 263: 1530–1534, 1988.

Szasz I., Sarkadi B., Schubert A., Gardos G., **Effects of lanthanum on calcium-dependent phenomena in human red cells**, *Biochim Biophys Acta* Vol. 512: 331–340, 1978.

Takahashi M., Seagar M.J., Jones J.F., Reber B.F., Catterall W.A., **Subunit structure of dihydropyridine-sensitive calcium channels from skeletal muscle.** *Proc. Natl. Acad. Sci.*, Vol. 84: 5478–5482, 1997.

Takasugi N., Tomita T., Hayashi I., Tsuruoka M., Niimura M., Takahashi Y., Thinakaran G., Iwatsubo T., **The role of presenilin cofactors in the gamma-secretase complex.** *Nature*, Vol. 422: 438–441 (2003).

Takeshima H., Nishimura S., Matsumoto T., Ishida H., Kangawa K., Minamino N., Matsuo H., Ueda M., Hanaoka M., Hirose T., et al.. **Primary structure and expression from complementary DNA of skeletal muscle ryanodine receptor.** *Nature*, Vol. 339: 439–445, 1989.

Tanzi R.E., Gusella J.F., Watkins P.C., Bruns G.A., St George-Hyslop P., Van Keuren M.L., Patterson D., Pagan S., Kurnit D.M. and Neve R.L., **Amyloid beta protein gene: cDNA, mRNA distribution, and genetic linkage near the Alzheimer locus.** *Science*, Vol. 235: 880–884, 1987.

Tarassishin L., Yin Y.I., Bassit B., Li Y.M., **Processing of Notch and amyloid precursor protein by gamma-secretase is spatially distinct.** *Proc. Natl. Acad. Sci. USA*, Vol. 101: 17050-17055, 2004.

Thastrup O., Cullen P.J., Drobak B.K., Hanley M.R., Dawson A.P., **Thapsigargin, a tumor promoter, discharges intracellular Ca^{2+} stores by specific inhibition of the endoplasmic reticulum Ca^{2+}-ATPase.** *Proc Natl Acad Sci USA*, Vol. 87: 2466–2470, 1990.

Thinakaran G., Borchelt D.R., Lee M.K., Slunt H.H., Spitzer L., Kim G., Ratovitsky T., Davenport F., Nordstedt C. and Seeger M., **Endoproteolysis of presenilin 1 and accumulation of processed derivatives in vivo.** *Neuron*, Vol. 17: 181–190, 1996.

Thyberg J., Moskalewski S., **Role of microtubules in the organization of the Golgi complex.** *Exp. Cell. Res.*, Vol.246:263-79, 1999.

Tsien R.W., Lipscombe D., Madison D.V., Bley K.R., Fox A.P., **Multiple types of neuronal calcium channels and their selective modulation.** *Trends Neurosci.*, Vol. 11: 431–438, 1988.

Vaca L., **SOCIC: The store-operated calcium influx complex.** *Cell Calcium*, Vol. 47: 199–209, 2010.

VanBaelen K., Vanoevelen J., Callewaert G., Parys J.B., DeSmedt H., Raeymaekers L., Rizzuto R., Missiaen L., Wuytack F., **The contribution of the SPCA1 Ca^{2+} pump to the Ca^{2+} accumulation in the Golgi apparatus of HeLa cells assessed via RNA-mediated interference.** *Biochem. Biophys. Res. Commun.*, Vol. 306:430–436, 2003.

Vangheluwe P., Sepulveda M.R., Missiaen L., Raeymaekers L., Wuytack F., Vanoevelen J., **Intracellular Ca^{2+}- and Mn^{2+}-transport ATPases.** *Chem.Rev.*, Vol. 109: 4733–4759, 2009.

Vanoevelen J., Raeymaekers L., Parys J.B., DeSmedt H., VanBaelen K., Callewaert G., Wuytack F., Missiaen L., **Inositol trisphosphate producing agonists do not mobilize the thapsigargin-insensitive part of the endoplasmic-reticulum and Golgi Ca^{2+} store.** *Cell Calcium*, Vol. 35: 115–121, 2004.

Vetrivel K.S., Cheng H., Lin W., Sakurai T., Li T., Nukina N., Wong P.C., Xu H., Thinakaran G., **Association of gamma-secretase with lipid rafts in post-Golgi and endosome membranes.** *J. Biol. Chem.*, Vol. 279: 44945-54, 2004.

Vetrivel K.S., Zhang Y. W., Xu H. and Thinakaran G. **Pathological and physiological functions of presenilins.** *Mol. Neurodegener.*, Vol. 1: 4, 2006.

Wang H.J., Guay G., Pogan L., Sauve R., Nabi I.R., **Calcium regulates the association between mitochondria and a smooth subdomain of the endoplasmic reticulum.** *J Cell. Biol.*, Vol. 150: 1489–1498, 2000.

Weingarten M.D., Lockwood A.H., Hwo S.Y., Kirschner M.W., **A protein factor essential for microtubule assembly.** *Proc. Natl. Acad. Sci. USA*, Vol. 72: 1858–1862, 1975.

Wuytack F., Raeymaekers L., Missiaen L., **Molecular physiology of the SERCA and SPCA pumps**, *Cell Calcium* Vol. 32: 279–305, 2002.

Yabe D., Nakamura T., Kanazawa N., Tashiro K., Honjo T., **Calumenin, a Ca^{2+}-binding protein retained in the endoplasmic reticulum with a novel carboxyl-terminal sequence, HDEF.** *J. Biol. Chem.*, Vol. 272: 18232–18239, 1997.

Yang S.N., Berggren P.O., **The role of voltage-gated calcium channels in pancreatic b-cell physiology and pathophysiology.** *Endocr. Rev.* Vol. 27: 621–676, 2006.

Yu G., Nishimura M., Arawaka S., Levitan D., Zhang L., Tandon A., Song Y. Q., Rogaeva E., Chen F. and Kawarai T., **Nicastrin modulates presenilin-mediated notch/glp-1 signal transduction and beta-APP processing.**, *Nature*, Vol. 407, 48–54, 2000

Yu M., Zhong L., Rishi A.K., Khadeer M., Inesi G., Hussain A., **Specific substitutions at amino acid 256 of the sarcoplasmic/endoplasmic reticulum Ca^{2+} transport ATPase mediate resistance to thapsigargin in thapsigargin-resistant hamster cells.** *J Biol Chem*, Vol. 273: 3542–3546, 1998.

Zampese E. and Pizzo P., **Intracellular organelles in the saga of Ca^{2+} homeostasis: different molecules for different purposes?**, *Cell. Mol. Life Sci.*, Vol. 69: 1077-1104, 2011.

Zampese E., Brunello L., Fasolato C., Pizzo P., **Ca^{2+} dysregulation mediated by presenilins in Familial Alzheimer's Disease: Causing or modulating factor?** *Current Trends in Neurology*, Vol.3: 1-9, 2009.

Zatti G., Burgo A., Giacomello M., Barbiero L., Ghidoni R., Sinigaglia G., Florean C., Bagnoli S., Binetti G., Sorbi S., Pizzo P., Fasolato C., **Presenilin mutations linked to familial Alzheimer's disease reduce endoplasmic reticulum and Golgi apparatus calcium levels.** *Cell Calcium,* Vol. 39: 539-50, 2006.

Zatti G., Ghidoni R., Barbiero L., Binetti G., Pozzan T., Fasolato C., Pizzo P., **The presenilin 2 M239I mutation associated with familial Alzheimer's disease reduces Ca^{2+} release from intracellular stores.** *Neurobiol. Dis.*, Vol. 15: 269-78, 2004.

Zerfaoui M., Fukuda M., Langlet C., Mathieu S., Suzuki M., Lombardo D., El-Battari A., **The cytosolic and transmembrane domains of the beta 1,6 N-acetylglucosaminyltransferase (C2GnT) function as a cis to medial/Golgi-targeting determinant.** *Glycobiology*, Vol. 12: 15-24, 2002.

Zhang H., Ma Q., Zhang J., Xu H., **Proteolytic processing of Alzheimer's β-amyloid precursor protein.** *J. of Neurochemistry*, Vol. 120: 9–21, 2012.

Zhang Y., Thompson R., Zhang H., Xu H., **APP processing in Alzheimer's disease.** *Molecular Brain*, Vol. 4: 3, 2011.